Aus dem Cologne Excellence Cluster on Cellular Stress Response in Aging-Associated Diseases (CECAD) der Universität zu Köln Direktor der Medizinischen Fakultät: Univ.-Prof. Dr. Gereon Fink

Exploration of immunomodulatory functions of ferroptosis

Inaugural-Dissertation zur Erlangung der Doktorwürde der Medizinischen Fakultät der Universität zu Köln

vorgelegt von Josephine Weber aus Forst (Lausitz) Dekan: Universitätsprofessor Dr. med. G.R. Fink

- 1. Gutachterin: Universitätsprofessorin Dr. rer. nat. S. von Karstedt
- 2. Gutachter: Universitätsprofessor Dr. rer. nat. H. Walczak

Erklärung

Ich erkläre hiermit, dass ich die vorliegende Dissertationsschrift ohne unzulässige Hilfe Dritter und ohne Benutzung anderer als der angegebenen Hilfsmittel angefertigt habe; die aus fremden Quellen direkt oder indirekt übernommenen Gedanken sind als solche kenntlich gemacht.

Bei der Auswertung des Materials habe ich Unterstützungsleistungen von folgenden Personen erhalten:

Frau Prerana Wagle (Bioinformatician at CECAD Cologne)

Frau Jenny Stroh (AG von Karstedt)

Frau Fatma Isil Yapici (AG von Karstedt)

Herrn Zhiyi Chen (AG von Karstedt)

Herrn Dr. Julian Nüchel (Center for Biochemistry, Medical Faculty, University of Cologne)

Prof. Dr. Alexander Quaas from the department of pathology at the University Clinic of Cologne Team of the Proteomics Facility (CECAD Cologne)

Team of the histological department of the Manolis Pasparakis laboratory

Weitere Personen waren an der Erstellung der vorliegenden Arbeit nicht beteiligt. Insbesondere habe ich nicht die Hilfe einer Promotionsberaterin/eines Promotionsberaters in Anspruch genommen. Dritte haben von mir weder unmittelbar noch mittelbar geldwerte Leistungen für Arbeiten erhalten, die im Zusammenhang mit dem Inhalt der vorgelegten Dissertationsschrift stehen.

Die Dissertationsschrift wurde von mir bisher weder im Inland noch im Ausland in gleicher oder ähnlicher Form einer anderen Prüfungsbehörde vorgelegt.

Die dieser Arbeit zugrunde liegenden Experimente sind von mir mit Teilunterstützung von der medizinisch-technischen Assistentin Frau Jenny Stroh und Isil Yapici als Mitglieder der AG von Karstedt durchgeführt und analysiert worden. Die Zucht und Versorgung der Versuchstiere, sowie deren Tötung wurden ohne meine Mithilfe von Frau Jenny Stroh durchgeführt. Ebenso wurden die Experimente beschrieben in 4.2.1. und 4.3.1. ohne meine Mithilfe von Frau Jenny Stroh durchgeführt. Dehydratisierungs -und Infiltrationsschritte erfolgten durch die histologische Abteilung der Arbeitsgruppe von Manolis Pasparakis. Später wurden histologische Schnitte von 20 Wochen alten Mäusen in Zusammenarbeit mit Prof. Dr. Alexander Quaas von der Abteilung für der Pathologie der Universitätsklinik Köln analysiert.

Die RNA Sequenzierung wurde von dem Cologne Center for Genomics durchgeführt (Illumina dye sequencing method, Lexogne QuantSeq 3´ library preparation protocol). Sequenzierte Daten wurden sodann an das Bioinformatische Institut CECAD zur Generierung der Datensätze übermittelt und von Frau Prerana Wagle zur Verfügung gestellt. Anschließend wurde mit der Unterstützung von Herrn Zhiyi Chen die Expressionsanalyse (DESeq2) durchgeführt. Die zu sequenzierenden Proben wurden in der Zellkultur durch mich generiert.

Die Erstellung der Proben für die massenspektrometrischen Experimente erfolgte alleinig durch mich. Die massenspektrometrische Messung und die Generierung der Erstdatensätze wurde ohne meine Mitarbeit in der Proteomics Facility des CECAD Köln durchgeführt und

ihrerseits zur Verfügung gestellt. Die weitere Softwareanalyse der Datensätze mit *Perseus* und *Instant Clue* erfolgte mit der Hilfe von Dr. Julian Nüchel.

Erklärung zur guten wissenschaftlichen Praxis:

Ich erkläre hiermit, dass ich die Ordnung zur Sicherung guter wissenschaftlicher Praxis und zum Umgang mit wissenschaftlichem Fehlverhalten (Amtliche Mitteilung der Universität zu Köln AM 132/2020) der Universität zu Köln gelesen habe und verpflichte mich hiermit, die dort genannten Vorgaben bei allen wissenschaftlichen Tätigkeiten zu beachten und umzusetzen.

Koln, den 15.01.2025	
Unterschrift:	

Danksagung

Ich möchte mich bei Prof. Dr. Silvia von Karstedt bedanken, die eine hervorragende Betreuerin dieser Dissertation war. Ich bewundere ihre unvergleichliche Begeisterung für die Wissenschaft und ihre herausragende Fähigkeit, ihre Studierenden wissenschaftlich zu leiten. Ich möchte mich bei ihr für die Möglichkeit bedanken, diese Dissertation in ihrem Labor durchführen zu können. Außerdem möchte ich meiner Laborkollegin Fatma Isil Yapici danken, die mich während dieser Dissertation sehr unterstützt hat. Sie hat mir wertvolle Ratschläge und Empfehlungen gegeben und war eine große Unterstützung bei diesem Projekt. Mein Dank gilt auch meinen Kollegen und Kolleginnen aus dem von Karstedt-Labor. Insbesondere möchte ich Jenny Stroh danken. Emotionale Unterstützung und Stabilität durfte ich außerdem durch meine Freunde, Freundinnen, meinen Partner und meine Familie erfahren. Ich bin sehr stolz darauf, mit einem so unterstützenden Umfeld gesegnet zu sein.

Table of contents

ABB	REVIATIONS	9
1.	SUMMARY	14
1.1.	Summary in German language	14
1.2.	Summary in English language	14
2.	INTRODUCTION	16
2.1.	Cell Death	16
2.1.	1. Apoptosis	17
	2.1.1.1. Extrinsic pathway	18
	2.1.1.2. Intrinsic pathway	19
2.1.	2. Autophagy	21
2.1.	3. Necrosis	22
	2.1.3.1. Necroptosis	22
	2.1.3.2. Pyroptosis	24
	2.1.3.3. Ferroptosis	26
	2.1.3.3.1. Mechanisms of ferroptosis	26
	2.1.3.3.2. Regulation of ferroptosis	30
2.2.	Inflammation and immune defence	34
2.2.	1. Necroinflammation	36
2.2.	2. Ferroptosis as an immunogenic form of cell death	37
3.	MATERIALS AND METHODS	38
3.1.	Materials	38
3.1.	1. Antibodies	38
3.1.	2. Buffers	38
3.1.	3. Cell culture materials	40
3.1.	4. Cell lines	41
3.1.	.5. Consumable materials and chemicals	41
3.1.	.6. Enzymes and enzyme buffers	44
3.1.	.7. Kits	44
3.1.	.8. Laboratory equipment	44
3.1.		45
3.2.	Methods	45
3.2.	1. Cell culture	45

	3.2.1.	Cultivation and passaging of cells	45
	3.2.1.	2. Cell count measurement	46
	3.2.1.	3. Cryopreservation and thawing	46
	3.2.1.	4. Cell viability assay	46
	3.2.1.	5. Ferroptotic supernatants	47
;	3.2.2.	Nucleic acid techniques	47
	3.2.2.	1. DNA Isolation	47
	3.2.2.	2. RNA Isolation	48
	3.2.2.	3. PCR/Genotyping	48
	3.2.2.	4. Determination of nucleic acid concentration	48
	3.2.2.	5. RNA Sequencing	49
;	3.2.3.	Protein Biochemistry	49
	3.2.3.	1. Protein lysation	49
	3.2.3.	2. Bicinchoninic acid assay and sample preparation	50
	3.2.3.	3. SDS PAGE	50
	3.2.3.	4. Western Blot	51
;	3.2.4.	Quantitative Mass Spectrometry	52
	3.2.4.	1. Cell culture preparation of samples	52
	3.2.4.	2. Enrichment of newly synthesised proteins	52
	3.2.4.	3. Reduction and Alkylation of resin-bound proteins and digestion	53
	3.2.4.	4. Desalting and stage tips	53
	3.2.4.	5. Mass Spectrometry analysis	54
;	3.2.5.	Cytokine Array	54
;	3.2.6.	Flow Cytometry	55
	3.2.6.	1. Analysis of data	56
;	3.2.7.	Mouse work	56
	3.2.7.	1. Mouse model	56
	3.2.7.	2. Histological techniques	56
	3.2	2.7.2.1. Paraffin sectioning	56
	3.2	.7.2.2. H&E staining	57
1.	RES	ULTS	58
1.1	. Ferro	ptosis-inducible systems	58
4	4.1.1.	Validation of a genetic model of ferroptosis induction in vitro	58
•	4.1.2.	Validation of an in vitro model of ferroptosis induction through small molecules	59
1.2	. Chara	acterisation of a ferroptosis-induced secretome	61
4	4.2.1.	Cytokine release in ferroptosis	61
4	4.2.2.	Quantitative secretome analysis	62
1.3	3. lmmı	unological responses of bystander immune cells to ferroptosis	69
4	4.3.1.	Ferroptosis-provoked cytokine release by immune cells	69

4.3.	.2. RNA sequencing analysis of ferroptotically primed immune cells	72
4.4.	Investigation of immunological responses to ferroptosis in vivo	74
5.	DISCUSSION	76
5.1.	Characterisation of a ferroptosis-induced secretome	76
5.2.	Inflammatory responses in bystander immune cells	78
5.3.	The influence of ferroptosis on cancer immunity	80
5.4.	Ferroptosis and inflammation in pathology – in vivo models	81
6.	REFERENCES	83
7.	APPENDIX	97
7.1.	List of Figures	97
7.2.	List of Tables	98
8.	PUBLICATIONS	99

Abbreviations

4-HNE	4-hydroxynonenal
4-Hydroxytamoxifen	4-OHT; tamoxifen
8-hydroxy-2'-	8-OHG
deoxyguanosine	
AA	Arachidonic acid
ACN	Acetonitrile
AdA	Adrenic acid
ACD	Accidental cell death
ACSL4	Long-chain acyl-coenzyme A synthase 4
ADCD	Autophagy-dependent cell death
AHA	Azidohomoalanine
AKI	Acute kidney injury
APAF-1	Apoptotic protease activating factor 1
APC	Antigen-presenting cell
APS	Ammonium persulfate
ARE	Antioxidant response element
ASC	Apoptosis-associated speck-like protein containing a caspase
	recruitment domain
ATM	Ataxia-telangiectasia mutated gene
ATP	Adenosine triphosphate
BAK	Bcl-2 homology antagonist/killer
BAX	Bcl-2 associated X protein
Bcl-2	B-cell lymphoma 2
ВН	Bcl-2 homology
BHT	Butylated hydroxytoluene
BH ₄	Tetrahydrobiopterin
BID	BH3 interacting domain death agonist
Bcl-2 homology	BH3 interacting-domain death agonist
BSO	Buthionine sulfoximine
C11-BODIPY ^{581/591}	Fluorescent dye C11-Boron-dipyrromethene
Capases	Cysteine aspartic proteases
CARD	Caspase recruitment domain
CBS	Cystathionine beta-synthase
CD	Cluster of differentiation

cGAS	Cyclic guanosine monophosphate—adenosine monophosphate
	synthase
CMA	Chaperon-mediated autophagy
CoA	Coenzyme A
CrmA	Cytokine response modifier A
СТВ	Cell Titer Blue
CXCL-2 (-11)	C-X-C motif chemokine 2 (-11)
Ctr	Control condition
c-FLIP	FLICE (FADD-like IL-1β-converting enzyme)-like inhibitory protein
DAI	DNA-dependent activator of IFN regulatory factors
DAMP	Damage-associated molecular patterns
DHODH	Dihydroorotate dehydrogenase
DIABLO	Direct IAP binding protein with low PI
DISC	Death-inducing signaling complex
DMSO	Dimethyl sulfoxide
DMT1	Divalent metal transporter 1
DNA	Deoxyribonucleic acid
DR	Death receptor
DTT	Dithiothreitol
Erastin	Eradicator of RAS and ST-expressing cells
ESCRT	Endosomal sorting complexes required for transport
FA	Formic acid
FACS	Fluorescent activated cell sorting
FADD	Fas-associated death domain protein
FADH	Flavine adenine dinucleotide
FASR	Fas cell surface death receptor
FCS	Fetal calf serum
FINO ₂	Ferroptosis inducer endoperoxide
Fer-1	Ferrostatin-1
FIN56	Ferroptosis inducer 56
FITC	Fluorescein isothiocyanate
FPKM	Fragments per kilobase of transcript per million mapped reads
FSC	Forward-scattered light
FSP1	Ferroptosis suppressor protein 1
GCH1	GTP cyclohydrolase 1
GCL	Glutamate-cysteine ligase

GO	Gene Ontology
GPX4	Glutathione peroxidase 4
GR	Glutathione reductase
GSDMD	Gasdermin D
GSH	Reduced glutathione
GSS	Glutathione synthetase
GSSG	Oxidised glutathione
H&E	Hematoxylin and eosin
HETE	5-hydroxyeicosatetraenoic acid
HMGB1	High mobility group protein B1
HPETE	Hydroperoxyeicosatetraenoic acid
HRP	Horseradish peroxidase
HSPA 5	Heat shock 70 kDa protein 5
HSPB1	Heat shock protein beta-1
IAP	Inhibitors of apoptosis
iBMDM	Immortalised bone marrow derived macrophages
ICAD	Inhibitor of caspase-activated deoxyribonuclease
ICD	Immunogenic cell death
IKBKE	Inhibitor of nuclear factor kappa-B kinase subunit epsilon
IKK	Inhibitor of nuclear factor kappa-B kinase epsilon
IFN	Interferon
IL1ra	Interleukin-1 receptor antagonist protein
IL-6	Interleukin 6
IL-8	Interleukin 8
IL-1beta	Interleukin 1 beta
IL-18	Interleukin 18
IL-33	Interleukin-33
IREB2	Iron response element binding protein 2
IRI	Ischaemia/reperfusion injury
IRP1/2	Iron regulatory proteins 1 and 2
KEAP1	Kelch-like ECH-associated protein 1
КО	Knock out
KRAS	Kirsten rat sarcoma viral oncogene homologue
LAMP2A	Lysosomal receptor lysosomal associated membrane protein 2A
LDCD	Lysosome-dependent cell death
LIP	Labile iron pool

LOX	Lipoxygenase
LPCAT3	Lysophosphatidylcholine acyltransferase 3
LPS	Lipopolysaccharide
L-ROS	Lipid reactive oxygen species
MCP-1	Monocyte chemoattractant protein-1
MEF	Mouse embryonic fibroblast
MHC-receptor	Major histocompatibility complex
ΜΙΡ1α	Macrophage inflammatory protein 1α
ML162	Molecular Libraries 162
MLKL	Mixed lineage kinase domain-like pseudokinase
MOMP	Mitochondrial outer membrane permeabilization
MPT	Mitochondrial permeability transition
MS	Mass spectrometry
NADH	Nicotinamide adenine dinucleotide
NADPH	Nicotinamide adenine dinucleotide phosphate
NCOA4	Nuclear receptor coactivator 4
Nec-1	Necrostatin-1
NF-kB	Nuclear factor kappa B
NLR	Nucleotide-binding domain and leucine-rich repeat containing gene
	family receptors (also referred to NOD-like receptors)
NLRC4	NLR Family CARD Domain Containing 4
NLRP1	NLR family pyrin domain containing 1
NLRP3	NLR family pyrin domain containing 3
NOX	NADPH oxidases
NOXA	phorbol-12-myristate-13-acetate-induced protein 1
NRF2	Nuclear factor erythroid 2-related factor
NSCLC	Non-small cell lung cancer
OXPHOS	Oxidative phosphorylation
PAGE	Polyacrylamide gel electrophoresis
PAMP	pathogen-associated molecular pattern
PDAC	Pancreatic ductal adenocarcinoma
PDX-1	Pancreatic and Duodenal Homeobox 1
PE	Phosphatidylethanolamine
PFA	Paraformaldehyd
PGE2	Prostaglandin E2
PGH2	Prostaglandin endoperoxide H2

PIK3C3C Phosphatidylinositol 3-Kinase Catalytic Subunit Type PL Glycerophospholipids PMA Phorbol 12-myristate-13-acetate PPR Pattern recognition receptor	pe 3
PMA Phorbol 12-myristate-13-acetate	
PPR Pattern recognition receptor	
PtdIns3P Phosphatidylinositol-3-phosphate	
PTGES3 Prostaglandin E synthase 3	
PUFA Polyunsaturated fatty acid	
PUMA p53 upregulated modulator of apoptosis	
RAGE Receptor for advanced glycation end-products	
RCD Regulated cell death	
RHIM domains RIP homotypic interaction motif domains	
RIPK1 Serine/threonine-protein kinase 1	
RIPK3 Serine/threonine-protein kinase 3	
ROS Reactive oxygen species	
RPKM Reads per kilo base of transcript per million mappe	d reads
RSL3 Ras-selective lethal 3	
SDS Sodium dodecyl sulfate	
SILAC Stable isotope labelling in cell culture	
SLC3A1 Solute carrier family 3 member 1	
SLC7A11 Solute carrier family 7 member 11	
SMAC Second mitochondria-derived activator of caspases	3
sMAF Small musculoaponeurotic fibrosarcoma	
SN Supernatant	
SOD Superoxide dismutase	
SSC Side-scattered light	
STEAP3 Six transmembrane epithelial antigen of prostate 3	
STING Stimulator of interferone genes	
STRING Search Tool for the Retrieval of Interacting Genes/F	Proteins
TCA cycle Tricarboxylic acid cycle	
TCR T-cell receptor	
TEMED Tetramethylethylenediamine	
TFRC Transferrin receptor	
TGFα Transforming growth factor α	
Th(1) T helper cells (1)	
TLR Toll-like receptor	

TLR4	Toll-like receptor 4
TNF	Tumor necrosis factor
TNFR	Tumor necrosis factor receptor
TNFR1	TNF receptor superfamily member 1A
TRADD	TNFR1-associated death domain protein
TRAIL	TNF-related apoptosis-inducing ligand
TRIF	Toll/interleukin-1 receptor domain-containing adaptor protein
	inducing interferon-β
ULK1	Unc-51 like kinase-1
UPW	Ultrapure water
VCAM	Vascular cell adhesion molecule 1
VEGF	Vascular Endothelial Growth Factor
WT	Wild type
XIAP	X-linked inhibitor of apoptosis
ZBP1	Z-DNA-binding protein
zVAD-fmk	Carbobenzoxy-valyl-alanyl-aspartyl-[O-methyl]-fluoromethylketone

1. Summary

1.1. Summary in German language

Der Verlust der Integrität der zellulären Plasmamembran im Rahmen verschiedener Zelltodmechanismen führt zur Freisetzung zytosolischen Inhalts in das umliegende Gewebe¹. Diese intrazellulären Überreste können als schadenassoziierte molekulare Muster (DAMPs) Mustererkennungsrezeptoren (PRRs) auf angeborenen Immunzellen aktivieren². Nekrotische Zelltodmechanismen werden daher als immunogene Formen des Zelltods angesehen. In der Zelltodforschung wurde in den letzten Jahren der Prozess der Nekroinflammation untersucht, welcher einen Zelltod beschreibt infolgedessen endogene zelluläre Proteine durch regulierte Nekrose freigesetzt werden und Entzündungsreaktionen verursachen².

Ferroptose ist eine kürzlich entdeckte Form der regulierten Nekrose³. Es wurde gezeigt, dass Ferroptose in pathologischen Vorgängen, wie beispielsweise Ischämie/Reperfusionsschäden (IRI)⁴, eine immunogene Form des Zelltods darstellt². Eine genaue Charakterisierung entzündlicher ferroptotischer Signalwege konnte jedoch bisher noch nicht erfolgen. Es scheint von großer Wichtigkeit diesen Zelltodweg genau zu verstehen und sein immunogenes Potenzial näher zu beschreiben. In diesem Projekt wird das Sekretom, das durch den Zusammenbruch der Plamamembran während Ferroptose in die Zellumgebung freigesetzt wird, untersucht und charakterisiert. Außerdem werden Zytokinantworten von Makrophagen, die durch ferroptotische Überstände stimuliert werden können, durch RNA-Sequenzierung und Enzym-gekoppelte Immunadsorptionsassays analysiert und quantifiziert.

1.2. Summary in English language

During tissue homeostasis-associated cell death, the loss of cellular plasma membrane integrity can result in the exposure of the cytosolic content to the surrounding tissue, a distinguishing feature of necrotic cell death pathways¹. These cytosolic remnants can function as damage-associated molecular patterns (DAMPs) and activate pattern recognition receptors (PRRs) on innate immune cells². Necrotic forms of cell death are therefore considered to be immunogenic forms of cell death, and the process wherein non-pathogen associated endogenous cellular proteins released through regulated necrosis cause inflammation has therefore been termed necroinflammation². Ferroptosis is a recently discovered form of regulated necrosis^{2,3}. Although ferroptosis has been proposed to represent an immunogenic form of cell death in a few pathologies, such as ischaemia/reperfusion injury (IRI)⁴, it remains poorly understood as to how exactly such an inflammatory ferroptotic signaling pathway might be carried out¹. However, it will be important to understand this cell death pathway and how it

might trigger inflammation in order to either interfere with it for the prevention of tissue damage during IRI or to specifically enhance it for harnessing an anti-tumour immune response. In this project, a secretome released into the cellular environment upon ferroptotic plasma membrane rupture will be investigated through mass spectrometry. Furthermore, this thesis aims to characterise and quantify cytokine responses of macrophages stimulated by ferroptotic supernatants through RNA-sequencing and enzyme-linked immunoabsorbant assays.

2. Introduction

2.1. Cell Death

A well-maintained equilibrium of cell survival, newly generated cells, and cell death is the foundation for the precisely maintained tissue homeostasis of living organisms. Approximately 10¹¹ damaged or unrequired cells are replaced each day by newly generated cells via mitosis in an adult human body keeping the equilibrium of biosynthesis and decomposition intact⁵. The imperative nature of cell death becomes further apparent when we look at the plethora of infections and human pathologies linked to either the stimulation or inhibition of cell death⁶. Neurodegenerative diseases can cause an augmented rate of abnormal cell death, whereas mutations in the cell cycle machinery have the power to prevent cell death, thereby causing cancerous growths^{7,8}. This highlights that both, excessive as well as decreased cell death rates can be pathological.

Although the first report of cell death dates back to 1842 when Carl Vogt studied the metamorphosis of amphibia9, it was not until a century later that the concept of physiological cell death became apparent. In the 1960s, the observation that cell death follows a biological plan^{10,11} and requires protein synthesis laid the groundwork for understanding cell death as a predetermined event in the development of organisms^{12,13}. Importantly, the distinction between a controlled, programmed cell death and an uncontrolled cell death referred to as necrosis, was made thereafter by Kerr and colleagues in the 1970s following their study of cell death morphologies^{14,15}. Apoptosis was for a long time considered to be the standard form of cell death. It is morphologically characterised by organelle and cellular shrinkage as well as membrane blebbing. It results in the formation of apoptotic bodies that are digested by phagocytes^{16,17}, thereby preventing cellular lysis and the release of intracellular content into the surrounding interstitial tissue. In the absence of potentially intracellular inflammatory or alarming substances, apoptosis was long considered a type of non-inflammatory cell death 18,19. In contrast, necrosis was described as a form of unregulated, accidental cell death that follows physiochemical insults²⁰ as well as trauma²¹. It results in the leakage of cellular content into the surroundings and is therefore considered an immunogenic form of cell death²¹. However, the elucidation of several novel cell death pathways that exhibit regulated forms of necrosis has challenged this rigid categorisation of regulated and unregulated cell death and has set the focus of cell death research on the physiology and the mechanisms of signalling pathways²⁰. The identification of a wide set of genetically encoded cell death mechanisms with differences in the execution and initiation of cell death^{22,23} has broadened the field and invited

researchers to further elucidate interconnecting networks between these individual cell death pathways (Figure 1).

The research of the past decades has shaped the current consensus on the classification of cell death into three different categories: I. cell death associated with heterophagy (I. apoptosis), II. cell death associated with eating of itself (II. autophagy) and III. cell death that does not involve digestion and is distinct from types I and II.^{23,24,25}.

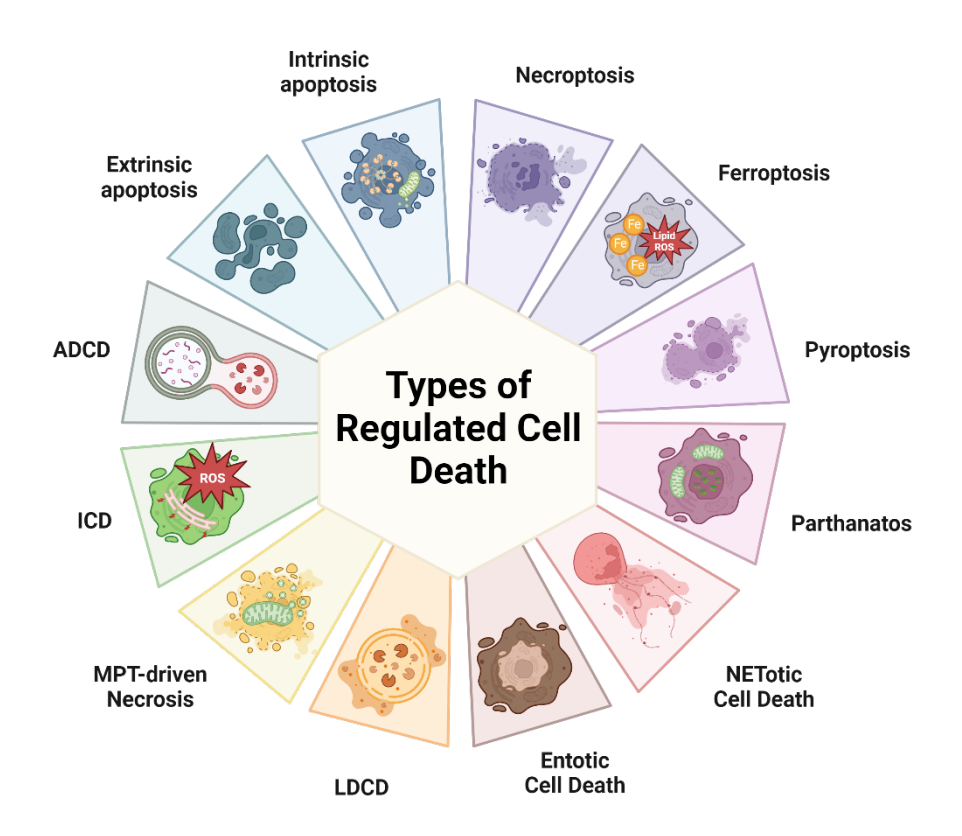


Figure 1. Major forms of cell death.

Depicted is a multitude of the most essential cell death subroutines uncovered in cell death research varying from autophagy-dependent cell death and apoptosis to different forms of regulated necrosis. Categorised into one group are also forms of cell death that converge on a common shared principle of death, such as immunogenic cell death (ICD). ADCD: Autophagy-dependent cell death, LDCD: lysosome-dependent cell death, MPT: mitochondrial permeability transition. Adapted from Galluzzi et al. 2018²³. The figure has been created using Biorender.

2.1.1. Apoptosis

Apoptosis is an evolutionarily conserved process that is indispensable for embryonic development, ageing and tissue homeostasis. This type of programmed cell death is not only critical for a functioning, quotidian cell turnover and equilibrated tissue renewal in the human body²⁶, it also exerts an important role as part of immune reactions against pathogens and noxious agents²⁷. Unlike necrosis, apoptosis depends on the availability of intracellular adenosine triphosphate (ATP) as well as cysteine aspartic proteases (caspases)^{28,29}.

Caspases can activate target molecules in a cleavage reaction that requires cysteine residues to be present in the caspase active site. These endoproteases feature one of the hallmarks of apoptosis^{26,30} and can functionally be clustered into initiator caspases (caspase 8, -9) and executioner caspases (caspase-3, -6, -7). Mechanistically, initiator caspases activate other caspases, whilst executioner caspases are crucial in the characteristic apoptotic breakdown of cells³¹. Although necrosis and apoptosis share a common biochemical network³², apoptosis is morphologically and mechanistically distinguishable¹⁴. Cells that succumb to apoptosis exhibit cell shrinkage, characterised by a dense cytoplasm and tightly packed organelles, plasma membrane blebbing, and condensed chromatin^{15,33,34}. Pyknosis, characterised by nuclear shrinkage, is followed by pyknotic nuclei membrane rupture and subsequent nuclear fragmentation known as karyorrhexis^{14,15}. Accordingly, dense purple nuclear chromatin fragments as well as dark eosinophilic cytoplasm become visible in histological H&E stainings of rounded, apoptotic cells²⁶. The prevailing notion of apoptosis as a type of immunologically silent cell death traces back to the fact that apoptosis results in the formation of apoptotic bodies. Cells that undergo apoptosis show loss of cell viability, while their plasma membranes remain intact, and express cell surface markers for phagocytic recognition by adjacent cells³⁵ 37

The initiation of apoptosis can either be triggered through an extrinsic signal in a transmembrane receptor-mediated fashion³⁸ or by the cell itself via intracellular receptors detecting damage⁶. These two pathways are interconnected³⁸ and ultimately converge on a last common pathway²⁶.

2.1.1.1. Extrinsic pathway

The extrinsic pathway of apoptosis is induced through an interaction between death receptors of the tumor necrosis factor receptor (TNFR) gene superfamily and death ligands $^{39-41}$. When natural killer cells or macrophages release death ligands such as FasL, tumor necrosis factor (TNF) - α or TNF-related apoptosis-inducing ligand (TRAIL), they bind to their corresponding death receptors (DRs) at the cellular membrane 40,42,43 . This receptor-ligand interaction initiates the formation of a death-inducing signalling complex (DISC) 44,45 on the cytoplasmic death domain of the ligand-bound DR, as well as the recruitment of monomeric procaspase 8 to the DISC 46 . The recruited cytoplasmic adaptor proteins fas-associated death domain (FADD) or TNFR1-associated death domain protein (TRADD) 47,48 facilitate the dimerisation of the death effector domain and activation of monomeric procaspase-8 to caspase-8 47,48 . The activation of procaspase-8, however, can be blocked at the DISC by the anti-apoptotic FLICE (FADD-like IL-1 β -converting enzyme)-inhibitory protein (c-FLIP) 44 .

Two distinct sub-pathways downstream of the Fas (cluster of differentiation 95 (CD95)/APO-1) pathway have been described. Which of two pathways is carried out is determined by the cell itself, following the type I/II concept⁴⁹. In this respect, executioner caspases are cleaved directly by sufficiently activated caspase 8 in type I cells⁵⁰. Alternatively, when effector caspase activation is blocked by high expression of x-linked inhibitor of apoptosis (XIAP)⁵⁰, caspase-8 cleaves BH3 interacting domain death agonist (BID) in type II cells⁵⁰. This results in the onset of the execution pathway by truncated BID (tBID) through the release of pro-apoptotic factors including second mitochondria-derived activator of caspases (SMAC)/direct IAP binding protein with low PI (DIABLO), which neutralises XIAP from mitochondria⁵¹. In this case, the caspase cascade is enforced via the mitochondrium⁵².

2.1.1.2. Intrinsic pathway

This non-receptor-mediated pathway is triggered by intracellular signals that can be of a positive or negative nature. Whereas positive signals include radiation, toxins, hyperthermia and viral infections that induce apoptosis⁵³, negative signals provoke failed apoptotic suppression thereby promoting pro-apoptotic molecules, such as p53 upregulated modulator of apoptosis (Puma), Bcl-2 associated X protein (Bax), and phorbol-12-myristate-13-acetateinduced protein 1 (Noxa)²⁶. Mitochondria-mediated apoptosis is regulated by the Bcl-2 family⁵⁴. These proteins are clustered into three different groups: proapoptotic BH3-only members; proapoptotic effector molecules, namely Bax and Bcl-2 homology antagonist/killer (Bak); and antiapoptotic Bcl-2 family proteins⁵⁵. Whereas BH3-only members promote the activation of Bax and Bak, they antagonise antiapoptotic proteins. In the event of a stimulus, mitochondrial permeability transition pores (MPTs) are opened, and Bax and Bak initiate the mitochondrial outer membrane permeabilisation (MOMP), representing the point of no return in the intrinsic pathway of apoptosis⁵⁶. MOMP leads to the release of proapoptotic proteins such as cytochrome c and SMAC/DIABLO⁵⁷⁻⁶⁰ from the mitochondrial intermembrane space into the cytosol⁶¹. While SMAC/DIABLO promote apoptosis by blocking inhibitors of apoptosis (IAP)⁶², cytochrome c binds to apoptotic protease activating factor 1 (Apaf1) monomers⁶². This mechanism initiates a conformational change of the molecule that in turn enables the chemical bond between deoxy ATP (dATP) and the oligomerisation domain of Apaf1⁶³. The exposure of its oligomerisation domains and its caspase recruitment domain (CARD) ultimately results in the recruitment of multiple Apaf-1 molecules and procaspase-9 proteins, causing the formation of an active heptameric complex called the apoptosome⁶⁴. Procaspase-9 is cleaved autocatalytically into its active form caspase-9 which in turn induces the execution pathway by activating the executioner procaspase-3⁶⁵.

The process of apoptotic cell death results in a final step that is characterised by the degradation of nuclear material and cytoskeletal proteins, DNA fragmentation, and the formation of apoptotic bodies²³. Both the intrinsic and extrinsic pathways lead to a final execution pathway that starts with the activation of executioner caspases 3, 6 and 7 through active initiator caspases (caspase-8 and -9). The process of degradation is carried out by endonucleases and proteases that are activated by the aforementioned executioner caspases²⁶. Caspase-3 cleaves the inhibitor of caspase-activated deoxyribonuclease (ICAD), resulting in its activation. Subsequently, CAD degrades inter-nucleosomal DNA and causes DNA fragmentation⁶⁶. The appearance of phosphatidylserine on the outer membrane as well as phospholipid asymmetry of apoptotic cells signal surrounding cells to prepare for phagocytosis⁶⁷.

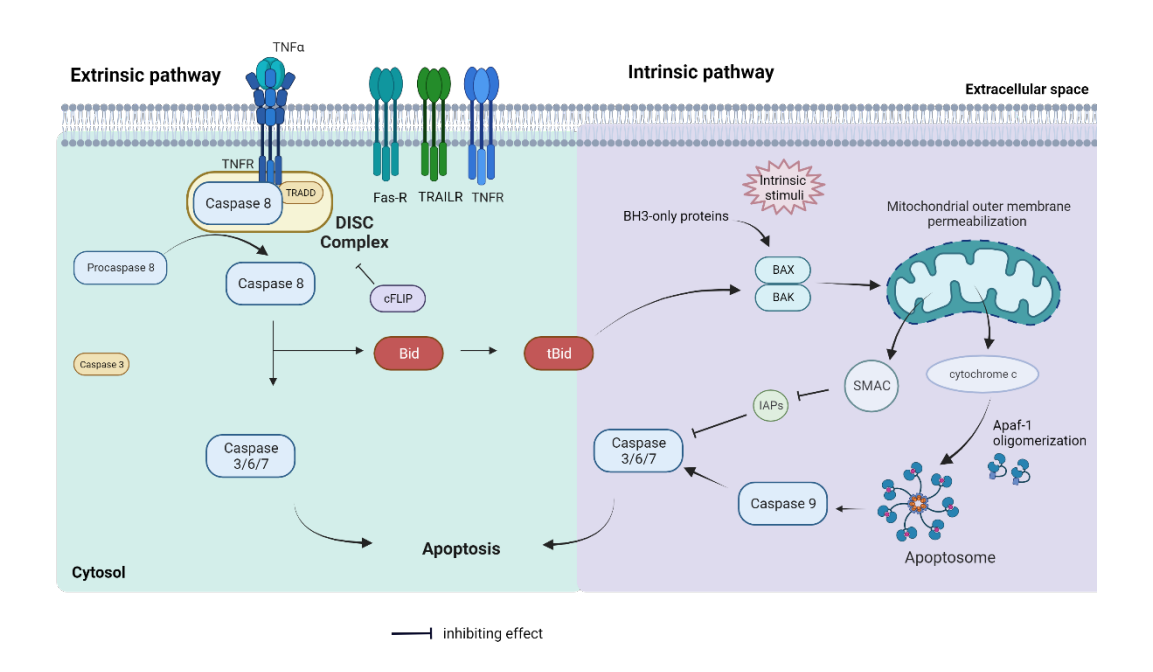


Figure 2. The extrinsic and intrinsic pathway of apoptosis.

Extrinsic apoptosis can be triggered by death ligands interacting with their corresponding death receptors, such as Fas-R, TRAILR and TNFR on the cellular plasma membrane. When TNF- α binds to the TNF-receptor, TRADD as well as procaspase-8 will be recruited to form a death-inducing signal complex (DISC). As a result, caspase-8 is cleaved into its active form and will in turn activate executioner caspases 3, 6 and 7. The activation of procaspase-8 can be blocked by c-FLIP. Alternatively, apoptosis can be induced by intrinsic signals. The proapoptotic effector molecules Bax and Bak will prompt membrane permeabilisation of the mitochondria. This leads to the release of cytochrome c and to the subsequent Apaf-1-mediated formation of an apoptosome. Procaspase-9 is activated and will cleave executioner caspases 3, 6 and 7. Concomitantly, proapoptotic proteins, such as Smac will prevent the inhibition of the executioner caspases by IAPs leading to apoptosis. Adapted from Elmore et al. 2007²⁶. The figure has been created using Biorender.

2.1.2. Autophagy

The catabolic process by which a cell can eat and digest itself was termed autophagy by the discoverer of lysosomes, Christian De Duve⁶⁸. Autophagy-dependent cell death constitutes type II of the three major forms of cell death²³. According to the Nomenclature Committee on Cell Death, it is a type of regulated cell death (RCD) that depends on the autophagic machinery²³. Conversely, morphological characteristics of autophagic cell death, such as accumulating autophagosomes in dying cells, can also be interpreted as a cell survival strategy⁶⁹. In this context, autophagy has been shown to be of great importance for the maintenance of cell homeostasis, as it rids the body of old cell debris and recycles biochemicals for the biosynthesis of new cellular structures or organelles⁷⁰. Autophagy is initiated in response to stressors and triggering factors, such as infectious pathogens or nutrient deprivation, and protects cellular maintenance through lysosomal degradation of intracellular cargo^{71,72}. Though the term autophagy is frequently used as a synonym for macroautophagy, the distinction between macroautophagy, microautophagy and chaperon-mediated autophagy (CMA)⁷³ should be considered when discussing its mechanistic profile.

Macroautophagy features the formation of double-membrane vesicles, known as autophagosomes, that digest large portions of cellular content. The initiation of this process is mediated by the unc-51 like kinase-1 (ULK1) complex that induces the generation of a phagophore⁷⁴. This process occurs at the requirement of class III phosphatidylinositol 3-kinase (Phosphatidylinositol 3-Kinase Catalytic Subunit Type 3 (PIK3C3C) in humans) which can synthesise the phospholipid phosphatidylinositol-3-phosphate (PtdIns3P) due to its heterotetrameric core (PIK3C3 complex I)⁷⁵. After the phagophore has expanded and closed, an autophagosome is formed in a subsequent step. Cell components that are destined for degradation become engulfed by the autophagosome and are ultimately digested after fusion with lysosomes to form an autophagolysosome⁷⁶. The degrading process is performed by lysosomal hydrolytic enzymes within the lumen⁷⁷. In contrast, microautophagy describes the digestion of specific damaged organelles that present conformant signalling molecules on the organelle surface to be recognised by various macroautophagic pathways. This process requires the fusion of lysosomes with determined organelles. The resulting autophagic vesicles are named after the engulfed organelle - for example, mitophagy for mitochondrial autophagy or micropexophagy for peroxisomal degradation. The aim of microautophagy is therefore cell survival⁷⁸.

CMA on the contrary is a receptor-mediated pathway and does not require vesicular trafficking. The engagement of a cytosolic chaperone with a biologically marked substrate is constitutive for this type of autophagic pathway. After the targeted protein is delivered to the lysosome, it

binds to the lysosomal receptor lysosomal associated membrane protein 2A (LAMP2A) and is ultimately transported into the lysosome for degradation⁷⁹.

While autophagy is known to occur concurrently with multiple forms of cell death, it has been shown to activate signalling pathways of other types of cell death, inter alia, ferroptosis⁸⁰. Ferritinophagy, a type of selective autophagy, is the process by which intracellular ferritin, an iron storage protein, is degraded⁸¹. This process results in an increased concentration of free iron within the cell, which in turn promotes ferroptosis⁷⁴. Autophagy-dependent ferroptosis is an applicable example of the interconnection of different types of cell death and underlines the complexity of cell death research.

2.1.3. Necrosis

Historically, necrosis was viewed as a form of accidental cell death, constituting an immediate and uncontrollable cellular demise in response to external forces, such as trauma, toxins, high pressure, temperature change, osmotic forces, or pH variations^{23,82}. It was described as an energy-independent form of cell death that can occur in the absence of ATP, ultimately resulting in the disruption of the biomembrane and lysis of the cell. However, the scientific community revised this idea of necrotic cell death as merely uncontrollable and introduced the concept of regulated necrosis as a class of newly discovered biochemical cell death pathways^{23,83}. Nevertheless, the umbrella term necrosis persists for all unregulated types of necrosis. Types of regulated necrosis include necroptosis, pyroptosis, ferroptosis, parthanatos, and NETosis⁸⁴. In this context, RCD, unlike accidental cell death, has emerged as a type of genetically controlled form of cell death that is governed by prescribed molecular machineries and pathways^{23,74}. At a stage where cellular adaptive responses and the cell's capacity to resist external disruptive signals are exhausted, the cell will commence a finely attuned molecular program of death⁸². Additionally, RCD is tightly regulated and can be modulated through genetic alterations or drugs targeting key substances⁷⁴. Morphologically, necrosis is associated with significant disruption of cellular organelles that encompass organelle rupture, distension and swelling^{14,85}. In the following, the different forms of regulated necrosis and their corresponding molecular pathways will be delineated.

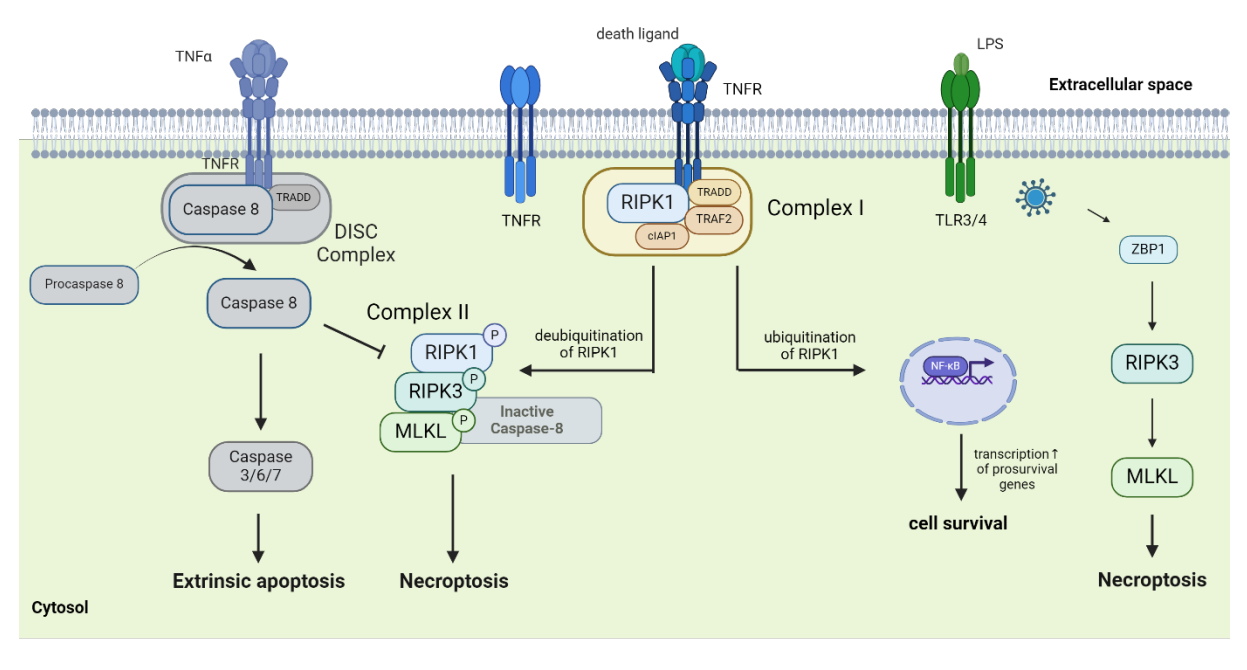
2.1.3.1. Necroptosis

Necroptosis is an inflammatory mode of cell death that is highly regulated by a genetically encoded predefined cell death machinery⁸⁶. It shares common characteristics with both, apoptosis and necrosis. Although necroptosis is a programmed form of cell death like

apoptosis, it results in the loss of metabolic function and loss of plasma membrane integrity which represent important features of necrotic cell death⁸⁶. Upon caspase-8 inhibition, necroptosis can be executed as an alternative death-signalling pathway to apoptosis⁸⁶. It is further performed in a caspase-independent manner and depends on protein phosphorylation rather than cleavage. Importantly, receptor-interacting serine/threonine-protein kinase 1 (RIPK1) and receptor-interacting serine/threonine-protein kinase 3 (RIPK3) are key players in the execution of necroptosis^{86,87}.

Necroptosis is thought to be a part of the mechanisms of the innate immune system to fend off pathogens, particularly in the context of viral infection which antagonises caspase-8 activity through expression of the viral protein cytokine response modifier A (CrmA)88,89. On a molecular level, it can be triggered by the interaction of death ligands with corresponding PRRs, such as toll-like receptor families (TLR), or death receptors, such as TNFR189. After TNFR1 stimulation, the cell can either commence a nuclear factor kappa B (NF-kB)-mediated pathway for cell survival or follow a signalling pathway resulting in apoptotic or necroptotic cell death⁸⁷. TNFR1 recruits TRADD protein and RIPK1 as well as various other signalling components to its cytosolic death domain forming complex I⁸⁹. In the case of necroptosis, inhibition of caspase-8 activity hinders apoptosis and leads to activation of RIPK1 through deubiquitination and the engagement of RIPK3⁸⁶. This process results in the ultimate formation of a high molecular weight complex, termed necrosome^{87,89}. In a crucial subsequent step, mixed lineage kinase domain-like pseudokinase (MLKL) is phosphorylated by RIPK3 and results in its oligomerisation and translocation to the plasma membrane via Golgi-microtubuleactin-dependent mechanisms 90,91. It was shown that MLKL activation during necroptosis is associated with the permeabilisation of the membrane and the consequent leakage of the intracellular content⁸⁹. Hence, necroptosis represents a lytic type of cell death that can lead to secondary inflammatory responses⁸⁹.

Alternatively, necroptosis can also be mediated by Z-DNA-binding protein (ZBP1)⁹². This protein consists of multiple binding domains⁹². Its N-terminal Z-DNA-binding domains function as sensors of nucleic acids, whereas its RIP homotypic interaction motif domains (RHIM domains) trigger necroptotic cell death signalling by recruiting RIPK3^{92,93}. As a result, RIPK3 autophosphorylation is once again induced and further results in the downstream signalling of necroptosis. Interestingly, the signalling domain of ZBP1 will activate type I Interferon (IFN) synthesis⁹⁴. ZBP1 has been described as an interferon (IFN)-inducing protein and will lead to the activation of the innate immune system. Together, ZBP1 can induce necroptosis in response to pathogen-associated molecular pattern (PAMP) and DAMP exposure and elicit an inflammatory response⁹².



- inhibiting effect

Figure 3. Pathways of necroptosis.

The inhibition of caspase-8 causes the execution of necroptosis instead of apoptosis. When death ligands, such as TNF bond to PRRs located on the plasma membrane, TRADD protein, RIPK1 and other signalling components are recruited to form complex I. RIPK1 activation results further in the recruitment and activation of RIPK3 and ultimately in the subsequent phosphorylation of MLKL (complex II). MLKL is thought to permeabilise the membrane leading to necroptotic cell lysis. Alternatively, necroptosis can be triggered by ZBP1, which is a sensor of nucleic acids. Upon activation, RIPK3 autophosphorylation is initiated and necroptosis is executed. In a non-lethal setting, the NF-kB-mediated pathway for cell survival is carried out instead of necroptosis. Adapted from Dai et al. 2021⁸⁷. The figure has been created using Biorender.

2.1.3.2. Pyroptosis

Pyroptosis is a type of regulated caspase-dependent cell death that occurs in response to pathogen infection⁹⁵. It constitutes a form of lytic cell death that is characterised by the release of the cellular content through plasma cell membrane pores formed by the pyroptosis executioner gasdermin D (GSDMD)⁹⁵. Although multiple research labs had observed pyroptotic cell death before the millennium, the term pyroptosis was only coined in 2001 by D'Souza and colleagues⁹⁶. It stems from the Greek words pyro (fire/fever) and to-sis (falling) which hints at its potential to trigger inflammation following cell death^{96,97}.

The signalling pathways of pyroptosis can be clustered into two groups: canonical and non-canonical pathways⁹⁵. Constitutively, canonical pyroptotic death involves the assembly of an inflammasome and the subsequent cleavage of caspase-substrate GSDMD⁹⁵. This pathway can be triggered by PAMPs, generally found in microbes, as well as DAMPs that are host-derived signals in response to stress or unbalanced tissue homeostasis⁹⁸. PAMPs and DAMPs can be recognised by PRRs located on the cellular membrane and cytosol to initiate the

formation of a multimolecular complex, the so-called inflammasome^{97,98}. It consists of three major components: a cytosolic sensor, such as Nod-like receptors (NLRs), the adaptor protein apoptosis-associated speck-like protein containing a caspase recruitment domain (ASC), and procaspase-1⁹⁹. Specifically, NLR family pyrin domain containing 1 (NLRP1), NLRP3, as well as NLR Family CARD Domain Containing 4 (NLRC4) are known to assemble inflammasomes¹⁰⁰. Subsequently, procaspase-1 is cleaved into mature caspase-1 which in its activated form cleaves executor protein GSDMD at the ASP 275 site 97,100. GSDMD, as part of the gasdermin superfamily, is a conserved protein⁹⁷. Upon cleavage, the N-terminal poreforming domain of GSDMD perforates the cell membrane and forms nonselective pores resulting in pyroptotic cell death⁹⁷. Interestingly, caspase-1 is not only crucial for the cleavage of GSDMD but can also cleave proinflammatory cytokines pro-IL-1beta and pro-IL-18. As a result of cell membrane perforation during pyroptosis, mature IL-1beta and IL-18 are released 97,101. Concomitantly, water enters the cell leading to cell swelling and osmotic lysis during pyroptosis¹⁰². In the non-canonical pathway, GSDMD can be processed by caspase-4/11 or caspase-5 which are activated by cytosolic lipopolysaccharide (LPS), also resulting in pyroptosis 97,103. Although pyroptosis shares common characteristics with apoptosis, such as DNA damage, nuclear condensation and caspase activity, it is important to acknowledge pyroptosis as a highly distinct form of immunogenic and regulated cell death with a high potential for inflammatory processes following plasma membrane leakage and the release of proinflammatory cytokines^{14,97}.

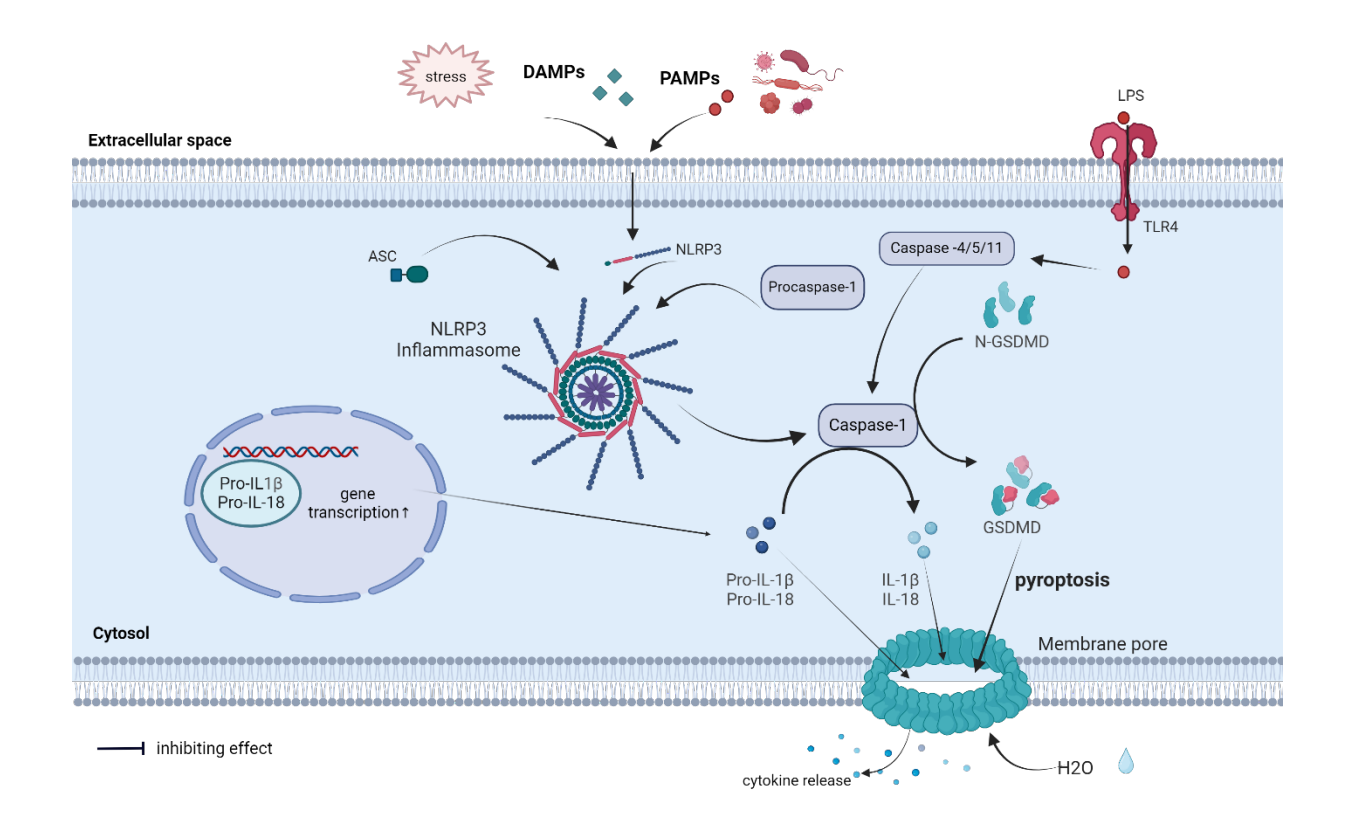


Figure 4. GSDMD-mediated pyroptosis.

Pyroptosis can be induced by PAMPs and DAMPs that are detected by PRRs located on cellular membranes and in the cytosol, initiating the assembly of a multi-molecular complex known as the inflammasome. This complex comprises three key components: a cytosolic sensor such as NLRs, ASC and procaspase-1. Following assembly, procaspase-1 is activated into mature caspase-1, which subsequently cleaves the executor protein GSDMD. This results in the formation of membrane pores leading to cell swelling and rupture. Caspase-1 can also process proinflammatory cytokines pro-IL-1beta and pro-IL-18. The perforation of the cell membrane during pyroptosis results in the release of pro-inflammatory cytokines and cellular contents. In the non-canonical pathway, GSDMD can undergo processing by caspase-4/11 or caspase-5, both of which are activated by cytosolic lipopolysaccharide, ultimately leading to pyroptosis. Adapted from Yu et al. 2021⁹⁷. The figure has been created using Biorender.

2.1.3.3. Ferroptosis

In the process of finding chemical compounds to selectively kill Kirsten rat sarcoma viral oncogene homologue (KRAS) mutant cells in non-small cell lung cancer (NSCLC) research, a new form of cell death, termed ferroptosis, was serendipitously identified and first named in 2012 by Brent R. Stockwell and colleagues in Cell¹⁰⁴. In recent years, this new form of nonapoptotic, iron-dependent regulated type of cell death has been shown to be distinguishable from other well-described forms of cell death, such as apoptosis and autophagy, and has become of particular interest in cell death research due to its unique pathway features 105. Ferroptosis is biochemically, morphologically and genetically to be differentiated from other types of regulated necrosis 106. In contrast to apoptosis and necroptosis, ferroptosis is characterised by its independence of caspases. The harmful impact on a cell preceding ferroptotic cell death is caused by the production of free lipid radicals, called lipid reactive oxygen species (L-ROS)^{105,107}. Biochemically, radicals are unstable chemical substances that contain unpaired electrons, rendering them highly reactive in their requirement for more molecular stability. Highly reactive radicals commonly attack nonradical chemical structures, thereby imposing immense oxidative stress on cells and launching a free radical chain reaction 108. In the context of ferroptosis, iron-dependent production of lipid peroxides upon lipid peroxidation, as a prominent example of a free radical chain reaction, are key events that drive ferroptotic cell death¹⁰⁷. Furthermore, the collapse of an antioxidant defence system displays a crucial moment in the execution of ferroptosis as it marks a turning point where cells ultimately fail to withstand oxidative stress and commence a cellular death pathway¹⁰⁷. Medically, research on oxidative stress and how it causes cell death appears to be indispensable when acknowledging its important role in tissue damage and a plethora of human pathologies 109.

2.1.3.3.1. Mechanisms of ferroptosis

The execution of ferroptosis is dependent on several biochemical structures and reactions and can be triggered by several cell death-provoking events¹⁰⁵. One of the hallmarks of ferroptosis

is the presence of intracellular ferrous iron (Fe²⁺)¹⁰⁷. Free ferric iron (Fe³⁺) is shuttled from the blood stream into the cell through a transferrin receptor-mediated import 110 and is reduced into divalent iron (Fe²⁺) by the catalyzing metalloprotease six-transmembrane epithelial antigen of prostate 3 (STEAP3)¹¹¹. The divalent metal transporter 1 (DMT1) ultimately releases iron from the endosome into a labile iron pool (LIP) in the cytoplasm that harbours chelatable, as well as redox-active iron, while excess iron is stored in ferritin^{111,112}. Redox-active iron (Fe²⁺) can react with hydrogen peroxide (H₂O₂) and result in the formation of hydroxyl radicals in a socalled Fenton reaction¹¹³. Therefore, a possible reason for the cell death-promoting potential of iron lies within its capacity to donate electrons to oxygen³. It thereby represents one of the major sources of reactive oxygen species (ROS) which, when accumulating, can cause ferroptosis³. Additionally, ROS is generated in the form of highly reactive superoxides (O₂ ·-) as a by-product of oxidative phosphorylation (OXPHOS) in mitochondria¹¹⁴. Routinely, OXPHOS is a part of cell respiration and a process by which ATP is generated in multicellular organisms to supply energy¹¹⁵. It is closely linked to the mitochondrial tricarboxylic acid cycle (TCA cycle) because of their mutually dependent functionality. Products, such as nicotinamide adenine dinucleotide (NADH) and flavine adenine dinucleotide (FADH2) are fed into the electron chain transport for OXPHOS¹¹⁶. Though superoxide dismutases (SODs) can convert superoxide molecules into water and non-radical hydrogen peroxide (H₂O₂), the molecule itself can then react with divalent iron, once again forming hydroxyl radicals¹¹⁴. ROS that are produced in the cell have the disruptive ability to oxidise intracellular macromolecules, preferentially polyunsaturated fatty acids (PUFAs) leading to ferroptosis^{3,114}.

PUFAs are important components of the lipid bilayer of cellular membranes. Unsaturated fatty acids, particularly arachidonic acid (AA) and adrenic acid (AdA), are activated through esterification with Coenzyme A (CoA)¹¹⁷. This process is mediated by long-chain acyl-coenzyme A synthase 4 (ACSL4), which was shown to be essential for ferroptosis¹¹⁸. Activated fatty acids are subsequently used for PUFA synthesis¹¹⁹. To this end, lysophosphatidylcholine acyltransferase 3 (LPCAT3) integrates acylated AA into membrane glycerophospholipids (PLs), phosphatidylethanolamine (PE) in particular¹²⁰. Methylene bridges that are found between fatty acids, render PUFAs highly vulnerable to radical attack due to abstractable carbon-hydrogen atoms¹¹⁹. In the case of abstracted allylic hydrogen, a lipid radical is formed (L') that subsequently produces lipid peroxyl radicals (LOO') in a reaction with oxygen. As a result of lipid peroxidation, hydroperoxides as well as new lipid radicals (L') are formed that can further abstract hydrogen on their part¹⁰⁹. Hence, the reaction of ROS with PUFAs triggers a radical chain reaction, referred to as lipid peroxidation that features the accumulation of lipid ROS¹⁰⁴. In a self-amplifying manner, accumulating lipid peroxides can gradually attack adjacent PUFAs¹²¹ and result in lipid autoxidation¹²². This process leads to the destabilisation

of the cellular membrane. The molecular mechanisms through which lipid peroxidation and oxidised PE-PUFAs lead to ferroptotic cell death remain unresolved, though the formation of pores in membranes causing loss of ionic homeostasis was hypothesised in the past^{123,124}. Loss of cellular integrity will ultimately lead to membrane rupture and ferroptotic cell death¹²⁴. It was shown that levels of oxygenated AA and AdA-containing PE species (AA-OOH-PE) were elevated upon ferroptosis induction and that ferroptosis could be impeded by ACSL4 inhibition¹²⁵. A different study demonstrated elevated levels of the lipid mediators 5-hydroxyeicosatetraenoic acid (HETE), 11-HETE and 15-HETE in the medium of ferroptotic cells¹²⁶. Given their contribution to PUFA synthesis and the generation of a lipid target pool, LPCAT3 and ACSL4 exert a critical role in the execution mechanism of ferroptosis.

Alternative to lipid peroxidation by ROS, PUFAs can be peroxidised enzymatically through lipoxygenase (LOX)¹²¹. In this context, divalent iron serves as a cofactor of LOX¹²¹. Following LOX-mediated oxidation of AA, lipid signalling mediator hydroperoxyeicosatetraenoic acid (HPETE) is formed¹²⁷. 12/15 lipoxygenase in particular is suggested to play an important part in ferroptosis as it was experimentally linked to lipid peroxidation upon glutathione peroxidase 4 (GPX4) inhibition causing ferroptosis¹²⁷. It is further associated with lipid peroxidation of the mitochondrial membrane in neurons¹²⁸. Taken together, free intracellular iron and membrane PL-PUFAs constitute essential prerequisites for ferroptosis.

The collapse of an antioxidant defence system is equally thought to exert a crucial role in the execution of ferroptosis. Antioxidant protection mechanisms aim to promote cell survival and mitigate oxidative stress through the conversion of radicals into non-harmful variants as well as the repair of lipid peroxidation. One of the key players of ferroptosis is the selenocysteinecontaining enzyme GPX4, which has been described as the principal regulator of ferroptosis as it is responsible for the reduction of lipid hydroperoxides ¹²⁹ and lipid peroxide repair ¹⁰⁷. It constitutively hydrolyzes lipid peroxides (L-OOH), including phospholipid hydroperoxides and cholesterol hydroperoxides, to lipid alcohols (L-OH) at the expense of reduced glutathione (GSH) levels³. Glutathione serves in this context as an electron donor for GPX4¹³⁰. The antioxidant function of GSH derives from its oxidation to GSSG by GPX4 which can then convert peroxides into their corresponding alcohols or water¹⁰⁵. In a recycling step, GSSG is then catalysed into its reduced form in a nicotinamide adenine dinucleotide phosphate (NADPH)-dependent reaction with the help of glutathione reductase (GR)¹³¹. Consequently, the formation of toxic lipid hydroxyl radicals that lead to the accumulation of lipid ROS (L-ROS) can be prevented by GSH-GPX4 activity. It was shown that GSH depletion as well as the inactivation of GPX4 induces ferroptosis through ROS-mediated lipid peroxidation ¹²⁹.

Importantly, the biosynthesis of GSH depends on the availability of the three amino acids glycine, glutamine and cysteine. Cystine is imported into the cell, while glutamate is exported

in a one-to-one transport via the antiporter system xc^{-132} . Cystine as the predominant form can be reduced to cysteine and used for GSH synthesis¹³³. Alternatively, cysteine can also be generated through the transsulfuration pathway¹³⁴. In this metabolic pathway, homocysteine, generated from methionine, is converted into cysteine by the enzymatic activity of cystathionine beta-synthase (CBS)¹³⁴. Once cysteine availability is ensured, glutamate-cysteine ligase (GCL) forms the GSH precursor Υ - glutamylcysteine by catalytically linking glutamate and cysteine. Glycin is added by glutathione synthesis (GSS) in an ensuing step to generate glutamylcysteinylglycine and complete GSH synthesis¹³⁵.

Taking into consideration that cysteine is a principal component of GSH, it becomes apparent that system xc⁻ exhibits pivotal importance in ferroptosis. System xc⁻ is a heterodimer composed of a heavy chain subunit (4F2) and a light chain subunit (xCT)¹⁰⁵. These subunits are encoded by the solute carrier family 3 member 1 (SLC3A1) gene and solute carrier family 7 member 11 (SLC7A11) gene, respectively¹³⁶. The small molecule eradicator of RAS and ST (erastin) was identified to be an inhibitor of system xc⁻ and can as such induce ferroptosis¹³⁷. Concerning the ferroptotic pathway structure, system xc⁻ is considered to be the most upstream player, while GPX4 activity is discussed to be the most downstream passage of the ferroptosis pathway^{105,136}. This notion can be supported by the observation of a functional tricarboxylic acid cycle (TCA cycle) as imperative for erastin-induced ferroptosis, whereas GPX4-induced ferroptosis appeared to be independent of TCA cycle functional OXPHOS and mitochondria^{110,138}.

Though GPX4 and system xc are essential parts of the lipid ROS-specific antioxidant defence system, recent research has elucidated two endogenous GPX4-independent systems to equally prevent ferroptotic cell death. Myristoylated ferroptosis suppressor protein 1 (FSP1; formerly known as AIFM2)/coenzyme Q₁₀ and GTP cyclohydrolase 1/tetrahydrobiopterin (GCH1/BH₄) can also impede lipid peroxidation, thereby preventing ferroptosis ¹³⁹. Ubiquinol (CoQ₁₀H₂), an internally produced lipophilic radical scavenger, can trap lipid peroxyl radicals and is thereby oxidised to ubiquinone (Coenzyme Q10; CoQ₁₀). Notably, emerging evidence suggests that ubiquinone can be converted into its reduced form (ubiquinol) by FSP1 as well as dihydroorotate dehydrogenase (DHODH) using NAD(P)H^{140,141,142}. Furthermore, GCH1 was introduced as another antioxidant system to suppress ferroptosis by producing the endogenous metabolite tetrahydrobiopterin (BH₄), which in turn also protects against lipid peroxidation ¹⁴³.

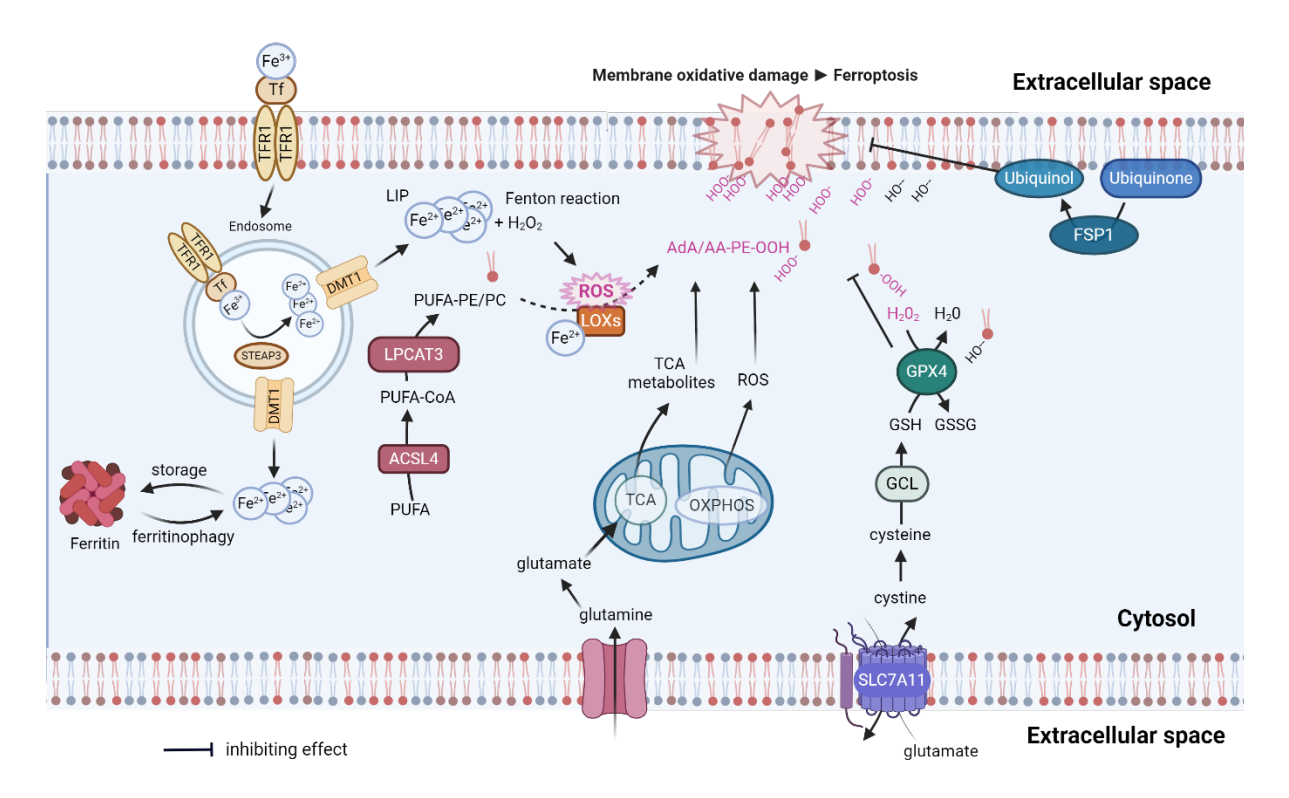


Figure 5. Schematic view of the ferroptosis pathway.

Iron is imported into cells via transferrin receptor-mediated mechanisms, converted into its active form by STEAP3 and released into the LIP by DMT1. Highly reactive hydroxyl radicals are generated in the Fenton reaction by the interaction of ferrous iron and hydrogen peroxide (H₂O₂). Superoxide radicals generated during oxidative phosphorylation in mitochondria can further contribute to ROS production. Subsequently, enzymatic and non-enzymatic peroxidation of PUFAs can occur leading to the accumulation of L-ROS. Lipid peroxidation disrupts the membrane integrity resulting in ferroptosis. ACSL4 and LPCAT3 facilitate PUFA activation and incorporation into cellular membranes. Ferroptosis can further be triggered by the failure of the cell's antioxidant defence system. The import of cystine, a precursor to cysteine, via the antiporter system xc⁻, is crucial for glutathione synthesis. GPX4 reduces lipid hydroperoxides to non-harmful lipid alcohols utilising glutathione as an electron donor. FSP1/coenzyme Q10 also plays an important role in preventing lipid peroxidation and subsequent ferroptotic cell death. Adapted from Bebber et al. 2020¹⁰⁵. The figure has been created using Biorender.

2.1.3.3.2. Regulation of ferroptosis

The regulation of ferroptosis can be implemented in one of two ways: either through positive regulation carried out by ferroptosis-driving substances or through negative regulators that prevent ferroptotic cell death. The most prominent mediators of ferroptosis are thought to be cell death-stimulating iron-metabolism, substances promoting lipid peroxidation, and inactivation of the cell death-protecting system xc⁻/glutathione/GPX4 axis^{144,145}.

The activation of system xc⁻ is vital for the import of cystine into the cell and for its use to synthesise glutathione. Contrary to the ferroptosis-protecting effect of system xc⁻, the synthetic small molecule erastin inhibits this antiporter and exhibits opposing implications in that it triggers ferroptosis¹⁰⁴. GSH is one of the most important cellular antioxidants and its constant intracellular provision depends on GPX4¹⁴⁶. Given that GPX4 activity leads to reduced L-ROS

production under healthy conditions, it is thought to be a vital factor for cellular protection from ferroptosis 129. Research has shown that cells undergo ferroptosis upon gene knockdown of GPX4 which was shown to be prevented by the application of iron chelators and antioxidants¹²⁹. Similar to gene knockdown of GPX4, Ras selective lethal 3 (RSL3) also leads to ferroptotic cell death by directly inhibiting GPX4¹⁴⁷. The transcription of GPX4 can be triggered by nuclear factor erythroid 2-related factor (NRF2)¹⁴⁸. This antioxidant transcription factor decouples in the cytosol from its negative regulator kelch-like ECH-associated protein 1 (KEAP1) when the cell is exposed to oxidative stress¹⁴⁸. It subsequently translocates from the cytosol to the nucleus, where it forms heterodimers with small musculoaponeurotic fibrosarcoma (sMAF) proteins, binds to antioxidant response elements (AREs) and primes the transcription of its target genes 148,149. NRF2 regulates a wide range of genes encoding proteins that exert an important role in ferroptosis, including anti-ferroptotic GPX4, system xc-, and ferritin^{148,150,151}. Besides its capacity to negatively regulate ferroptosis and to render cells less sensitive to ferroptotic cell death, NRF2 was conversely shown to increase the expression of heme oxygenase-1 in neuroblastoma, which mediates the decomposition of heme leading to an augmented labile Fe (II) pool¹⁵². Thereby, cells become more vulnerable to ferroptosis induction¹⁵². Hence, NRF2 shows ambiguous mechanisms and displays positive as well as negative regulatory functions in the context of ferroptosis.

Furthermore, heat shock protein beta-1 (HSPB1) was recently introduced as a negative mediator of ferroptotic cancer cell death. Mechanistically, it limits intracellular iron uptake as well as lipid ROS accumulation, thereby protecting against ferroptotic cell death¹⁵³.

Additionally, autophagy-related genes were determined to be involved in the promotion of ferroptosis¹¹¹. Active iron is released by the previously mentioned process of ferritinophagy, whereby stored complexed iron is liberated from ferritin nanocages via cargo receptor nuclear receptor coactivator 4 (NCOA4) in the lysosome⁸¹. Experimental knockdown or overexpression of NCOA4 showed reciprocal results concerning the regulation of ferroptosis: knockdown of NCOA4 blocked ferritinophagy and ferroptotic cell death¹⁵⁴, while overexpression of NCOA4 enhanced ferritinophagy and fueled ferroptosis¹⁵⁵.

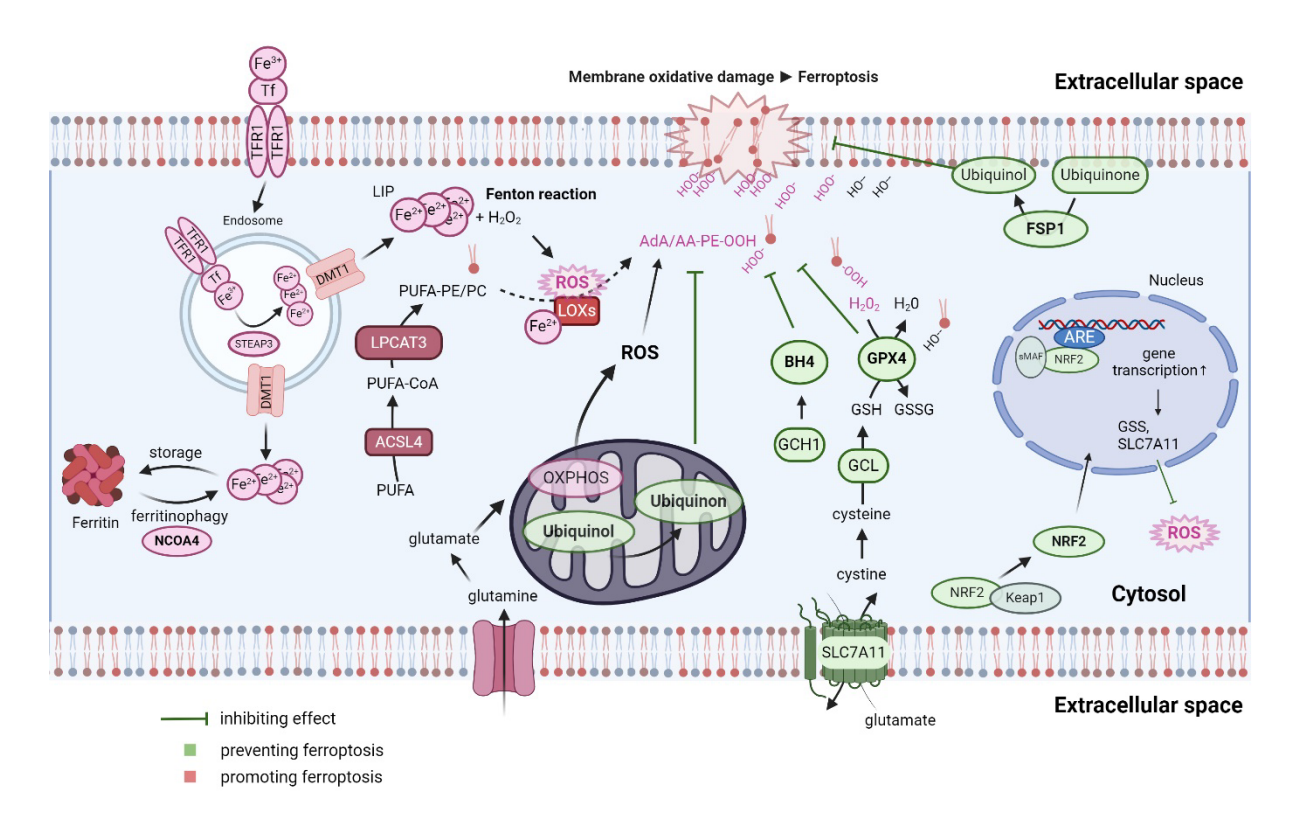


Figure 6. Endogenous positive and negative regulators of ferroptosis.

Depicted in green are mechanisms or biomolecular pathways that protect the cell against ferroptosis. Positive regulators or molecular processes which promote ferroptosis are illustrated in red colour. Most important ferroptosis-promoting mechanisms include the cell death-stimulating iron-metabolism and lipid peroxidation-promoting substances. NCOA4 is also thought to be a positive regulator as it releases active iron from ferritin nanocages and thereby facilitates ferroptosis. The xc-/glutathione/GPX4 axis, however, protects efficiently against ferroptotic cell death. The expression of GPX4 can be induced by the transcription factor NRF2. In reaction to oxidative stress, NRF2 dissociates from its inhibitor KEAP1, in the cytosol. This allows NRF2 to translocate to the nucleus, where it forms heterodimers with sMAF proteins, binds to ARE and initiates the transcription of target genes. FSP1/coenzyme Q10 and GCH1/BH4 also play important roles in preventing lipid peroxidation and subsequent ferroptotic cell death. Adapted from Yapici and Bebber et al. 2024¹⁵⁶. The figure has been created using Biorender.

RSL3- or erastin-induced cell death can be prevented by lipid peroxidation inhibitors known as ferrostatin-1 (Fer-1) and liproxstatin-1¹⁵⁷. These small molecules operate as lipid ROS scavengers by removing oxidising free radicals¹⁵⁷. Further, lipophilic antioxidants, such as vitamin E, trolox and butylated hydroxytoluene (BHT), can also be applied as ferroptosis-inhibiting drugs to prevent lipid peroxidation¹²³. In addition to exogenous ferroptosis inhibitors, cells have developed endogenous mechanisms to hinder lipid peroxidation and block ferroptosis, notably using the FSP1-CoQ₁₀-NAD(P)H pathway. As mentioned earlier, FSP1 acts as a negative regulator of ferroptosis because it quenches the accumulation of L-ROS^{140,141}. Similarly, lipid peroxidation can be counteracted by the administration of PUFAs that harbor the hydrogen isotope deuterium rendering PUFAs more resistant to oxidation¹²¹. In contrast to its role as a ferroptosis-protecting substance, NADPH simultaneously acts as an electron donor for NADPH oxidases (NOX)¹⁵⁸. This enzyme family can reduce oxygen to superoxides, thus promoting ferroptosis through the generation of ROS^{104,158}.

The successful inhibition of experimentally induced ferroptosis can further be achieved through the application of iron chelators, such as deferoxamine 104, deferiprone, and ciclopirox olamine¹²³. Membrane impermeable iron chelators are involved in lysosomal iron chelation, while lipophilic iron chelators are linked to the LIP¹¹¹. Since ferrous iron is a crucial prerequisite for ferroptosis, iron chelators constitute a highly efficient way to prevent ferroptosis by restricting divalent redox-active iron 144. Reversely, several genes and proteins involved in iron metabolism were recently identified to be positive regulators of ferroptosis. In adjustment to adequate intracellular levels of iron, iron regulatory proteins 1 and 2 (IRP1/2) regulate iron uptake, export and storage in response to iron abundance or iron depletion 159,160. Of note, iron response element binding protein 2 (IREB2), the gene encoding IRP2, was identified to be crucial for erastin-induced ferroptosis 104,160. IRPs can alter expression levels of proteins involved in iron metabolism, such as ferritin and transferrin receptor 160. Suppressed gene expression of the transferrin receptor (TFRC) results in decreased iron uptake and prevents ferroptosis 110. Oncogenic-RAS-harbouring cancer cells that are sensitive to ferroptosis have shown a profile of heightened TFRC1 and decreased ferritin expression compared to ferroptosis-resistant cells¹⁴⁷. These findings support the idea of elevated levels of intracellular available iron in promoting ferroptosis.

Ferroptosis inducers can be classified into 4 mechanisms of action: Class 1 inducers target system xc⁻, which prevents cystine uptake and GSH synthesis leading to ferroptosis. Substances inhibiting system xc⁻ include small molecule inhibitor erastin, sorafenib, sulfasalazine, and the amino acid glutamate. GPX4 constitutes the target molecule of class 2 inducers, namely RSL3 and ML162. Class 3 inducers trigger ferroptosis through the depletion of GPX4 and ubiquinone (FIN56). Lastly, class 4 ferroptosis inducers, endoperoxide compounds (FINO₂), provoke lipid peroxidation, resulting in ferroptotic cell death 123,161. Alongside these pharmacological ferroptosis inducers, cell death can also be triggered by 4hydroxynonenal (4-HNE) because it controls transcription factors NRF2 and cell-cycle regulators¹²³. This secondary oxidation product is generated by the degradation of AAs and longer PUFAs, suggesting that 4-HNE acts as a downstream inducer of ferroptosis following lipid peroxidation¹²³. 4-HNE has further been hypothesised to act as a potential end effector in ferroptosis and to cause plasma membrane rupture 162. Interestingly, recent evidence showed that the endosomal sorting complexes required for transport (ESCRT)-III are associated with the repair of plasma membrane damage during ferroptosis 163. The depletion of ESCRT-III promoted ferroptosis, suggesting that it negatively regulates ferroptosis 163.

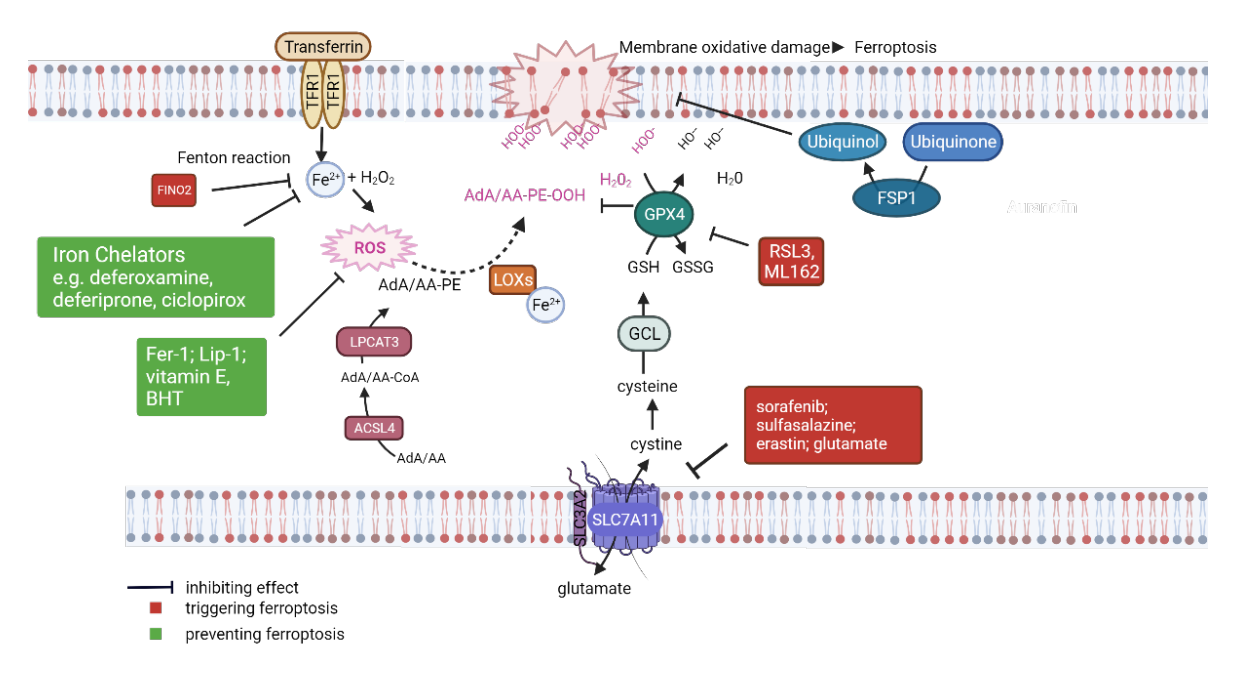


Figure 7. Exogenous ferroptosis inhibitors and inducers.

Class 1 inducers target system xc-, which hampers cystine uptake and glutathione (GSH) synthesis, ultimately leading to ferroptosis (depicted in the red box). Substances inhibiting system xc- include the small molecule inhibitor erastin, sorafenib, sulfasalazine, and the amino acid glutamate. Class 2 inducers focus on GPX4, such as RSL3 and ML162. FINO2 induces lipid peroxidation, resulting in ferroptotic cell death. Effective suppression of experimentally induced ferroptosis can be accomplished by utilising iron chelators, including deferoxamine, ciclopirox olamine, and deferiprone. Cell death induced by RSL3 or erastin can be blocked by lipid peroxidation inhibitors, such as Fer-1 and Lip-1. Additionally, lipophilic antioxidants such as vitamin E, and BHT can also serve as ferroptosis-inhibiting agents to prevent lipid peroxidation. Adapted from Yapici and Bebber et al. 2024¹⁵⁶. The figure has been created using Biorender.

2.2. Inflammation and immune defence

As a result of an activated immune system, immune cells and immunologic factors are recruited to the tissue of interest, causing a process known as inflammation. The immune system comprises two subsystems: the innate immune system, which responds in a quick and non-specific manner to danger signals, and the adaptive immune system¹⁶⁴.

Front-line host defence is provided by innate immune cells such as dendritic cells, natural killer cells, granulocytes, B lymphocytes, and bone marrow-derived monocytes that differentiate into macrophages in tissues. Pathogens are quickly recognised and instantly eliminated through phagocytosis carried out by phagocytes (neutrophil granulocytes, macrophages and dendritic cells). Additionally, innate immune cells can recognise and digest complexes consisting of pathogen-derived antigens coupled with host-derived antibodies to present pathological antigens on their cell surface and trigger an immune response. These antigens are presented via major histocompatibility receptors (MHC-receptors) and can then be recognised by corresponding immune cells of the adaptive immune system. This process mainly takes place after the migration of antigen-presenting cells (APCs) to secondary lymphatic organs and

lymph nodes. Simultaneously, innate immune cells can secrete cytokines that function as important messenger substances between innate and adaptive immunity. Hence, multiple mechanisms result in the activation of the antigen-specific and highly effective adaptive immune system¹⁶⁴.

Adaptive immunity encompasses cell-mediated and humoral-mediated mechanics. Naïve T lymphocytes are equipped with T-cell receptors (TCRs) that can recognise specific pathological antigens and differentiate into effector T cells. Whereas CD4-positive T cells help to eliminate pathogens, CD8-positive T cells show cytotoxic capacity to directly kill infected or degenerated cells. The antigen-specific activation of a T cell is followed by its proliferation in secondary lymphatic organs to generate a force of cell-mediated defence against invading pathogens. This process can take hours or days, which underlines the more specific and yet slower immune response of adaptive immune cells compared to the innate immune system. In addition to cell-mediated adaptive immunity, B cells that have differentiated into plasma cells can produce antigen-specific antibodies against invading microbes. In this case of humoral-mediated immune defence, the response is executed by macromolecules. Both T and B cells can develop immunological memory during an immune response to primary exposure to a pathogen (primary immune response). Due to memory cells, an immune response can be launched and implemented more rapidly in case of exposure to a known pathogen (secondary immune response)

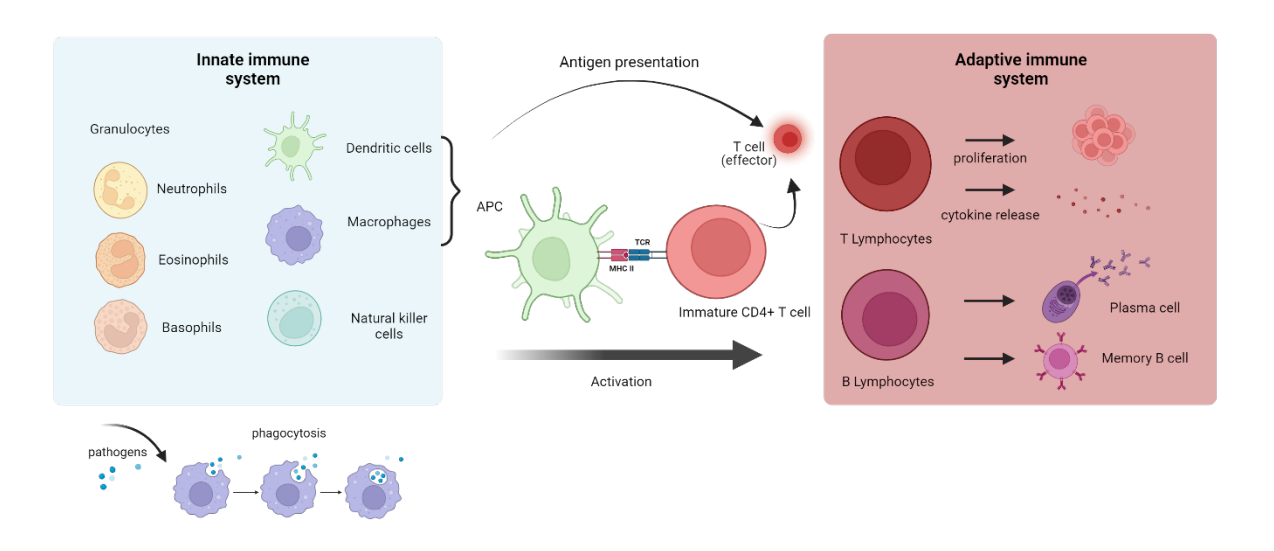


Figure 8. Innate and adaptive immunity.

The immune system consists of two main branches: the quick and nonspecific innate immune system, and the adaptive immune system. Innate immune cells encompass granulocytes, dendritic cells, natural killer cells, and macrophages, which quickly recognise and eliminate pathogens through phagocytosis. They also present antigens via MHC-receptors leading to the activation of the adaptive immune system. T and B lymphocytes are cells of the adaptive immune system. T lymphocytes differentiate into effector cells upon recognising specific antigens, aiding in pathogen elimination. B lymphocytes produce antibodies against pathogens. Adapted from Janeway et al. 2001¹⁶⁴. The figure has been created using Biorender.

2.2.1. Necroinflammation

A key characteristic of regulated necrosis pathways is the disruption of plasma membrane integrity^{105,167}. This unique aspect of regulated necrosis leads to the release of cytosolic components, which are then exposed to the surrounding tissue. Several of these released cytosolic factors act as immune signaling molecules, known as DAMPs^{2,105}. They are defined as endogenous molecules encoded by the host's endogenous genome that function as immunogenic signals when released into the extracellular space^{2,168}. In addition to DAMPs, alarmins released during cell death or injury also have the capacity to trigger inflammatory immune responses^{105,169}. Synergistically with PAMPs, DAMPs and alarmins operate as ligands that stimulate PRRs that are expressed on the plasma membranes of innate immune cells¹⁰⁵. Upon stimulation of PRRs, such as TLRs and NLRs, a signalling cascade is initiated to activate downstream transcription factors and to produce immune factors, such as chemokines and cytokines^{170,171}. Immunogenic cell death results in the recruitment and activation of immune cells, which is hypothesised to induce further necrotic cell death pathways, culminating in a necroinflammatory auto-amplification loop²¹. This inflammatory process is referred to as necroinflammation if regulated necrosis initiated this immune activation^{2,105}.

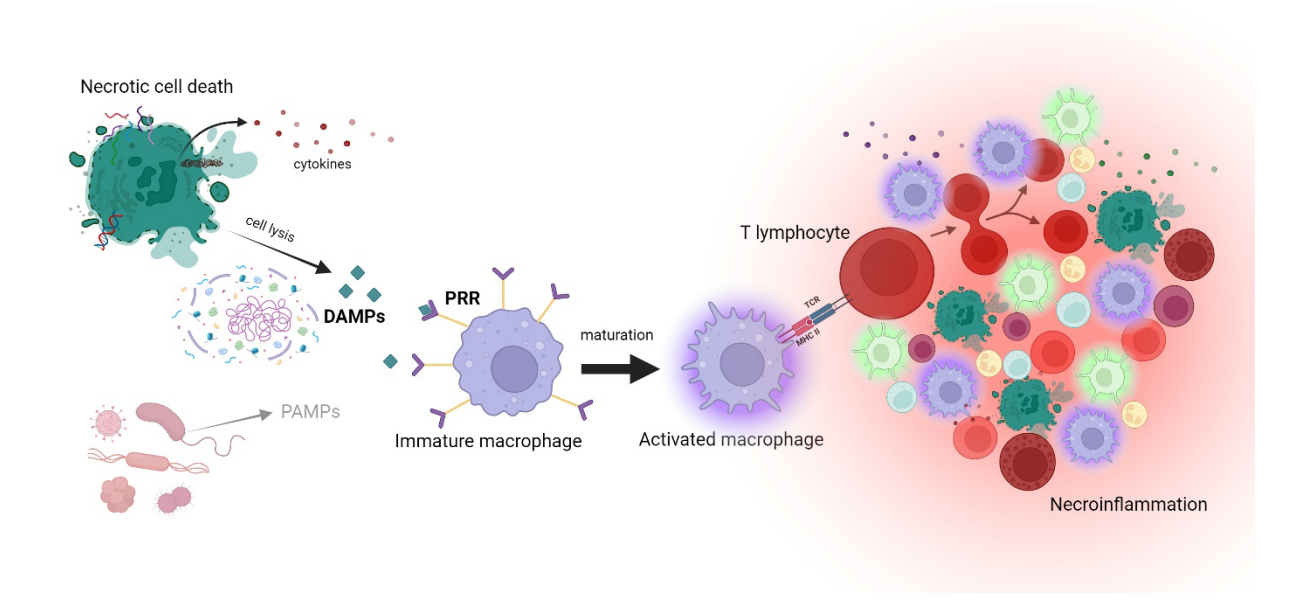


Figure 9. Necroinflammation.

Regulated necrosis pathways are characterised by the disruption of plasma membrane integrity, leading to the release of the cytosolic content. Endogenous noninflammatory components and cell organelles of viable cells can be recognised as DAMPs when released, secreted or exposed during cell death, and acquire immunomodulatory functions. DAMPs and alarmins can be recognised by PRRs on plasma membranes of innate immune cells. Consequently, inflammatory signalling cascades are triggered that lead to the production of immune factors and the activation of adaptive immune cells, potentially leading to further necrotic cell death pathways. If regulated necrosis triggers immune activation, the resulting inflammatory process is termed necroinflammation. Adapted from Sarhan et al. 2018². The figure has been created using Biorender.

2.2.2. Ferroptosis as an immunogenic form of cell death

As a lytic form of cell death, ferroptosis is thought to result in plasma membrane rupture and the release of the cellular content into the surroundings¹⁷². The formation of pores in the membrane has been observed to result in the bursting of the plasma membrane in other types of lytic cell death, namely necroptosis¹⁷³ and pyroptosis¹⁰¹, and is carried out by the effectors MLKL and gasdermin D respectively¹⁶². Interestingly, recent evidence suggested that membrane rupture in ferroptosis is linked to the formation of membrane nanopores, leading to an imbalance in osmotic forces¹⁶³. Although several end effectors have been hypothesised to be crucial for the disruption of the plasma membrane in ferroptosis 162, the mechanisms by which cellular lysis is caused, remain obscure. However, mounting evidence demonstrates that ferroptosis can be inflammatory, as lipid peroxidation-induced rupture of the plasma membrane¹⁷⁴ results in sterile inflammation¹³⁶. Furthermore, a growing body of literature indicates that ferroptotic cell death causes the release of DAMPs, which in turn initiate inflammatory signalling pathways^{2,4}. Recent studies have suggested further that ferroptosis is closely associated with overt inflammatory signatures exhibiting elevated levels of proinflammatory cytokines in damaged tissues 175-178. Released cytokines from ferroptotic cells can be altered by the aforementioned ESCRT-III, which bridges inflammatory signalling and ferroptotic membrane rupture, and indicates that the inflammatory potential of ferroptosis can be modulated 163. In addition, ESCRT-III was shown to influence the activation of macrophages that were exposed to ferroptotic supernatants¹⁶³. The interval between membrane damage and membrane rupture displays a highly delicate time frame in which cells are still able to produce biomolecules, such as cytokines, to signal a lethal process¹⁷⁹. The investigation of processes occurring in this crucial time frame in ferroptosis is an integral part of this thesis. Recently, it was shown that high-iron diets or GPX4 depletion rendered mice more susceptible to experimental pancreatitis compared to unexposed mice¹⁸⁰. Furthermore, in a model of Krasdriven pancreatic ductal adenocarcinoma (PDAC), increased macrophage infiltration in the tumour microenvironment of Kras-driven mice with Gpx4 depletion or a high-iron diet could be observed¹⁸⁰.

3. Materials and methods

3.1. Materials

3.1.1. Antibodies

Table 3-1 Primary antibodies used in this study

Antibody	Size	Source	Supplier
Anti-mouse	53-55 kDa	rat	Biolegend (Sa14-2)
CD14 antibody			
Isotype Ctrl	53-55 kDa	rat	Biolegend
CD14 antibody			
Anti-GPX4	22 kDa	rabbit	Abcam

Table 3-2 Secondary antibodies used in this study

Antibody	Dilution	Size	Source	Supplier
anti-mouse HRP	1:10 000	42 kDa	goat	Thermo Fischer
anti-rabbit HRP	1:10 000	75 kDa	goat	Thermo Fischer

3.1.2. Buffers

All buffers used in this study were prepared using distilled water from the Milli-H₂O system.

Table 3-3 Buffers used in this study

Buffer	Ingredients
Blocking Buffer	5% no-fat dry milk powder
	dissolved in 50ml 1x PBST
Blotting Buffer	1x Transfer Buffer
CASYton	OMNI Life Science
EDTA	14.16 g (0.5 M) EDTA
	dissolved in 80ml ddH₂O
FACS Buffer	2% FBS
	50 ml 1x PBS
LDS Sample Buffer	Invitrogen [™]
Sample Buffer	400 μl LDS Sample Buffer
	100 µl 1 M DTT
Lysis Buffer	30 mM Tris-HCl
	120 mM NaCl

2 mM KCI 1% Triton-X-100 dissolved in 1000 ml ddH₂O SDS-Running buffer 1x TGS 80 g NaCI 2.0 g KCI 14.4 g Na2HPO4 2.4 g KH₂PO₄ dissolved in 800 ml ddH₂O 10x PBST 1 L 10x PBS 5 ml Tween-20 Phosphatase Inhibitor Solution 1 tablet of phosphatase inhibitor dissolved in 1 ml ddH2O PI FACS buffer 50 ml 1x PBS 2% FBS 0.1% propidium iodide PI Lysis Buffer 200 μl protease inhibitor solution 200 μl phosphatase inhibitor solution dissolved in 1 ml ddH2O Protease Inhibitor Solution 1 tablet of protease inhibitor solution 200 μl phosphatase inhibitor solution dissolved in 1 ml ddH2O Stripping Buffer 5% no-fat dry milk powder 0.05% NaN₃ dissolved in 50 ml PBST 48.4 g Tris base 11.4 ml glacial acetic acid 20 ml 0.5 M EDTA dissolved in 800 ml ddH2O TE-buffer (Tris-EDTA buffer) 0,5 ml 1M Tris-HCl (pH8 or 7.5) (10 mM Tris-HCl) 0,1 ml 0,5 M EDTA (1 mM) 49.4 ml ddH2O 10x TGS Buffer 250 mM Tris 1.92 M glycine 1% SDS dissolved in 800 ml ddH2O		2 mM EDTA
1% Triton-X-100 dissolved in 1000 ml ddH₂O SDS-Running buffer 1x TGS 80 g NaCl 2.0 g KCl 14.4 g Na2HPO4 2.4 g KH₂PO₄ dissolved in 800 ml ddH₂O 10x PBST 1 L 10x PBS 5 ml Tween-20 Phosphatase Inhibitor Solution 1 tablet of phosphatase inhibitor dissolved in 1 ml ddH2O PI FACS buffer 50 ml 1x PBS 2% FBS 0.1% propidium iodide PI Lysis Buffer 200 μl protease inhibitor solution dissolved in 1 ml ddH2O Protease Inhibitor Solution 1 tablet of protease inhibitor solution 200 μl protease inhibitor solution dissolved in 1 ml ddH2O Stripping Buffer 5% no-fat dry milk powder 0,05% NaN₃ dissolved in 50 ml PBST 10x TAE Buffer 48.4 g Tris base 11.4 ml glacial acetic acid 20 ml 0.5 M EDTA dissolved in 800 ml ddH2O TE-buffer (Tris-EDTA buffer) 0,5 ml 1M Tris-HCl (pH8 or 7.5) (10 mM Tris-HCl) 0,1 ml 0,5 M EDTA (1 mM) 49.4 ml ddH2O 10x TGS Buffer 250 mM Tris 1.92 M glycine 1% SDS		
dissolved in 1000 ml ddH₂O SDS-Running buffer 1x TGS 80 g NaCl 2.0 g KCl 14.4 g Na2HPO4 2.4 g KH₂PO₄ dissolved in 800 ml ddH₂O 10x PBST 1L 10x PBS 5 ml Tween-20 Phosphatase Inhibitor Solution 1 tablet of phosphatase inhibitor dissolved in 1 ml ddH2O PI FACS buffer 50 ml 1x PBS 2% FBS 0.1% propidium iodide PI Lysis Buffer 200 μl protease inhibitor solution 200 μl phosphatase inhibitor solution 40 μl phosphatase inhibitor solution 200 μl phosphatase inhibitor solution 200 μl phosphatase inhibitor solution 40 μl phosphatase inhibitor solution 200 μl phosphatase inhibitor solution 40 μl phosphatase inhibitor solution 41 tablet of protease inhibitor solution 42 μl phosphatase inhibitor solution 43 μl phosphatase inhibitor solution 44 μl phosphatase inhibitor solution 45 μl phosphatase inhibitor solution 46 μl phosphatase inhibitor solution 47 μl phosphatase inhibitor solution 48 μl phosphatase inhibitor solution 49 μl phosphatase inhibitor solution 40 μl phosphatase inhibitor solution 40 μl phosphatase inhibitor solution 40 μl phosphatase inhibitor solu		
10x PBS		
2.0 g KCI 14.4 g Na2HPO4 2.4 g KH ₂ PO ₄ dissolved in 800 ml ddH ₂ O 10x PBST 1 L 10x PBS 5 ml Tween-20 Phosphatase Inhibitor Solution 1 tablet of phosphatase inhibitor dissolved in 1 ml ddH2O PI FACS buffer 50 ml 1x PBS 2% FBS 0.1% propidium iodide PI Lysis Buffer 200 µl protease inhibitor solution 200 µl phosphatase inhibitor solution 200 µl phosphatase inhibitor solution dissolved in 1 ml ddH2O Protease Inhibitor Solution 1 tablet of protease inhibitor (cOmplete TM) dissolved in 1 ml ddH2O Stripping Buffer 5% no-fat dry milk powder 0,05% NaN ₃ dissolved in 50 ml PBST 10x TAE Buffer 48.4 g Tris base 11.4 ml glacial acetic acid 20 ml 0.5 M EDTA dissolved in 800 ml ddH2O TE-buffer (Tris-EDTA buffer) 0,5 ml 1M Tris-HCl (pH8 or 7.5) (10 mM Tris-HCl) 0,1 ml 0,5 M EDTA (1 mM) 49.4 ml ddH2O 10x TGS Buffer 250 mM Tris 1.92 M glycine 1% SDS	SDS-Running buffer	1x TGS
14.4 g Na2HPO4 2.4 g KH₂PO₄ dissolved in 800 ml ddH₂O 10x PBST 1 L 10x PBS 5 ml Tween-20 Phosphatase Inhibitor Solution 1 tablet of phosphatase inhibitor dissolved in 1 ml ddH2O PI FACS buffer 50 ml 1x PBS 2% FBS 0.1% propidium iodide PI Lysis Buffer 200 µl protease inhibitor solution 200 µl phosphatase inhibitor solution 200 µl phosphatase inhibitor solution dissolved in 1 ml ddH2O Protease Inhibitor Solution 1 tablet of protease inhibitor (cOmplete™) dissolved in 1 ml ddH2O Stripping Buffer 5% no-fat dry milk powder 0,05% NaN₃ dissolved in 50 ml PBST 10x TAE Buffer 48.4 g Tris base 11.4 ml glacial acetic acid 20 ml 0.5 M EDTA dissolved in 800 ml ddH2O TE-buffer (Tris-EDTA buffer) 0,5 ml 1M Tris-HCl (pH8 or 7.5) (10 mM Tris-HCl) 0,1 ml 0,5 M EDTA (1 mM) 49,4 ml ddH2O 10x TGS Buffer 250 mM Tris 1.92 M glycine 1% SDS	10x PBS	80 g NaCl
2.4 g KH₂PO4 dissolved in 800 ml ddH₂O 10x PBST 1 L 10x PBS 5 ml Tween-20 Phosphatase Inhibitor Solution 1 tablet of phosphatase inhibitor dissolved in 1 ml ddH2O PI FACS buffer 50 ml 1x PBS 2% FBS 0.1% propidium iodide PI Lysis Buffer 200 µl protease inhibitor solution 200 µl phosphatase inhibitor solution 200 µl phosphatase inhibitor solution dissolved in 1 ml ddH2O Protease Inhibitor Solution 1 tablet of protease inhibitor (cOmplete™) dissolved in 1 ml ddH2O Stripping Buffer 5% no-fat dry milk powder 0,05% NaN₃ dissolved in 50 ml PBST 10x TAE Buffer 48.4 g Tris base 11.4 ml glacial acetic acid 20 ml 0.5 M EDTA dissolved in 800 ml ddH2O TE-buffer (Tris-EDTA buffer) 0,5 ml 1M Tris-HCI (pH8 or 7.5) (10 mM Tris-HCI) 0,1 ml 0,5 M EDTA (1 mM) 49,4 ml ddH2O 10x TGS Buffer 250 mM Tris 1.92 M glycine 1% SDS		2.0 g KCI
dissolved in 800 ml ddH₂O 10x PBST 1 L 10x PBS 5 ml Tween-20 Phosphatase Inhibitor Solution 1 tablet of phosphatase inhibitor dissolved in 1 ml ddH2O PI FACS buffer 50 ml 1x PBS 2% FBS 0.1% propidium iodide PI Lysis Buffer 200 μl protease inhibitor solution 200 μl phosphatase inhibitor solution dissolved in 1 ml ddH2O Protease Inhibitor Solution 1 tablet of protease inhibitor (cOmplete™) dissolved in 1 ml ddH2O Stripping Buffer 5% no-fat dry milk powder 0,05% NaN₃ dissolved in 50 ml PBST 10x TAE Buffer 48.4 g Tris base 11.4 ml glacial acetic acid 20 ml 0.5 M EDTA dissolved in 800 ml ddH2O TE-buffer (Tris-EDTA buffer) 0,5 ml 1M Tris-HCl (pH8 or 7.5) (10 mM Tris-HCl) 0,1 ml 0,5 M EDTA (1 mM) 49.4 ml ddH2O 10x TGS Buffer 250 mM Tris 1.92 M glycine 1% SDS		14.4 g Na2HPO4
10x PBST 1 L 10x PBS 5 ml Tween-20 Phosphatase Inhibitor Solution 1 tablet of phosphatase inhibitor dissolved in 1 ml ddH2O PI FACS buffer 50 ml 1x PBS 2% FBS 0.1% propidium iodide PI Lysis Buffer 200 μl protease inhibitor solution 200 μl phosphatase inhibitor solution dissolved in 1 ml ddH2O Protease Inhibitor Solution 1 tablet of protease inhibitor solution 200 μl phosphatase inhibitor solution dissolved in 1 ml ddH2O Stripping Buffer 5% no-fat dry milk powder 0,05% NaN₃ dissolved in 50 ml PBST 10x TAE Buffer 48.4 g Tris base 11.4 ml glacial acetic acid 20 ml 0.5 M EDTA dissolved in 800 ml ddH2O TE-buffer (Tris-EDTA buffer) 7,5 ml 1M Tris-HCl (pH8 or 7.5) (10 mM Tris-HCl) 0,1 ml 0,5 M EDTA (1 mM) 49,4 ml ddH2O 10x TGS Buffer 250 mM Tris 1.92 M glycine 1% SDS		2.4 g KH ₂ PO ₄
5 ml Tween-20 Phosphatase Inhibitor Solution 1 tablet of phosphatase inhibitor dissolved in 1 ml ddH2O PI FACS buffer 50 ml 1x PBS 2% FBS 0.1% propidium iodide PI Lysis Buffer 200 µl protease inhibitor solution 200 µl phosphatase inhibitor solution dissolved in 1 ml ddH2O Protease Inhibitor Solution 1 tablet of protease inhibitor (cOmplete™) dissolved in 1 ml ddH2O Stripping Buffer 5% no-fat dry milk powder 0.05% NaN₃ dissolved in 50 ml PBST 10x TAE Buffer 48.4 g Tris base 11.4 ml glacial acetic acid 20 ml 0.5 M EDTA dissolved in 800 ml ddH2O TE-buffer (Tris-EDTA buffer) 0,5 ml 1M Tris-HCl (pH8 or 7.5) (10 mM Tris-HCl) 0,1 ml 0,5 M EDTA (1 mM) 49,4 ml ddH2O 10x TGS Buffer 250 mM Tris 1.92 M glycine 1% SDS		dissolved in 800 ml ddH₂O
Phosphatase Inhibitor Solution 1 tablet of phosphatase inhibitor dissolved in 1 ml ddH2O PI FACS buffer 50 ml 1x PBS 2% FBS 0.1% propidium iodide PI Lysis Buffer 200 μl protease inhibitor solution 200 μl phosphatase inhibitor solution dissolved in 1 ml ddH2O Protease Inhibitor Solution 1 tablet of protease inhibitor (cOmplete™) dissolved in 1 ml ddH2O Stripping Buffer 5% no-fat dry milk powder 0,05% NaN₃ dissolved in 50 ml PBST 10x TAE Buffer 48.4 g Tris base 11.4 ml glacial acetic acid 20 ml 0.5 M EDTA dissolved in 800 ml ddH2O TE-buffer (Tris-EDTA buffer) 0,5 ml 1M Tris-HCl (pH8 or 7.5) (10 mM Tris-HCl) 0,1 ml 0,5 M EDTA (1 mM) 49,4 ml ddH2O 10x TGS Buffer 250 mM Tris 1.92 M glycine 1% SDS	10x PBST	1 L 10x PBS
dissolved in 1 ml ddH2O PI FACS buffer 50 ml 1x PBS 2% FBS 0.1% propidium iodide PI Lysis Buffer 200 µl protease inhibitor solution 200 µl phosphatase inhibitor solution dissolved in 1 ml ddH2O Protease Inhibitor Solution 1 tablet of protease inhibitor (cOmplete TM) dissolved in 1 ml ddH2O Stripping Buffer 5% no-fat dry milk powder 0,05% NaN₃ dissolved in 50 ml PBST 10x TAE Buffer 48.4 g Tris base 11.4 ml glacial acetic acid 20 ml 0.5 M EDTA dissolved in 800 ml ddH2O TE-buffer (Tris-EDTA buffer) 0,5 ml 1M Tris-HCl (pH8 or 7.5) (10 mM Tris-HCl) 0,1 ml 0,5 M EDTA (1 mM) 49,4 ml ddH2O 10x TGS Buffer 250 mM Tris 1.92 M glycine 1% SDS		5 ml Tween-20
PI FACS buffer 50 ml 1x PBS 2% FBS 0.1% propidium iodide PI Lysis Buffer 200 μl protease inhibitor solution 200 μl phosphatase inhibitor solution dissolved in 1 ml ddH2O Protease Inhibitor Solution 1 tablet of protease inhibitor (cOmplete™) dissolved in 1 ml ddH2O Stripping Buffer 5% no-fat dry milk powder 0,05% NaN₃ dissolved in 50 ml PBST 10x TAE Buffer 48.4 g Tris base 11.4 ml glacial acetic acid 20 ml 0.5 M EDTA dissolved in 800 ml ddH2O TE-buffer (Tris-EDTA buffer) 0,5 ml 1M Tris-HCl (pH8 or 7.5) (10 mM Tris-HCl) 0,1 ml 0,5 M EDTA (1 mM) 49,4 ml ddH2O 10x TGS Buffer 250 mM Tris 1.92 M glycine 1% SDS	Phosphatase Inhibitor Solution	1 tablet of phosphatase inhibitor
2% FBS 0.1% propidium iodide PI Lysis Buffer 200 µl protease inhibitor solution 200 µl phosphatase inhibitor solution dissolved in 1 ml ddH2O Protease Inhibitor Solution 1 tablet of protease inhibitor (cOmplete™) dissolved in 1 ml ddH2O Stripping Buffer 5% no-fat dry milk powder 0,05% NaN₃ dissolved in 50 ml PBST 10x TAE Buffer 48.4 g Tris base 11.4 ml glacial acetic acid 20 ml 0.5 M EDTA dissolved in 800 ml ddH2O TE-buffer (Tris-EDTA buffer) 0,5 ml 1M Tris-HCl (pH8 or 7.5) (10 mM Tris-HCl) 0,1 ml 0,5 M EDTA (1 mM) 49,4 ml ddH2O 10x TGS Buffer 250 mM Tris 1.92 M glycine 1% SDS		dissolved in 1 ml ddH2O
0.1% propidium iodide PI Lysis Buffer 200 µl protease inhibitor solution 200 µl phosphatase inhibitor solution dissolved in 1 ml ddH2O Protease Inhibitor Solution 1 tablet of protease inhibitor (cOmplete™) dissolved in 1 ml ddH2O Stripping Buffer 5% no-fat dry milk powder 0,05% NaN₃ dissolved in 50 ml PBST 10x TAE Buffer 48.4 g Tris base 11.4 ml glacial acetic acid 20 ml 0.5 M EDTA dissolved in 800 ml ddH2O TE-buffer (Tris-EDTA buffer) 0,5 ml 1M Tris-HCl (pH8 or 7.5) (10 mM Tris-HCl) 0,1 ml 0,5 M EDTA (1 mM) 49,4 ml ddH2O 10x TGS Buffer 250 mM Tris 1.92 M glycine 1% SDS	PI FACS buffer	50 ml 1x PBS
PI Lysis Buffer 200 µl protease inhibitor solution 200 µl phosphatase inhibitor solution dissolved in 1 ml ddH2O Protease Inhibitor Solution 1 tablet of protease inhibitor (cOmplete™) dissolved in 1 ml ddH2O Stripping Buffer 5% no-fat dry milk powder 0,05% NaN₃ dissolved in 50 ml PBST 10x TAE Buffer 48.4 g Tris base 11.4 ml glacial acetic acid 20 ml 0.5 M EDTA dissolved in 800 ml ddH2O TE-buffer (Tris-EDTA buffer) 0,5 ml 1M Tris-HCl (pH8 or 7.5) (10 mM Tris-HCl) 0,1 ml 0,5 M EDTA (1 mM) 49,4 ml ddH2O 10x TGS Buffer 250 mM Tris 1.92 M glycine 1% SDS		2% FBS
200 µl phosphatase inhibitor solution dissolved in 1 ml ddH2O Protease Inhibitor Solution 1 tablet of protease inhibitor (cOmplete™) dissolved in 1 ml ddH2O Stripping Buffer 5% no-fat dry milk powder 0,05% NaN₃ dissolved in 50 ml PBST 10x TAE Buffer 48.4 g Tris base 11.4 ml glacial acetic acid 20 ml 0.5 M EDTA dissolved in 800 ml ddH2O TE-buffer (Tris-EDTA buffer) 0,5 ml 1M Tris-HCl (pH8 or 7.5) (10 mM Tris-HCl) 0,1 ml 0,5 M EDTA (1 mM) 49,4 ml ddH2O 10x TGS Buffer 250 mM Tris 1.92 M glycine 1% SDS		0.1% propidium iodide
dissolved in 1 ml ddH2O Protease Inhibitor Solution 1 tablet of protease inhibitor (cOmplete™) dissolved in 1 ml ddH2O Stripping Buffer 5% no-fat dry milk powder 0,05% NaN₃ dissolved in 50 ml PBST 10x TAE Buffer 48.4 g Tris base 11.4 ml glacial acetic acid 20 ml 0.5 M EDTA dissolved in 800 ml ddH2O TE-buffer (Tris-EDTA buffer) 0,5 ml 1M Tris-HCl (pH8 or 7.5) (10 mM Tris-HCl) 0,1 ml 0,5 M EDTA (1 mM) 49,4 ml ddH2O 10x TGS Buffer 250 mM Tris 1.92 M glycine 1% SDS	PI Lysis Buffer	200 μl protease inhibitor solution
Protease Inhibitor Solution 1 tablet of protease inhibitor (cOmplete [™]) dissolved in 1 ml ddH2O Stripping Buffer 5% no-fat dry milk powder 0,05% NaN₃ dissolved in 50 ml PBST 10x TAE Buffer 48.4 g Tris base 11.4 ml glacial acetic acid 20 ml 0.5 M EDTA dissolved in 800 ml ddH2O TE-buffer (Tris-EDTA buffer) 0,5 ml 1M Tris-HCl (pH8 or 7.5) (10 mM Tris-HCl) 0,1 ml 0,5 M EDTA (1 mM) 49,4 ml ddH2O 10x TGS Buffer 250 mM Tris 1.92 M glycine 1% SDS		200 μl phosphatase inhibitor solution
Stripping Buffer 5% no-fat dry milk powder 0,05% NaN3 dissolved in 50 ml PBST 10x TAE Buffer 48.4 g Tris base 11.4 ml glacial acetic acid 20 ml 0.5 M EDTA dissolved in 800 ml ddH2O TE-buffer (Tris-EDTA buffer) 0,5 ml 1M Tris-HCl (pH8 or 7.5) (10 mM Tris-HCl) 0,1 ml 0,5 M EDTA (1 mM) 49,4 ml ddH2O 10x TGS Buffer 250 mM Tris 1.92 M glycine 1% SDS		dissolved in 1 ml ddH2O
Stripping Buffer 5% no-fat dry milk powder 0,05% NaN3 dissolved in 50 ml PBST 10x TAE Buffer 48.4 g Tris base 11.4 ml glacial acetic acid 20 ml 0.5 M EDTA dissolved in 800 ml ddH2O TE-buffer (Tris-EDTA buffer) 0,5 ml 1M Tris-HCl (pH8 or 7.5) (10 mM Tris-HCl) 0,1 ml 0,5 M EDTA (1 mM) 49,4 ml ddH2O 10x TGS Buffer 250 mM Tris 1.92 M glycine 1% SDS	Protease Inhibitor Solution	1 tablet of protease inhibitor
0,05% NaN ₃ dissolved in 50 ml PBST 48.4 g Tris base 11.4 ml glacial acetic acid 20 ml 0.5 M EDTA dissolved in 800 ml ddH2O TE-buffer (Tris-EDTA buffer) 0,5 ml 1M Tris-HCl (pH8 or 7.5) (10 mM Tris-HCl) 0,1 ml 0,5 M EDTA (1 mM) 49,4 ml ddH2O 10x TGS Buffer 250 mM Tris 1.92 M glycine 1% SDS		(cOmplete [™]) dissolved in 1 ml ddH2O
dissolved in 50 ml PBST 48.4 g Tris base 11.4 ml glacial acetic acid 20 ml 0.5 M EDTA dissolved in 800 ml ddH2O TE-buffer (Tris-EDTA buffer) 0,5 ml 1M Tris-HCl (pH8 or 7.5) (10 mM Tris-HCl) 0,1 ml 0,5 M EDTA (1 mM) 49,4 ml ddH2O 10x TGS Buffer 250 mM Tris 1.92 M glycine 1% SDS	Stripping Buffer	5% no-fat dry milk powder
10x TAE Buffer 48.4 g Tris base 11.4 ml glacial acetic acid 20 ml 0.5 M EDTA dissolved in 800 ml ddH2O TE-buffer (Tris-EDTA buffer) 0,5 ml 1M Tris-HCl (pH8 or 7.5) (10 mM Tris-HCl) 0,1 ml 0,5 M EDTA (1 mM) 49,4 ml ddH2O 10x TGS Buffer 250 mM Tris 1.92 M glycine 1% SDS		0,05% NaN₃
11.4 ml glacial acetic acid 20 ml 0.5 M EDTA dissolved in 800 ml ddH2O TE-buffer (Tris-EDTA buffer) 0,5 ml 1M Tris-HCl (pH8 or 7.5) (10 mM Tris-HCl) 0,1 ml 0,5 M EDTA (1 mM) 49,4 ml ddH2O 10x TGS Buffer 250 mM Tris 1.92 M glycine 1% SDS		dissolved in 50 ml PBST
20 ml 0.5 M EDTA dissolved in 800 ml ddH2O TE-buffer (Tris-EDTA buffer) 0,5 ml 1M Tris-HCl (pH8 or 7.5) (10 mM Tris-HCl) 0,1 ml 0,5 M EDTA (1 mM) 49,4 ml ddH2O 10x TGS Buffer 250 mM Tris 1.92 M glycine 1% SDS	10x TAE Buffer	48.4 g Tris base
dissolved in 800 ml ddH2O TE-buffer (Tris-EDTA buffer) 0,5 ml 1M Tris-HCl (pH8 or 7.5) (10 mM Tris-HCl) 0,1 ml 0,5 M EDTA (1 mM) 49,4 ml ddH2O 10x TGS Buffer 250 mM Tris 1.92 M glycine 1% SDS		11.4 ml glacial acetic acid
TE-buffer (Tris-EDTA buffer) 0,5 ml 1M Tris-HCl (pH8 or 7.5) (10 mM Tris-HCl) 0,1 ml 0,5 M EDTA (1 mM) 49,4 ml ddH2O 10x TGS Buffer 250 mM Tris 1.92 M glycine 1% SDS		20 ml 0.5 M EDTA
mM Tris-HCl) 0,1 ml 0,5 M EDTA (1 mM) 49,4 ml ddH2O 10x TGS Buffer 250 mM Tris 1.92 M glycine 1% SDS		dissolved in 800 ml ddH2O
0,1 ml 0,5 M EDTA (1 mM) 49,4 ml ddH2O 10x TGS Buffer 250 mM Tris 1.92 M glycine 1% SDS	TE-buffer (Tris-EDTA buffer)	0,5 ml 1M Tris-HCl (pH8 or 7.5) (10
49,4 ml ddH2O 10x TGS Buffer 250 mM Tris 1.92 M glycine 1% SDS		mM Tris-HCl)
10x TGS Buffer 250 mM Tris 1.92 M glycine 1% SDS		0,1 ml 0,5 M EDTA (1 mM)
1.92 M glycine 1% SDS		49,4 ml ddH2O
1% SDS	10x TGS Buffer	250 mM Tris
		1.92 M glycine
dissolved in 800 ml ddH2O		1% SDS
		dissolved in 800 ml ddH2O

3.1.3. Cell culture materials

Table 3-4 Cell culture materials

Name	Supplier	Cat. No
Cell scraper	Roth	EKX9.1
CASYcups	OLS OMNI LS	638326
Casy ton	OLS OMNI LS	2501037
DMEM high glucose	Thermo Fisher	41966052
DMEM GlutaMax	Life Technologies	61965059
Dialysed FBS one shot 50 ml	Life Technologies	A3382001
Fetal Calf Serum	Sigma Aldrich	10500064
L-Arginine HCI 13C6	Silantes	201203902
L-Arginine HCI 13C,15N	Silantes	201603902
4,4,5,5-D4-L-Lysine 2HC 2H	Silantes	211103913
L-Lysine HCl 13C,15N	Silantes	211603902
Millex sterile filter	Merck	SLGV033RS
PBS	Thermo Fisher	10010056
Penicillin-Streptomycin	Sigma Aldrich	P4333-100ML
RPMI 1640 Medium	Thermo Fisher	765656
Single-use syringe luer lock	VWR	613-2006
SILAC DMEM high glucose	Enzo	AES-0420
Spin filter sterile	VWR	516-0233
Reagent Reservoirs	VWR	613-1174
75 cm ² Cell Culture Flask	Greiner	658175
175 cm ² Cell Culture Flask	Sigma Aldrich	C7481-50EA
6 Well Cell Culture Plate	Greiner	657160
	CELLSTAR®	
24 Well Cell Culture Plate	Greiner	662160
	CELLSTAR®	
96 Well Cell Culture Plate	Greiner	655180
	CELLSTAR®	
5 ml Serological pipettes	Starlab	E4860-0511
10 ml Serological pipettes	Starlab	E4860-1011
25 ml Serological pipettes	Starlab	E4860-2511

3.1.4. Cell lines

Table 3-5 Cell lines used in this study

Cell line	organism	Tissue	Cell type	Culture medium
CL45 ¹⁸¹	Mus	Bone marrow	macrophage	DMEM GlutaMax
	musculus			+ 10% FBS
CL13 ¹⁸¹	Mus	Bone marrow	macrophage	DMEM GlutaMax
	musculus			+ 10% FBS
H441 ¹⁸²	Homo	Lung (NSCLC)	epithelial	RPMI 10% (21875-091)
(RRID:CVCL_1561)	sapiens,			+ 10% FBS
	human			
MEF ¹⁸³	Mus	Embryo/embryo	fibroblast	DMEM high glucose
(RRID:CVCL_4240)	musculus	fibroblast		+ 10% FBS
Pfa1 ¹²⁷	Mus	Embryo/embryo	fibroblast	DMEM high glucose
	musculus	fibroblast		+ 10% FBS
RAW264.7 ¹⁸⁴	Mus	Abelson murine	macrophage	DMEM GlutaMax +
(RRID:CVCL_0493)	musculus	leukemia virus- induced tumour		10% FBS
THP1 ¹⁸⁵	Homo	Peripheral blood	monocyte	RPMI 1640 Medium
(RRID:CVCL_0006)	sapiens			+ 10% FBS

3.1.5. Consumable materials and chemicals

Table 3-6 Consumable materials and chemicals

Name	Supplier	Cat. No
Acrylamide/Bis-acrylamide, 30% solution	Roth	3029.2
Agarose Biozym	Biozym Scientific	840000
Amersham Hybond P 0.45 PVDF	GE Healthcare	10600023
Amicon Ultra-15, 3 kDa	Sigma Aldrich	UFC900308
Ammonium persulfate (APS)	Sigma Aldrich	431532
Azidohomoalanine (AHA)	AnaSpec	S8636-100ML
Bacto-tryptone	VWR	J859
Beta-estradtiol	Sigma Aldrich	E2758
Blotting Pad	VWR	732-0606
BODIPY™ 581/591 C11	Invitrogen	D3861
HyClone Bovine Serum Albumin	Thermo Fisher	777600
Calcium chloride (CaCl ₂)	Sigma Aldrich	C1016-500G

CL-Xposure Film	Thermo Fisher	34089
Cover slips	VWR	6311577
Developer G153 A	Agfa	#HT536
Developer G153 B	Agfa	#HT536
DMSO	PAN Biotech	P60-36720100
Dithiothreitol (DTT)	VWR	441496P
EDTA	VWR	1.084.520.250
Entellan	Merck	107961.0500
Eosin G-solution 0.5%	VWR	1.09844.1000
Ethanol	VWR	20.821.330
FACS tube	VWR	734-0000
Ferrostatin-1 (Fer-1)	Sigma Aldrich	SML0583-5MG
Fixer G354	Agfa	#2828Q
Hematoxylin solution	Sigma Aldrich	MHS32-1L
Histology cassettes	Simport Scientific	13226358
Immersion oil	Leica	11513838
Immobilon Classico Western HRP	Merckmillipore	WBLUC0500
substrate		
Isopropanol	Roth	EG-No. 200-661-7
L-Proline	Sigma Aldrich	P5607-25G
Leucin	Enzo	AES-0420
Methanol	Sigma Aldrich	34860-2.5L-R
ML210	Sigma Aldrich	SML0521-5MG
Nonfat dried milk powder	PanReac AppliChem	8V015284
NuPAGE LDS Sample Buffer (4x)	Thermo Fisher	NP0008
Sodium pyruvate	Sigma Aldrich	S8636-100ML
N,N,N',N'-Tetramethylethylenediamine	Sigma Aldrich	T9281
(TEMED)		
Tris	VWR	1,083,872,500
Tris-HCI	VWR	648313-250
Triton X-100	VWR	1,086,031,000
Tween-20	VWR	0777-1L
Paraformaldehyd (PFA)	Merck	4022536045948
PCR master mix	New England Biolabs	M3003E
Phosphatase Inhibitors (PhosSTOP TM)	Sigma Aldrich	4906837001

Phorbol 12-myristate-13-acetate (PMA)	Sigma Aldrich	1658
Polysine slides	Thermo Scientifc	J2800AMZ
Ponceau S	Sigma Aldrich	P3504-50G
Potassium chloride (KCI)	Sigma Aldrich	7447-40-7
L-Proline	Sigma Aldrich	P5607-25G
Propidium iodide (PI)	Bectin Pharma	14289
Protease Inhibitors (cOmplete [™])	Sigma Aldrich	4693132001
RSL3	Selleckchem	S8155
Sodium Azide (NaN ₃)	Sigma Aldrich	S2002-100G
Sodium chloride (NaCl)	VWR	1,064,045,000
Sodium hydrogen phosphate (Na ₂ HPO ₄)	VWR	1,065,861,000
Sodium pyruvate	Sigma Aldrich	S8636-100ML
Sodium selenite	Sigma Aldrich	S5261
SYBR Safe stain	Thermo Fisher	S33102
Tamoxifen (4-hydroxy-tamoxifen/4-OHT)	Biomol GmbH	Cay14854-5
Tris	VWR	1.083.872.500
Tris HCI	VWR	648313-250
Triton-X-100	VWR	1.086.031.000
Trypsin-EDTA (1X)	Thermo Fisher	745065
Urea	Sigma Aldrich	U5378-1KG
Xylene	Applichem	251769.2714
100 bp DNA Ladder	New England	N3231S
	Biolabs	
3 kDa, Amicon Ultrafiltration tube	Sigma Aldrich	UFC900308
500 μl centrifuge tube	VWR	211-2612
1.5 ml centrifuge tube	VWR	211-2135
2 ml centrifuge tube	VWR	211-0034
15 ml Falcons	Starlab	E1415-0200
50 ml Falcons	Starlab	E1450-0200
200 μl Graduated Filer Tip, Refill	Starlab	S1120-8710
1000 μl Graduated Filer Tip, Refill	Starlab	S1126-7710
10 μl pipet tips	VWR	613-0364
200 μl pipet tips	VWR	612-5755
1000 μl pipet tips	VWR	612-5756
5x Trans-Blot Turbo Transfer Buffer	Bio-Rad	1704270
10x TGS (Tris/Glycine/SDS Buffer)	Bio-Rad	161-0772

3.1.6. Enzymes and enzyme buffers

Table 3-7 Enzymes and enzyme buffers used in this study

Enzymes	Supplier	Cat. No
Pfu PCR Mastermix	Biotechrabbit	350300201
Proteinase K	VWR	1.245.680.100

3.1.7. Kits

Table 3-8 Kits used in this study

Name	Supplier	Cat. No
CellTiter-Blue® Cell Viability Assay	Promega	G8081
Click chemistry capture kit	Jena	CLK-1065
	Bioscience	
DC Protein Assay	Bio-Rad	774985
Human XL Cytokine Array Kit	R&D system	ARY022B
Mouse XL Cytokine Array Kit	R&D system	ARY028

3.1.8. Laboratory equipment

The laboratory equipment used for this study was obtained from AGFA, Amersham Biosciences, BD Bioscience, BINDER, Eppendorf, Bio-Rad, Enspire, Leica, Stuart, TECHNE, Thermo Fisher Scientific and WTW.

Table 3-9 Equipment used in this study

Device	Company
AGFA CP1000 X-Ray Film Processor	AGFA
BD LSR-Fortessa Analyzer	BD Biosciences
Binder CB CO2 incubator	BINDER
CASY Cell Counter + Analyzer	OLS OMNI Life Science
Centrifuge 5810 R	Eppendorf
Centrifuge 5430 R	Eppendorf
Centrifuge 5418 R	Eppendorf
ChemiDoc [™] MP Imaging system	Bio-Rad
Dri-Block DB-2d	TECHNE
Histology Flattening Table HI 1220	Leica
Histology Water Bath HI 1210	Leica

Hypercassette	Amersham Biosciences
Mini-PROTEAN® Glass Plates	Bio-Rad
Mini-PROTEAN® Short Plates	Bio-Rad
Mini-PROTEAN® Tetra System	Bio-Rad
Mini See-saw Rocker	Stuart
Multimode Plate Reader	Enspire
Nanodrop 8000c	Thermo Fischer
Paraffin Embedding Station EG 1150H	Leica
pH Meter inoLab® 7110	WTW
Rotary Microtome RM 2255	Leica
Rotator SB3	Stuart
See-saw rocker SSM4	Stuart
Thermo Cycler T100 [™]	Bio-Rad
Trans-Blot® Turbo™ Mini-size nitrocellulose	Bio-Rad
Trans-Blot® Turbo™ Mini-size Transfer Stacks	Bio-Rad
Trans-Blot® Turbo™ Transfer System	Bio-Rad

3.1.9. **Primers**

Table 3-10 Primers used in this study

Gene	Primer sequence 5' → 3'
GPX4 WT F	CTG CAA CAG CTC CGA GTT C
GPX4 C	CTG CAA CAG CTC CGA GTT C
GPX4 Mut F	CCA GTA AGC AGT GGG TTC TC
PDX1 Cre F	CTG GAC TAC ATC TTG AGT TGC
PDX1 Cre R	GGT GTA CGG TCA GTA AAT TTG

3.2. Methods

3.2.1. Cell culture

3.2.1.1. Cultivation and passaging of cells

The immortalised bone marrow-derived macrophage cell lines (iBMDMs) provided by E. Latz/ F. Schmidt as well as RAW264.7 macrophages were cultured in DMEM GlutaMax. The medium used for culturing Pfa1 and mouse embryonic fibroblast (MEF) cells was DMEM high glucose. H441 and THP1 cells were grown in RPMI medium. All media contained 10% heat-inactivated

fetal calf serum (FCS) and 1% Penicillin-Streptomycin. Adherent cells were washed with 3 ml

of 2xPBS and detached with 2 ml Trypsin-EDTA. After 5 minutes of incubation at 37°C, 8 ml of

culture medium was added and 9 ml were replaced with 11 ml of fresh medium. The

macrophage cell lines had to be scraped off the bottom since they would not detach upon

incubation with trypsin. Depending on the growth rate, the cells were split 1:10 in 75 cm² flasks

every two or three days. Routinely, cells were cultured at 37°C with 5% CO₂.

DMEM glutamax: DMEM, 10% FBS, 1% Penicillin-Streptomycin DMEM high glucose: DMEM, 10% FBS, 1% Penicillin-Streptomycin

RPMI 1640: 10% FBS, 1% Penicillin-Streptomycin

3.2.1.2. Cell count measurement

After the cells had been detached with trypsin, 100 µl of cell suspension was added to a

CASYcup with 10 ml of counting CASYton solution. The number of cells was then detected by

the CASY Cell Counter and Analyzer (OLS OMNI Life Science). The cells are detected

electrically as they pass through a measuring pore. Viable cells are able to exclude the electric

current, whereas dead cells cannot exclude the current and are in the following detected with

the volume of their nucleus.

3.2.1.3. Cryopreservation and thawing

Cells were cultured in 175 cm² cell culture flasks for cryopreservation until they reached 80%

confluency. After trypsinisation, cells were centrifuged at 1200 rpm for 3 minutes. The

supernatant was subsequently discarded, and cells were resuspended in a freezing medium.

Cryovials were placed in isopropanol-freezing containers at -80°C overnight and preserved at

-150°C for long-term storage.

The cryovials were thawed at room temperature and added to 10 ml of culture medium. To

eliminate the DMSO of the freezing medium, the cells were centrifuged at 1200 rpm for 3

minutes and resuspended in 12 ml of culture medium. Cells were then cultured in 75cm2 cell

culture flasks as described above.

Freezing medium: FCS containing 10% DMSO

3.2.1.4. Cell viability assay

The viability of the cells was detected by using the CellTiter-Blue (CTB) cell viability assay.

Viable cells reduce the non-fluorescent resazurin dye to the fluorescent product resorufin,

46

which can be detected at a wavelength of 530-560nm by a plate reading fluorometer or a spectrophotometer.

For the viability assays of the cell lines Pfa1, MEF and H441, 2,000 (Pfa1) / 5,000 (MEF) / 10,000 (H441) cells per 100 μ l were seeded one day prior to treatment in 96-well plates. Cells were incubated 24 hours after seeding with a 1:3 dilution series of RSL3 (highest concentration: 1 μ M) and Fer-1 (highest concentration: 5 μ M) for 24 hours. The azidohomoalanine (AHA) viability assay was performed with 100 μ M as the highest concentration. Ferroptosis induction with 1 μ M tamoxifen and/or 5 μ M Fer-1 was started when cells were seeded (total incubation time: 48hr).

After 1.5 to 4 hours incubation with 5 μ I of CTB per well, the absorbance was measured by a Multimode Plate Reader (EnVision). Treatment conditions were compared to control conditions with DMSO.

3.2.1.5. Ferroptotic supernatants

Ferroptotic supernatants were obtained from cultured H441, MEF and Pfa1 cells that succumbed to ferroptosis. For these experiments, 100,000 MEF cells, 200,000 H441 cells and 25,000 Pfa1 cells were seeded in 6-well plates. Ferroptosis induction in MEF and H441 was attained by treatment with 1 μ M RSL3 and rescued with 5 μ M Fer-1 24 hours after seeding. Supernatants were collected 24 hours after treatment. Ferroptosis of Pfa1 cells was triggered with 1 μ M of 4-Hydroxytamoxifen (4-OHT; tamoxifen) and equally rescued with Fer-1. In this case, supernatants were collected and filtered to eliminate cell debris 72 hours after seeding. Untreated cells were used as a control condition.

3.2.2. Nucleic acid techniques

3.2.2.1. DNA Isolation

DNA isolation was performed to verify the genotypes of the different mouse breeding lines in the in vivo experiment. Firstly, ear biopsies of the mice were lysed overnight at 56° C in 200 µl of lysis buffer containing 100 mM Tris/HCl, 5 mM EDTA, 0,2% SDS, 200 mM NaCl and 2 µl proteinase K. After the lysis, 200 µl of 100% isopropanol was added and samples were centrifuged at 13,000 rpm for one minute. This resulted in the precipitation of the DNA. The remaining supernatant could then be discarded. Afterwards, 200 µl of 75% ethanol was added to the DNA pellet and the samples were again centrifuged for one minute at 13,000 rpm to rid them of undesirable protein contamination. Lastly, 200 µl TE-buffer was added to the isolated DNA and further used for PCR (see 3.2.2.3.).

3.2.2.2. RNA Isolation

RNA isolation was performed with iBMDM cell lines CL13 and CL45 as well as with RAW264.7 cells. Before the stimulation of the macrophages with 1 ml of ferroptotic supernatant, 400.000 to 500.000 cells were seeded in 6-well plates one day in advance. After 24 hours of stimulation, cells were placed on ice and washed with 1 ml of sterile PBS. Consequently, each well was incubated for 5 to 10 minutes with 350 μ l RA1 buffer (Macherey and Nagel kit) containing 20 mM DTT. Further steps of the isolation process were followed as instructed by the manufacturer. The isolated RNA was eluted with 40 μ l nuclease-free H₂O and measured by the NanoDrop 8000 (Thermo Fisher).

3.2.2.3. PCR/Genotyping

PCR was performed to verify the genotypes of the mouse breeding line. The melting temperature of oligonucleotides was adapted for each primer pair. The PCR Master Mix was used for the preparation of PCR samples and added to the according primers. The duration of elongation was adapted to the size of the PCR product (1 min/kb).

Table 3-11 Components used for PCR

Component	Amount
PCR Master mix	25 μΙ
Forward primer	1 μΙ
Reverse primer	1 μΙ
DNA template	50-80 ng (2 μl)
Distilled water	Ad 50 μl

Table 3-12 PCR program for amplification of DNA fragments

Step	Time [sec]	Temp. [°C]	Cycle
Initial activation	120-180	94	1
Denaturation	30	94	
Annealing	30	primer specific	28-33
Elongation	size dependent	72	
Final elongation	300	72	1

3.2.2.4. Determination of nucleic acid concentration

Nucleic acid concentration and purity of RNA were measured by NanoDrop 8000 (Thermo Fisher). The purity of RNA was determined by the ratio of absorbance at 260 nm to 280/230

nm. A ratio of OD260/OD280 between 1.8 and 2.6 and a ratio of OD260/230 above 1.5 were considered as pure grade.

3.2.2.5. RNA Sequencing

Quality control and sequencing of the isolated RNA was performed by the Cologne Center for Genomics with the Illumina dye sequencing method following the Lexogne QuantSeq 3´ library preparation protocol (12,500 million reads per sample). Sequenced data was handed over to the CECAD Bioinformatics facility and presented to us as raw count data generated by Prerana Wagle. This data was analysed for differential expression using the negative binomial model DESeq2 for R Programming.

Before read count data can be used for differential gene expression analysis, a normalisation procedure needs to be applied to account for the technical biases of the sequenced reads. However, standard normalization methods, such as reads per kilobase of transcript per million mapped reads (RPKM) and fragments per kilobase of transcript per million mapped reads (FPKM), are not appropriate for analysing differential gene expression. In this study, DESeq2 was used to normalise data to account for two types of technical variation: library size (number of reads that map in a sample) and library composition bias. DESeq2 employs negative binomial modelling to account for variability in the variance between biological replicates (biological bias) within the same group. To this end, DESeq2 calculates the dispersion estimate for each gene as an additional parameter. As a result, non-differentially expressed genes will be more similar between the samples, and genes with high dispersion levels that are assumed to not follow modelling assumptions will be exposed. This can then be linked to a biological phenomenon. DESeq2 has been shown to have enhanced specificity and sensitivity in correctly identifying differentially expressed genes compared to other methods¹⁸⁶.

3.2.3. Protein Biochemistry

3.2.3.1. Protein lysation

The cells were washed twice with 1000 µl ice-cold PBS to remove any remaining serum. Consequently, cells were lysed with 80-100 µl lysis buffer containing protease inhibitor solution. The cells were scraped and transferred into microcentrifuge tubes. Cellular debris was removed by centrifuging the samples at 4°C for 20 minutes and 13,000 rpm. Lysates were stocked at -20°C until further use. The absorbance of each sample was measured at 750 nm with the Multimode Plate Reader (Enspire). The lowest value of absorbance was used as a reference to adjust protein concentration.

3.2.3.2. Bicinchoninic acid assay and sample preparation

The protein concentrations were determined through the DC Protein Assay (Bio-Rad) according to the manufacturer's instructions for the Microplate Assay Protocol. This colourimetric assay for protein concentration is based on the reaction of an alkaline copper tartrate solution and Folin reagent as published by Lowry¹⁸⁷.

The lowest value of absorbance was used as a reference to adjust protein concentration. Samples were measured at 750nm with the multimode plate reader (Enspire).

3.2.3.3. SDS PAGE

The sodium dodecyl sulfate polyacrylamide gel electrophoresis (SDS-PAGE) is a biochemical method to separate charged proteins by their molecular masses in an electric field. The anionic detergent SDS covers the intrinsic charge of the proteins and thereby provides a uniform charge-to-mass ratio. Before loading the gel, the samples are heated to denature the proteins. The proteins will be separated through a discontinuous electrophoretic system that consists of a stacking gel and a separating gel with different pore sizes due to differing polyacrylamide percentages and unequal pH levels. The stacking gel has a neutral pH level and smaller pore sizes in comparison to the separating gel (basic pH level). Under the application of an electric field, the negatively charged proteins will migrate in a running buffer (TRIS-Glycine-SDS-buffer) across the gel towards the positive electrode (anode). Small molecules migrate faster than larger ones.

Table 3-13 Electrophoresis gel composition

	Volume for 2 gels with 1 mm thickness		
Component	12.5% Separating gel	10% Separating gel	5% Stacking gel
MilliQ water	4.9 ml	6.1 ml	3 ml
30% Acrylamide	6.3 ml	5 ml	700 μΙ
1.5 M Tris, pH8.8	3.8 ml	3.8 ml	-
0.5 M Tris, pH6.8	-	-	1.3 ml
TEMED	7.5 µl	7.5 µl	5 μl
10% APS	75 μl	75 µl	33 µl

Gel electrophoresis of proteins was performed using the Mini-PROTEAN® Tetra Cell Electrophoresis and Blotting Apparatus by Bio-Rad. Stacking gel with a polyacrylamide

percentage of 5% and either 10% or 12.5% separation gel (Table 3-13) were used for SDS-

PAGE performances in this thesis. After mixing the samples with the sample buffer, they were

heated at 80°C for 10 minutes to denature the proteins. The sample wells of the polymerised

gel were loaded and collected for 30 minutes at 80V in 1X running buffer in the stacking gel.

This was followed by the separation of the proteins in the separation gel at 180 V for 1.5 hours.

Running buffer (1x): 25 mM TRIS, 192 mM Glycine, 0.1% SDS, pH8

Sample buffer: 400 µl LDS sample Buffer, 100 µl 1M DTT

3.2.3.4. Western Blot

The transfer of proteins is achieved through an electric current that pulls the negatively charged

proteins from the polyacrylamide gel in the direction of an anode into a polyvinylidene fluoride

(PVDF) or a nitrocellulose membrane. This was performed at 2.5 V for 7 minutes in 1x transfer

buffer with the Trans-Blot Turbo transfer system (Bio-Rad). In this thesis, only polyvinylidene

fluoride membranes were used. They were activated through immersion in 100% methanol for

45 seconds before the transblotting procedure. Subsequently, the membrane was placed in a

1x transfer buffer for 5 minutes. After the protein transfer, membranes were blocked with 5%

no-fat dry milk powder in phosphate-buffered saline with 0.1% Tween-20 (1x PBST) for 1 hour

at room temperature.

In the case of primary phospho-antibodies, the membrane was washed three times with 1x

PBST to remove the remaining milk powder before it was incubated with a primary antibody.

Generally, primary antibodies were incubated with the membranes overnight at 4°C. Following

three washing steps with 1xPBST for 10 minutes each, the membranes were incubated at

room temperature with the adequate secondary antibody conjugated with horseradish

peroxidase (HRP) (Table 3-2) for a minimum of 60 minutes. After three more washing steps

with 1x PBST, Western HRP Substrate (WBLUC0500, Merckmillipore) was added onto the

membrane. Chemiluminescence signals were detected through HRP enzyme reaction using

CL-Xposure films (34089, Thermo Fisher Science) and Curix 600 (AGFA).

In order to remove any remaining antibody complexes from the membrane, a stripping buffer

was applied for 10 minutes. The stripping was followed by three washing steps and 5% no-fat

dry milk powder 1x PBST blockage. Beta-Actin was used as a loading control in all cases.

Stripping buffer: 200 mM glycine, pH 2.5, 1% SDS

Transfer buffer (1x): 200 ml 5x transfer buffer, 500 ml nanopure water, 200 ml ethanol

PBST (10x): 80 mM Na₂HPO₄, 1.5 M NaCl, 20 mM KH₂PO₄, 30 mM KCl, 0.5% Tween-20

Blocking buffer: 5% no-fat dry milk powder dissolved in 50 ml 1x PBST

51

3.2.4. Quantitative Mass Spectrometry

All experimental steps were performed following instructions published by Eichelbaum and Krijgsveld with adjustments¹⁸⁸.

3.2.4.1. Cell culture preparation of samples

Before protein enrichment and digestion for mass spectrometry-based quantitative secretome analysis, Pfa1 cells underwent pulsed stable isotope labelling in cell culture (SILAC). In this experimental step, 1,000,000 Pfa1 cells were seeded into four 175 cm² flasks. The induction of ferroptosis was prompted by instant tamoxifen treatment (1 µM) in two out of four flasks. Cells were grown for 24 hours reaching a confluency of 80% and washed with pre-warmed PBS. Intracellular amino acids were depleted for 30 minutes by using an amino-acid-free SILAC medium obtained from Enzo. Penicillin Streptomycin (1%), dialysed FBS (10%), 100 mg Proline, Pyruvate (1:100) as well as 160 mM Leucin were added to SILAC medium before usage. After the depletion process, cells were incubated for 24 hours in a labelling medium containing 100 µM AHA, amounting to a total time of incubation of 48 hours. Intermediate SILAC amino acids (0,84 µl/ml ¹³C₆ -Arg; 1.46 µl/ml d₄ -Lys) were fed to control cells, while heavy SILAC amino acids (0,84 μ l/ml $^{13}C_6$ $^{15}N_4$ -Arg; 1.46 μ l/ml $^{13}C_6$ $^{15}N_2$ -Lys) were incubated with knock-out Pfa1 cells. Supernatants from both conditions were collected, centrifuged at 12,000 rpm for 5 minutes and filtered to get rid of cellular debris. For the prevention of proteolysis, one pill of Complete 50x protease inhibitor was added to the supernatant before freezing at -80°C.

3.2.4.2. Enrichment of newly synthesised proteins

In this step a cu(I)-catalysed Azide-Alkyne click chemistry reaction was performed to bind all labelled proteins in the samples to alkylated agarose beads. This allowed for stringent washing and the subsequent elimination of serum proteins. In this reaction, the methionine analogue AHA reacted as an azide-functionalised molecule with washed alkylated agarose beads and resulted in the formation of a stable conjugate crosslinked via a triazole moiety. The presence of a metal catalyst (oxidation state I) is essential for this reaction since terminal alkynes are fairly unreactive towards azides. The thawed supernatant was first concentrated in 15 ml ultrafiltration tubes (cut off: 3kDa) to a volume of 400 µl by centrifugation at 4000 g. The click chemistry reaction was conducted following the manufacturer's instructions from the click chemistry capture kit obtained from Jena Bioscience with slight alterations. 100 µl of resin was used per reaction and washed with 900 µl of ultrapure water (UPW). The 400 µl concentrated

medium was added to 400 μ l of Urea lysis buffer before adding the mix to the 100 μ l of washed resin. To catalyze the reaction, 800 μ l of a 2x catalyst solution containing 835 μ l UPW, 125 μ l Reaction Additive 1 and 20 μ l Copper(II)sulfate were added and rotated end-over-end for 18 hours at room temperature.

3.2.4.3. Reduction and Alkylation of resin-bound proteins and digestion

The resin-bound proteins were centrifuged for 5 minutes at 1000 g to dispose of the residual lysis buffer remaining in the tube. This step was repeated with 900 μ I UPW to avoid clumping in a potential interaction with the SDS buffer. After 500 μ I SDS buffer and 5 μ I 1M DTT were added to the remaining resin, it was heated at 70°C for 15 minutes. To ensure homogeneity of the SDS buffer, it is important to warm it to room temperature before usage. The heating process was followed by a cooling period (at room temperature) of 15 minutes. The resin was centrifuged again for 5 minutes at 1000 g and the remaining supernatant was discarded. Subsequently, 500 μ I 40 mM-Chloracetamine-SDS wash (CAA) was added to the resin and incubated for 30 minutes in the dark.

The click chemistry reaction between the agarose beads and the proteins allowed for stringent washing of the proteins to rid the resin of serum and other background proteins. For this process, a spin column was loaded with the resin and placed in an epi rack. The resin was then washed with 20 ml of each of the following solutions: SDS wash buffer, 8 M urea/100 mM Tris-HCl (pH 8), 20% isopropanol, and 20% acetonitrile (ACN).

The first part of protein digestion was attained with the addition of 500 μ l digestion buffer (50 mM TEAB, 2 mM CaCl2, 10% ACN per ml buffer) to the capped spin column. The resuspended resin was then transferred to a clean tube and pelleted by centrifugation. In the following, 200 μ l buffer was left on the resin, while the rest was discarded. Lastly, 1 μ g/ml trypsin and 0.5 μ g/ml LysC were incubated with the resin at 37°C overnight in the shaker at 800 rpm.

3.2.4.4. Desalting and stage tips

Peptides were loaded onto Pierce C-18 tips which enable fast and efficient desalting of peptides before mass spectrometry analysis. To this end, resins were pelleted by centrifugation for 5 minutes at 1000 g to transfer the peptide-containing supernatant into a clean tube. The resin was washed again with 500 μ I UPW to collect the peptides remaining in the pellet. These were added to the previously aspirated supernatant and acidified with 20 μ I of 10% formic acid (FA). Stage tips were equilibrated by passing through sequentially 20 μ I of methanol, 20 μ I of 80% ACN containing 0,1% FA and 20 μ I of 0.1% FA (2600 rpm, 2 minutes). Subsequently, the samples were loaded onto the stage tip in 200 μ I portions (2600 rpm, 2 minutes). The passage

of 30 μ l of 0.1% FA and two times 30 μ l of 80% ACN enabled the elution of the peptides from the C-18 stage tip (2600 rpm, 3 minutes). Before sample submission in triplicates, stage tips were dried with the help of a syringe.

3.2.4.5. Mass Spectrometry analysis

Quality control and mass spectrometry-based quantification of submitted samples were performed by the Proteomics Facility of the CECAD. Data was further processed using MaxQuant 2.0.3. The provided data showed Intensities (log2) as well as ratios (log2) of all measured protein channels (M/L, H/L, H/M) of each sample. Perseus 189 (Perseus 1.6.15), a software platform to interpret protein quantification and interaction, and detect significant protein signatures, was used for normalisation and statistical analysis in collaboration with Dr. Julian Nüchel from the Center for Biochemistry, Cologne. In order to test for significant differences regarding the presence of proteins in the secretome of Pfa1 cells in WT and KO conditions, a one-way t-test was deployed and visualised using the Interactive Scientific Data Analysis tool Instant Clue¹⁹⁰. Perseus was further used for 1D Enrichment analysis with a determined threshold value of 0.5 which allowed for the analysis of functional enrichments of quantified proteins and the characterisation of enriched pathway categories. Protein-protein interaction networks were visualised using the STRING database (Search Tool for the Retrieval of Interacting Genes/Proteins) as they contribute to the comprehension of biological processes.

3.2.5. Cytokine Array

Cytokine immunoassays were performed as preliminary experiments by Jenny Stroh according to protocols from R&D systems. For this, 100,000 cells were seeded per cell line and treated for 24 hours with RSL3 (1 μ M) or left untreated. When investigating macrophages for cytokine secretion, THP1 cells and RAW264.7 cells were stimulated with untreated supernatants (control) and ferroptotic supernatants (RSL3 treatment) of H441 and MEFs 24 hours after seeding, respectively. In this step, Fer-1 (5 μ M) was added to prevent cell death of the macrophage cell lines. PMA was used before the experiment to differentiate human monocytes (THP1 cells) in cell culture into macrophages¹⁹¹.

This membrane-based approach allowed for the screening of selected human and murine cytokines and chemokines. When supernatants are incubated with the cytokine array nitrocellulose membranes containing cytokine-specific capture antibodies, target proteins present in human (H441) and murine (MEF) control and treatment-conditioned supernatants

bind to the membranes. Captured proteins are detected with biotinylated detection antibodies and visualised through chemiluminescent signals.

3.2.6. Flow Cytometry

Flow cytometry is a commonly used procedure to analyse cells. The cells pass one by one through the sheath fluid of a cytometer. Due to a laser beam, light is scattered in different directions as soon as cells pass the beam. The light that is scattered in a sideward direction is directly proportional to the cells' complexity and granularity. The more granules the cell has, the more side-scattered light (SSC) will be detected. Conversely, the forward-scattered light (FSC) is directly proportional to the size of the cell. Since fluorescent light can also be detected by a cytometer, fluorescent dyes or fluorescent-labelled antibodies can bind to the cells and therefore be used to acquire information about a specific cell population. SSC, FSC, as well as dye-specific fluorescence signals can be converted into digital signals by the correspondent detectors. This data set can then be processed by a computer software.

Fluorescent activated cell sorting (FACS) experiments were generally performed with 24-well plates. Plates were placed on ice and the medium of each well was transferred into FACS tubes. Samples were washed once with 1x PBST and detached by a 5-minute incubation with 200 μ l of trypsin. The detached cells were then added into each corresponding FACS tube and centrifuged for 5 minutes at 4°C at 1200 rpm. After the supernatants were discarded, 200 μ l of FACS buffer was used to resuspend the cell pellets.

To quantitatively determine the number of dead Pfa1 cells in differently treated samples, 5000 cells were seeded in 24-well plates and treated instantly with tamoxifen (1 μ M) and/or Fer-1 (5 μ M). After an incubation period of 72 hours, cell viability was measured using the fluorescent dye Propidium iodide (PI). For these experiments, 0,1% PI was added to the FACS buffer. In order to assess the intracellular levels of ROS in H441 and MEF cells, 25,000 cells were seeded in 24-well plates. While cell death was induced with 100 nM RSL3 24 hours after seeding and 5 hours before FACS analysis, 5 μ M Fer-1 were used to rescue cell death. The fluorescent dye Bodipy-C11 was incubated with the cells at 37°C for 30 minutes prior to FACS sample preparation as described above. In the case of fluorescent-labelled antibody (CD14) detection, samples were incubated in the dark with 100 μ I of antibody for 60 minutes at room temperature after centrifuging. Lastly, the samples were washed twice with 500 μ I of FACS buffer to avoid false results due to the remaining antibody and resuspended in 200 μ I of FACS buffer. For this, 500,000 iBMDMs (CL13 and CL45) and RAW264.7 were seeded in 6-well plates and stimulated for 24 hours with ferroptotic and control supernatants 24 hours after seeding.

FACS buffer: 50 ml 1x PBS, 2% FBS

PBST 10x: 80 mM Na₂HPO₄, 1.5 M NaCl, 20 mM KH₂PO₄, 30 mM KCl, 0.5% Tween-20

3.2.6.1. Analysis of data

FACS data was analysed using FlowJo software 10.6.2. All experimental data are presented as means \pm SEM using the GraphPad Prism 8 software. Comparisons were made by paired two-tailed t-test. A value of *p < 0.05 (**p < 0.01) was considered statistically significant. p > 0.05, *p < 0.03325, **p < 0.0021, ***p < 0.0002, ****p<0.0001.

3.2.7. Mouse work

Mice were maintained on a 12-hour light/dark cycle by Jenny Stroh with water and food ad labium throughout the project.

3.2.7.1. Mouse model

In this thesis, mice were genetically engineered according to the Cre-loxP-system and crossed following a systematic breeding pattern. This approach allowed for a site-specific recombination event through the cut of a specific DNA sequence in the double-stranded DNA at both loxP sites. In the case of this study, pancreatic and duodenal homeobox 1 (PDX-1) as a pancreas-specific protein ensured the pancreas-specific expression of Cre recombinase, while floxed GPX4 alleles targeted by Cre resulted in genetic GPX4 deletion and ferroptosis of pancreatic cells. PDX-1-Cre^{+/-} mice¹⁹² were initially crossed with GPX4^{FI/FI} mice¹⁹³. The offspring was then crossed again (PDX1-Cre; GPX4^{WT/FL}) and resulted in three different genotypes: PDX1-Cre; GPX4^{WT/WT}, PDX1-Cre; GPX4^{WT/FL}, PDX1-Cre; GPX4^{FL/FL}.

3.2.7.2. Histological techniques

3.2.7.2.1. Paraffin sectioning

Mice were sacrificed at 20 weeks of age by Jenny Stroh for the collection of the pancreas, spleen and lung. For histological analysis, paraffin sectioning was used. Resected organs were transferred to tissue cassettes and fixated in 4% paraformaldehyd (PFA) overnight for a maximum of 24 hours for preservation of cell structure and minimisation of autolytic processes. Dehydration and infiltration steps were performed by the histological department of the Manolis Pasparakis lab. For organ embedding, tissue blocks were transferred into the well of a base mould and immersed in paraffin. After solidification of the cubes at room temperature, paraffin blocks were cut into 4 μ m slices, mounted on individual microscope slides and dried overnight.

3.2.7.2.2. H&E staining

Hematoxylin and Eosin Y stainings (H&E) of tissue sections were performed following the protocol indicated below (see table 3-14). Whereas Hematoxylin stains negatively charged structures in the tissue and visualised them in blue colour, Eosin appeared in red. Initially, paraffin was removed by immersing the slides in xylene and ethanol. After rehydration and staining, sections were ultimately mounted in mounting medium and sealed with coverslips.

Table 3-14 H&E staining protocol

Step	Staining reagent	Time	Comment
1	Xylene	20 min	Deparaffinisation
2	100% EtOH	2 min	Deparaffinisation
3	96% EtOH	2 min	Deparaffinisation
4	75% EtOH	1 min	Deparaffinisation
5	tap water	1 min	Excess hematoxylin removal
6	Hematoxylin	4 min	nuclei staining
7	tepid tap water	short wash	Excess hematoxylin removal
8	tap water	15 min	
9	distilled H ₂ O	short wash	
10	Eosin	1 min	cytoplasm staining
11	tap water	rinse 7x	Excess eosin removal
12	75% EtOH	1 min	Dehydration
13	96% EtOH	1 min	Dehydration
14	100% EtOH	1 min	Dehydration
15	Xylene	1 min	removal of ethanol

4. Results

In the context of a large effort to better understand the immunomodulatory functions of ferroptosis, this study aims to explore different aspects of ferroptosis as an immunogenic form of cell death. Given the fact that cell death occurs in a plethora of human diseases and autoimmune disorders, as well as medical events including cancer^{8,168}, the elucidation of putative inflammatory processes triggered by ferroptosis as a type of lytic cell death constitutes an immensely promising repository for the pursuit of innovative treatment strategies and targeted immunotherapies. In this respect, the question arises as to whether an inflammatory stimulus could be caused by ferroptosis. To this end, it is of great interest to explore the nature of DAMPs and alarmins that are actively secreted or released by ferroptotic cells. In this thesis, quantitative secretome analysis was used to first study the immunogenic factors and molecules in ferroptotic supernatants that could potentially lead to cell death-induced inflammation. Secondly, inflammatory responses in bystander immune cells after ferroptotic cell death were investigated. For this purpose, 3'RNA sequencing enabled a precise analysis of alterations in gene expression and the corresponding transcriptome in murine macrophages in response to stimulation with ferroptotic supernatants. This experiment aimed to explore potential inflammatory signatures and pathways involved in ferroptosis. While assessing the link between inflammation and ferroptosis in vitro, inflammatory consequences of ferroptosis in vivo were also investigated. PDX1-Cre expressing mice were crossbred with floxed GPX4 mice (PDX1-Cre; GPX4^{flox/flox} mice) to obtain a targeted genetic knockout of GPX4 in the pancreas. This specific experimental setup was designed to observe the influence of GPX4 deletion on tissue homeostasis in vivo and to detect signs of inflammatory responses, such as immune cell infiltration.

4.1. Ferroptosis-inducible systems

4.1.1. Validation of a genetic model of ferroptosis induction in vitro

In order to explore the biological repercussions of ferroptosis and its immunological consequences in vitro, it was necessary to first establish an in vitro system that displays susceptibility to ferroptosis. PFa1^(flox/flox), an immortalised mouse embryonic fibroblast cell line with floxed GPX4 alleles was provided by Marcus Conrad and used to specifically delete the key enzyme GPX4 and to genetically induce ferroptosis¹²⁷. When treated with 4-Hydroxytamoxifen (4-OHT), GPX4 is knocked out (Figure 10A, 10B) and cell death occurs as visualised by PI incorporation rate (Figure 10C, 10D). Cell death was prevented in cells treated with tamoxifen and the ferroptosis-selective antioxidant Fer-1 (Figure 10C). The sole

application of Fer-1, however, did not show any effects on cell viability (Figure 10C). Collectively, the results convey that ferroptosis is inducible in this model through the genetic knockout of GPX4, which can be prevented through the application of the ferroptosis-specific antioxidant Fer-1.

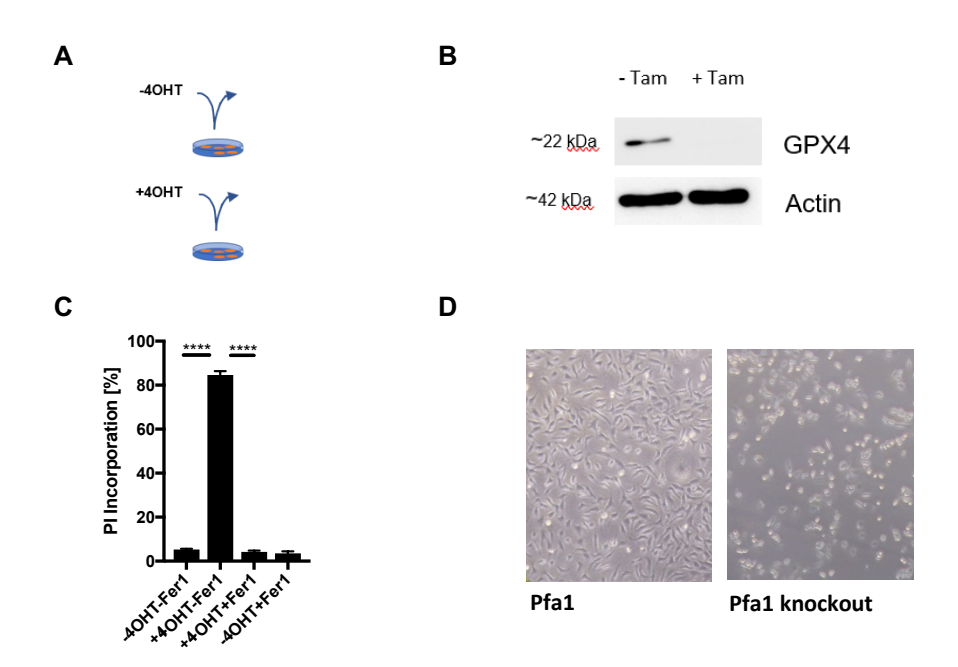


Figure 10. Ferroptosis is induced in murine Pfa1 cells through genetic knockout of GPX4. (A) Pfa1 cells were either treated with 4-OHT [1 μ M] for 72 hours or left untreated. (B) Western Blot analysis of Pfa cells demonstrates GPX4 knockout in cells treated with 4-OHT. β -actin was used as a loading control. (C) Quantification of cell viability in Pfa cells in the presence or absence of 4-OHT and Fer-1. PI staining was used to detect nonviable cells via FACS analysis. Mean values \pm SEM from biological triplicates (n = 3) are shown. (D) Visualisation of Pfa1 cell viability in cell culture \pm 4-OHT.

4.1.2. Validation of an in vitro model of ferroptosis induction through small molecules

Besides the inducibility of ferroptosis through a genetic knockout of key elements protecting from ferroptosis, induction of ferroptosis through small molecules, such as RSL3, provides an alternative way to attain cell death 129,137. RSL3 treatment of the human NSCLC cell line H441 (Figure 11A, 11B) and wildtype MEF cells (Figure 11C, 11D) leads to ferroptosis through GPX4 inhibition. Cell death was prevented in both cell lines through Fer-1. Whereas loss of cell viability in H441 cells could be observed at a concentration of 100 nM RSL3, for MEFs this seemed to be around 330 nM.

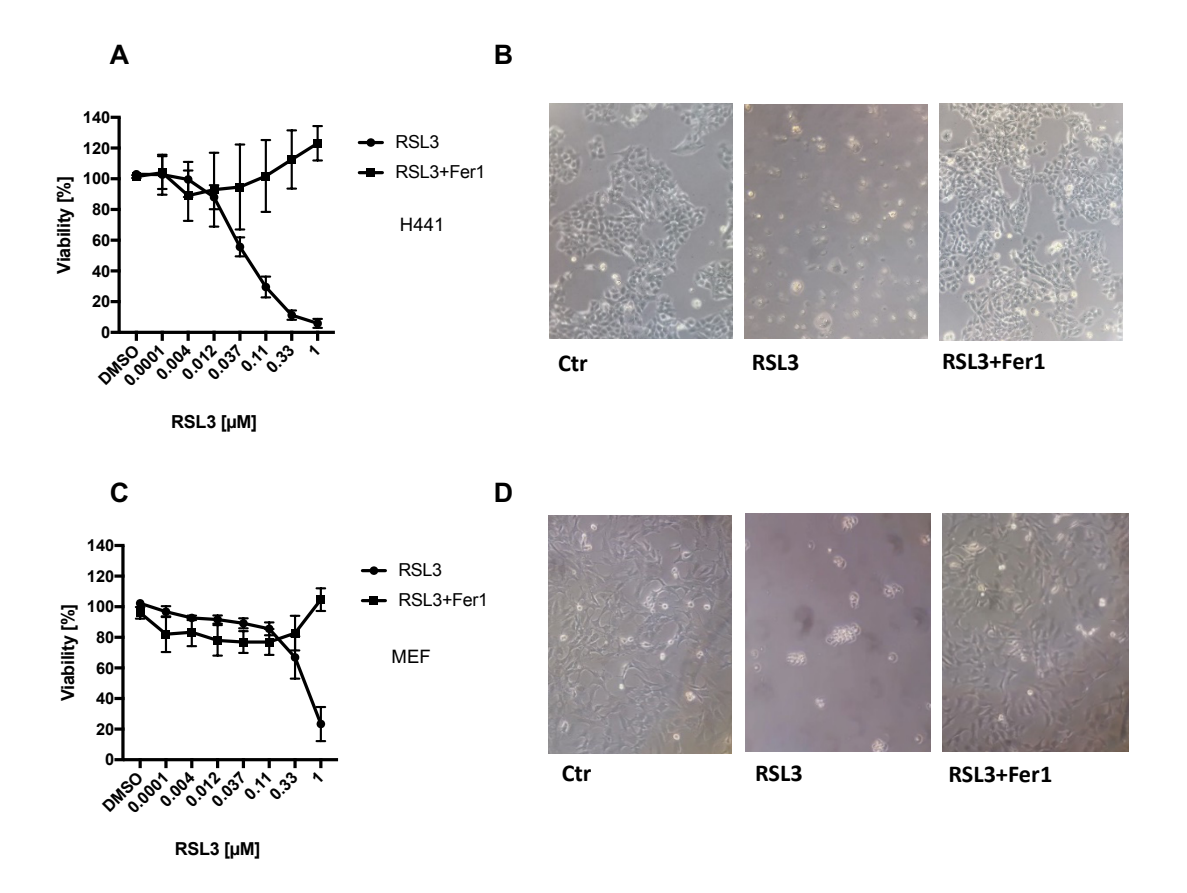


Figure 11. H441 and MEF cells display loss of cell viability upon GPX4 inhibition with RSL3. Cell viability was determined by Cell Titer Blue. (A) NSCLC cells (H441) cells were treated with DMSO, RSL3 [1 μ M] and Fer-1 [5 μ M] alone or in combination as indicated with a 1:3 dilution series for 24 hours. (B) Visualisation of H441 cell viability in cell culture \pm RSL3 and \pm Fer-1. (C) MEF cells were treated with DMSO, RSL3 [1 μ M] and Fer-1 [5 μ M] alone or in combination as indicated with a 1:3 dilution series for 24 hours. (D) Visualisation of MEF cell viability \pm RSL3 and \pm Fer-1.

The accumulation of intracellular lipid ROS upon ferroptosis induction was described to be one of the hallmarks of ferroptosis and is thought to be the executioner of death¹⁰⁷. Elevated levels of lipid ROS in dying cells are therefore highly indicative of ferroptotic cell death. To this end, the fluorescent dye C11-Boron-dipyrromethene (C11-BODIPY^{581/591}) was used to specifically stain for lipid peroxidation in both cell lines H441 and MEF and assessed through FACS analysis. Both cell lines displayed significantly increased levels of intracellular lipid ROS upon ferroptosis induction (Figure 12). In contrast, lipid ROS-levels decreased when treated with 5 µM of the ferroptosis inhibitor Fer-1.

Together, these data indicate that treatment with the GPX4-targeting small molecule RSL3 indeed induces lipid ROS and ferroptosis in the cellular systems tested here, and that cell death can be inhibited by Fer-1.

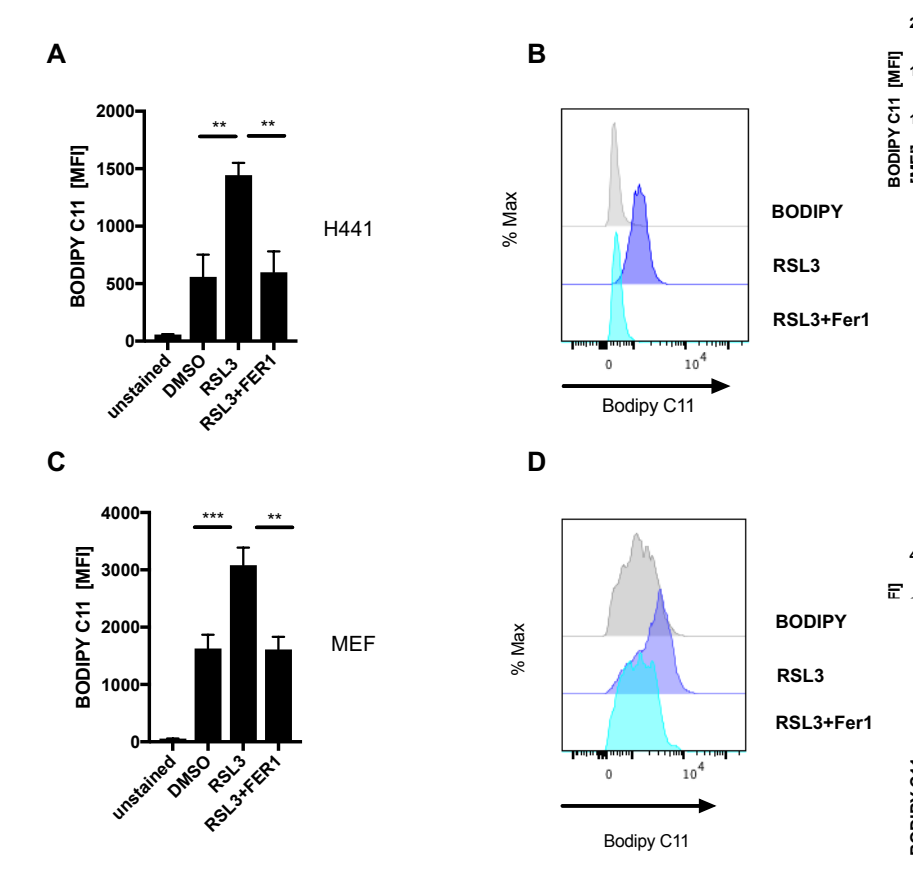


Figure 12. H441 and MEF cells exhibit increased levels of lipid ROS upon induction of ferroptosis which can be reverted by co-treatment with Fer-1.

(A and B) H441 cells were exposed to DMSO, RSL3 [100 nM] or RSL3 + Fer-1 [5 μ M] for 5 hours. During the last 30 minutes, 5 μ M C11-BODIPY^{581/591} was added to each well. Basal levels of intracellular lipid ROS were determined as MFI-mean fluorescence intensity by flow cytometry. Error bars show SEM. n=3. (C and D) MEF cells were exposed to DMSO, RSL3 [100 nM] or RSL3 + Fer-1 [5 μ M] for 5 hours. During the last 30 minutes, 5 μ M C11-BODIPY^{581/591} was added to each well. Basal levels of intracellular lipid ROS were determined as MFI-mean fluorescence intensity by flow cytometry. Error bars show SEM. n=3.

4.2. Characterisation of a ferroptosis-induced secretome

4.2.1. Cytokine release in ferroptosis

Having established that RSL3 treatment faithfully induces ferroptosis in H441 and MEF cells, the study next determined whether this resulted in the release of chemo- and cytokines. To this end, H441 cells and MEF cells were again treated with RSL3 to induce ferroptosis and the respective supernatants were collected. The small protein size of cytokines and chemokines spanning from 5 to 20 kDa impede the precise detection of these proteins through mass spectrometry. Due to the apparent risk of indistinct analysis, supernatants obtained after the induction of ferroptosis in H441 and MEF cells were analysed in the lab for chemo- and cytokine content in two sets of cytokine arrays (Figure 13A, 13B). Proteins are quantified using the same method as a chemiluminescent Western Blot.

Strikingly, both cell lines displayed intensified signals in comparison to the corresponding untreated control cells. In the human cell line H441 transforming growth factor α (TGF α) and

macrophage inflammatory protein 1α (MIP1 α) showed intensified signals, whereas vascular endothelial growth factor (VEGF) and Interleukin-1 receptor antagonist protein (IL1ra) appeared to be upregulated in the murine cell setting. This result suggests an increase in cytokine secretion triggered by ferroptosis and encouraged further investigations on a larger scale. Taken together, it seemed conceivable that a ferroptotic stimulus of yet unknown identity induces the release of immunological factors such as chemo- and cytokines from the dying cells themselves.

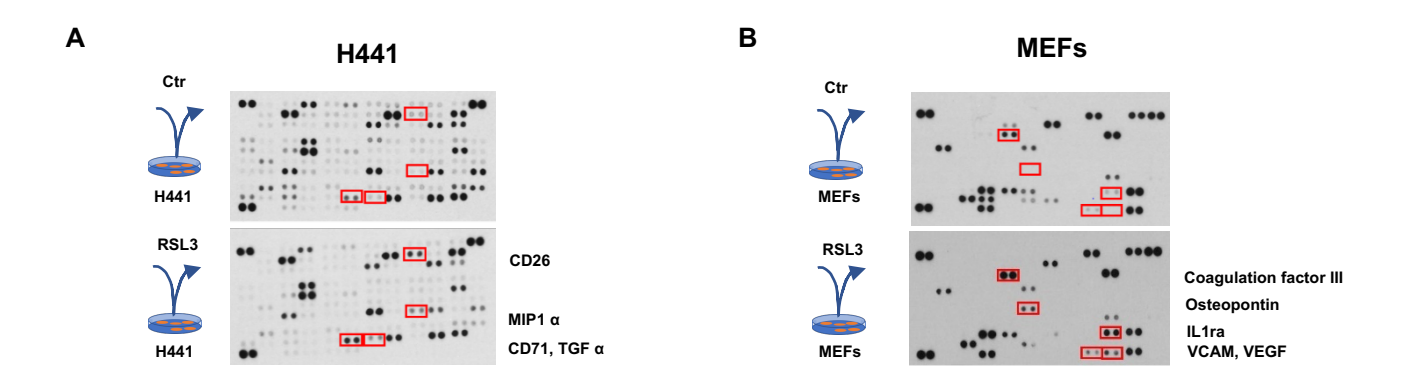


Figure 13. Cytokine array analysis of supernatants from ferroptotic H441 and MEF cells display augmented cytokine contents. (A) H441 cells were treated for 24 hours with RSL3 [1 μ M] or left untreated (Control; Ctr). Supernatants were filtered and chemokine/cytokine composition was analysed by the proteome profiler human XL Cytokine Array Kit (R&D). (B) MEF cells were treated for 24 hours with RSL3 [1 μ M] or left untreated (Ctr). Supernatants were filtered and chemokine/cytokine composition was analysed by the proteome profiler human XL Cytokine Array Kit (R&D).

4.2.2. Quantitative secretome analysis

In addition to the previous experiment, a mass spectrometry-based quantitative secretome analysis was conducted to further investigate the secretome of ferroptotic cells and their immunomodulatory potential. To this end, pulsed SILAC and click chemistry were combined to identify the molecules that are exposed to the surrounding environment of cells succumbing to plasma membrane rupture in the process of ferroptosis. Medically, it could be highly beneficial to gain an understanding of the inflammatory tissue microenvironment following ferroptosis to develop novel therapeutic strategies for the number of human pathologies associated with ferroptosis.

Generally, mass spectrometry (MS) is an analytical method for the identification of compounds based on the atomic or molecular masses of their constituents. In the field of biology and biochemistry, proteomics utilises MS as a tool to comprehend metabolic pathways as well as the structure and functions of proteins expressed by cells¹⁹⁴. In this thesis, a metabolic labelling technique was applied, as it provides an eminent method to characterise and quantitatively compare two or more conditions of cells, for example, treated vs. untreated cells or knockout

mutants vs. wildtype¹⁸⁸. SILAC labelling is achieved through the incorporation of isotopemarked amino acids into the proteome during translation of protein synthesis and cell proliferation in cell culture. In this experimental setup, amino acids carrying a light isotope (14N, 12C) were incubated with healthy proliferating Pfa1 cells (control condition), whilst amino acids with heavy isotopes (15N instead of 14N and/or 13C instead of 12C) were administered into cell culture of Pfa1 cells with the induced knockout of GPX4 (knockout condition). Amino acids that are most commonly used for protein labelling are arginine and lysine. For analysis, proteins could quickly be combined into one sample after cell cultivation, since the two cell conditions had been rendered metabolically distinguishable (Figure 14). This is highly advantageous for the elimination of confounding factors in the further course of sample preparation 195,196. Although proteins containing heavy amino acids differ in their isotopic composition, they do not act differently from their "light" analogues during sample preparation, chromatography, or mass spectrometry analysis. The isotope signature of the proteins accomplished by SILAC labelling is essential for the relative quantification of proteins following MS. If samples of knockout and control conditions are prepared in a ratio of 1:1, a signal pair with a specific mass difference can be obtained for each peptide providing a ratio between the two conditions. The relative ratios of the peptide signals in the mass spectrum correspond to the ratio of the peptides from the sample that are to be compared, which allows for quantification.

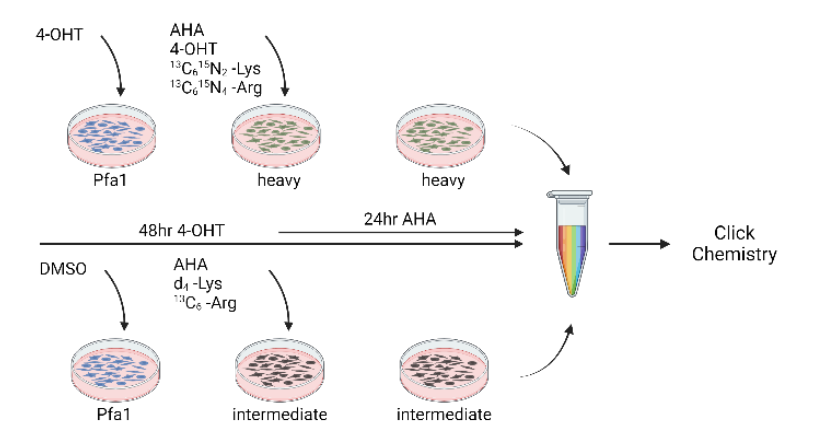


Figure 14. SILAC model.

Quantitative secretome analysis: schematic illustration of experimental setup in cell culture using SILAC labelling.

Furthermore, the click chemistry method was used for sample preparation prior to mass spectrometry to enable stringent washing of the samples, ridding them of hindering serum proteins. Routinely, cells are cultured in a serum-free medium for standard mass spectrometry analysis to enable the detection of low-abundant secretory factors which would otherwise be masked by high-abundant serum proteins. Ferroptosis induction of cells cultured under these circumstances, however, has been shown to be ineffective because the iron-carrier protein transferrin is provided to cells in large part by the serum¹¹⁰. Importantly, transferrin ensures the

cell's supply with iron by binding and delivering it to the intracellular space¹¹⁰. Hence, transferrin constitutes an essential prerequisite for ferroptosis. The quantitative secretome analysis technique applied in this thesis provides an option to circumvent the presented issue, because it allows for cell cultivation under normal conditions (medium containing 10% bovine serum) through a click chemistry reaction, whilst ensuring the detection of low-abundance proteins, which are part of the proteins of interest in this experiment.

One of the major components that facilitates the cu(I)-catalysed azide-alkyne click chemistry reaction is the azide-bearing methionine-analogue azidohomoalanine (AHA). In order to preclude the possibility of toxicity on the conditional knockout cell line (Pfa1) used in this experiment, as well as the possibility of interference between AHA and the agent tamoxifen used for GPX4 knockout induction, two viability assays with different time conditions were conducted. Neither loss of cell viability after 24 hours of incubation with AHA, nor relevant differences between single treatment with tamoxifen and combinational treatment with tamoxifen and AHA could be observed (Figure 15A-C). Interestingly, cell viability was attenuated when substituting DMEM high glucose medium with SILAC medium and amounted to approximately 40% cell death 48 hours after ferroptosis induction with tamoxifen (Figure 15D).

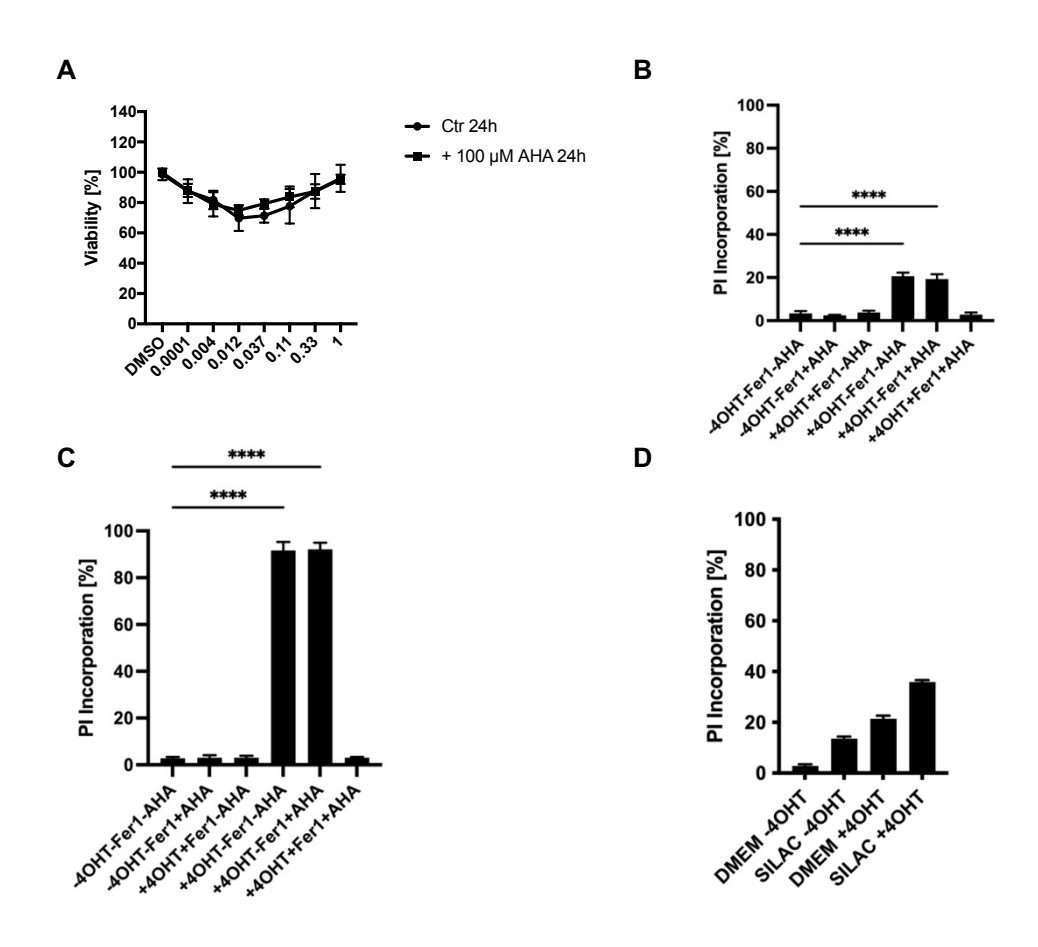


Figure 15. AHA does not display toxicity on Pfa1 cells or interference with 4-OHT and Fer-1.

(A) Pfa1 cells were treated with AHA [100 μ M] for 24 hours and displayed no toxicity. Cell viability was determined by Cell Titer Blue. (B) Pfa cells were incubated for 24 hours \pm AHA and for 48 hours \pm 4-OHT and \pm Fer-1 to analyse drug interference. PI staining and FACS analysis were used to detect nonviable cells. Mean values \pm s.e.m. from biological triplicates (n = 3) are shown. (C) Pfa1 cells were analysed and incubated for 48 hours \pm AHA and for 72 hours \pm 4-OHT and \pm Fer-1 to analyse drug interference. PI staining and FACS analysis were used to detect nonviable cells. Mean values \pm s.e.m. from biological triplicates (n = 3) are shown. (D) Quantification of cell viability in Pfa cells that were incubated for 48 hours \pm 4-OHT in DMEM high glucose medium and in SILAC medium. PI staining and FACS analysis were used to detect nonviable cells. Mean values \pm s.e.m. from biological triplicates (n = 3) are shown.

As a consequence of the antecedent results, the duration of incubation with tamoxifen and AHA was determined to be 48 hours and 24 hours, respectively. The induction of ferroptosis via GPX4 knockout with tamoxifen (knockout condition) was initiated at the same time as Pfa1 cells were seeded. The starting point of the labelling process of proteins present in the supernatants, as well as the incorporation of AHA into the newly synthesised proteins, was chosen to be 24 hours and not 48 hours after seeding, as 48 hours of incubation with tamoxifen was observed to roughly conform to the onset of ferroptotic cell death. Taken together, the aim was to label newly translated proteins from cells that succumbed to ferroptosis with heavy amino acids (knockout condition), while also preparing them to form a bioconjugate in an experimentally downstream click chemistry reaction through the incorporation of AHA (azide). In contrast, the control condition as a reference was incubated and labelled with light amino acids. It was not treated with tamoxifen but equally incubated with AHA. Supernatants of both conditions were merged after cell culture and concentrated using ultrafiltration (Millipore Amicon ultra-15, 3 kDa). For mass spectrometry analysis of complex biological samples, the breakdown of proteins into smaller peptides or amino acids through proteolysis is highly important. Therefore, the samples were digested, purified, and desalted after cell culture as described in 3.2.4. (see 3.2.4.2. until 3.2.4.4.). The prepared samples were delivered to the CECAD Proteomics Facility. After the submission of the project, proteins were measured by using liquid chromatography in combination with modern mass spectrometry (LC-MS). The CECAD Proteomics Facility uses nano ultra-high-performance liquid chromatography (UHPLC) systems that are followed by quadrupole Orbitrap hybrid mass spectrometry.

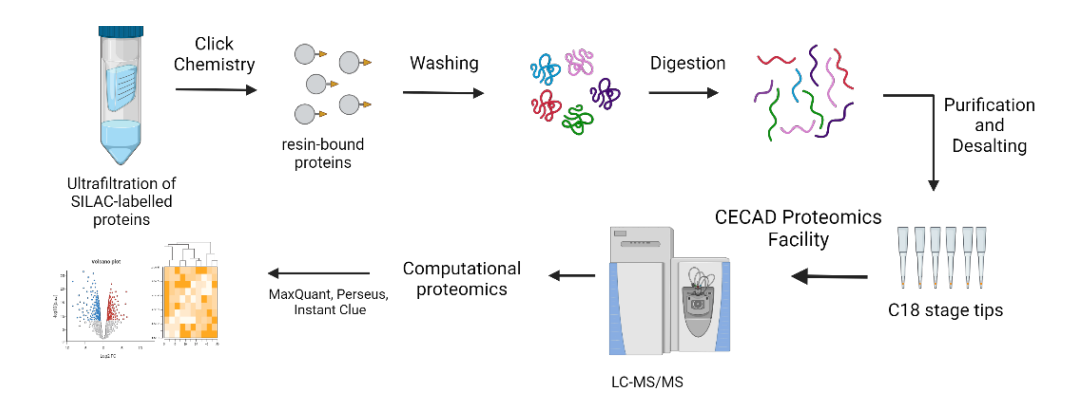


Figure 16. Mass spectrometry-based proteomics workflow for secretome analysis.

Depicted is the workflow following cell culture preparation for mass spectrometry. The samples were concentrated in ultrafiltration tubes. Proteins are extracted by chemical disruption and bound to agarose beads in a click chemistry reaction. Subsequently, samples were reduced, alkylated and enzymatically digested. Peptides were desalted and loaded onto C18 stage tips for high-performance liquid chromatography. Ultimately, peptides were quantified using mass spectrometry. Data analysis and visualisation were performed using bioinformatic platforms.

Following data acquisition, sample analysis and statistical data evaluation were performed using the quantitative proteomic software Perseus 1.6.15¹⁸⁹. As noted before, it is highly important to generate a 1:1 SILAC ratio between the control and knockout conditions, based on even cell counts, starting volumes and total protein concentrations. The objective included the investigation of a difference in the number of proteins secreted by ferroptotic cells compared to untreated, viable cells.

In total, SILAC experiments were generated in three biological replicates which consisted of one knockout and one control condition, respectively. As a result of MS data analysis, a total number of 589 different protein groups were identified in the experiment, 110 of which were detected in all three of the samples. Normalised H(knockout)/M(control) ratios for each detectable protein were obtained. SILAC ratios were linearised by converting them into their log2-values, enabling their use as a parameter to evaluate variations of protein concentration levels between the two conditions under comparison. Positive ratios suggest that there was a higher amount of a particular protein in the supernatant of the ferroptotic cells (knockout condition) than in the supernatant of untreated cells (control condition), potentially due to regulatory processes in the cells in response to ferroptosis induction. Contrarily, negative ratios imply a higher amount of a protein in the control condition than in the knockout condition. Additionally, a t-test was performed to determine the protein groups that significantly differ between the two conditions. In total, a number of 23 proteins listed in table 4-1, which displayed t-test significance (p < 0.05), were found. Three proteins out of 23, elongation factor 1-beta and 1-delta (Eef1b; Eef1b2; Eef1d), as well as heat shock 70 kDa protein 5 (HSPA5), also known as 78 kDa glucose-regulated protein (Grp-78), or immunoglobulin heavy-chain-binding protein (BiP), were detected in all three samples.

Table 4-1 Proteins detected with t-test significance.

Gene name	Protein name	Enriched in KO/CTR
Hspa5	78 kDa Glucose-regulated protein	CTR
	Heat shock 70kDa protein 5	
Eef1b; Eef1b2	Elongation factor 1-beta	КО
Eef1d	Elongation factor 1-delta	КО

Mcfd2	Multiple coagulation factor deficiency	CTR
	protein 2 homologue	
Ptges3	Prostaglandin E synthase 3	CTR
Erp44	Endoplasmic reticulum resident protein	CTR
	44	
Naca	Nascent polypeptide-associated	CTR
	complex subunit alpha	
Ybx1	Nuclease-sensitive element-binding	CTR
	protein 1	
Rbbp4	Histone-binding protein RBBP4	CTR
Sf3a1	Splicing factor 3A subunit 1	CTR
Ppa1	Inorganic pyrophosphatase	CTR
Cdc42	Cell division control protein 42 homolog	CTR
Anxa2	Annexin A2	CTR
Gabarapl2	Gamma-aminobutyric acid receptor-	CTR
	associated protein-like 2	
Pfdn5	Prefoldin subunit 5	CTR
Arhgdia	Rho GDP-dissociation inhibitor 1	CTR
Tubb5	Tubulin beta-5 chain	CTR
Uba1	Ubiquitin-like modifier-activating	КО
	enzyme 1	
Erh	Enhancer of rudimentary homolog	КО
Gm9242	predicted pseudogene 9242	КО
Tpm3-rs7	Tropomyosin 3, related sequence 7	КО
Sfpq	Splicing factor, proline- and glutamine-	КО
	rich	
Snrpa	U1 small nuclear ribonucleoprotein A	КО

According to the analysis, HSPA5, for example, showed negative H/M ratios in all three replicates suggesting that the protein amount of HSPA5 in untreated cells was higher than in ferroptotic cells. Levels of HSPA5 in particular were demonstrated in recent years to be increased during ferroptosis in KRAS mutant pancreatic cancer cells¹⁹⁷. HSPA5 was also shown by Zhu et al. to negatively regulate ferroptosis in human pancreatic cancer cells via HSPA5-GPX4 signalling and consequently mitigating the chemotherapeutic effects¹⁹⁸. In terms of inflammation, scientists have interestingly described that extracellular HSPA5 displays anti-inflammatory effects rather than proinflammatory^{199,200}.

Furthermore, different scatter plots were generated for the graphical visualisation of the high-dimensional data set with the software tool Instant Clue, designed by Hendrik Nolte and colleagues¹⁹⁰. Each dot in the depicted volcano plots (A-C) represents a detected protein, plotting significance (-log t-test p-value) versus t-test difference on the y and x axes, respectively. If the difference in protein concentration between the knockout and the control condition was rather small, they are graphed with a t-test difference close to 0. Proteins that are not part of the common plot line, however, could indicate up- or downregulations of proteins related to ferroptotic cell death. The volcano plot (C) visualises Reactome pathway database analysis and shows that a group of proteins involved in the degradation of the extracellular matrix is upregulated in the knockout condition, which aligns with cells undergoing ferroptosis.

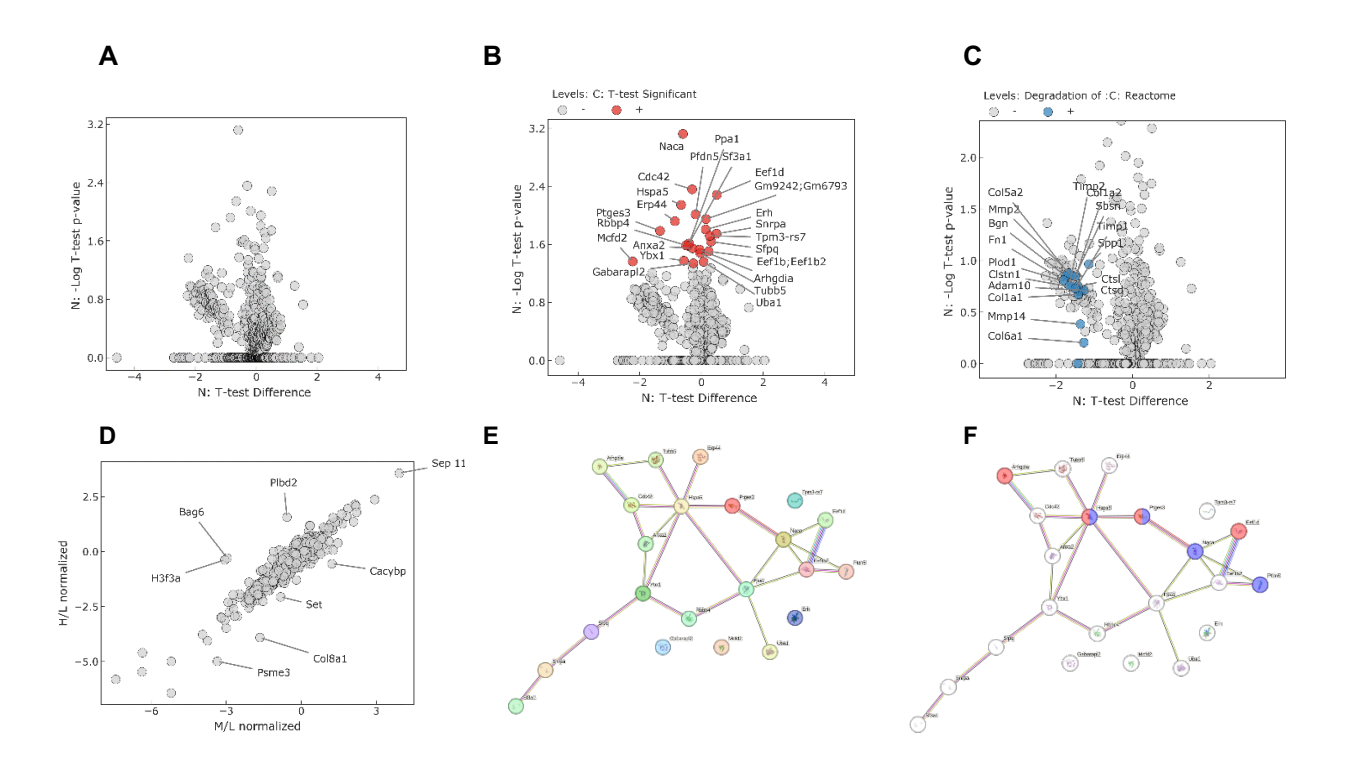


Figure 17. Quantitative secretome analysis

(A) Volcano plot of identified proteins. The x-axis shows the t-test difference of each identified protein. The y-axis shows the corresponding -log10 P-values. T-test (p-value < 0.05). (B) The volcano plot from (A) is overlaid: Grey = detected proteins secreted by Pfa1 cells; Red = detected proteins secreted by Pfa1 cells with significant change in abundance. T-test (p-value < 0.05). (C) The volcano plot from (A) is overlaid with proteins associated with the degradation of the extracellular matrix marked in blue colour. T-test (p-value < 0.05). (D) Volcano plot of identified proteins. The x-axis shows M/L ratio, y-axis shows H/L ratio. (E) Interaction network of differentially expressed proteins analysed with STRING 12.0 database (full STRING network, interaction score of 0.400). (F) Interaction network of differentially expressed proteins analysed with STRING 12.0 database and gene-set enrichment analysis. Gene Ontology used as a classification system: heat shock protein binding in red, unfolded protein binding in blue.

In summary, the data revealed that protein concentrations indeed differed between the control and knockout conditions, suggesting that the secretion profile of cells may be altered during ferroptosis. This difference in protein abundance could provide insights into how ferroptosis influences cellular signaling, particularly regarding how membrane damage and rupture are

associated with changes in the secretome. Nevertheless, it is important to note that capturing the full scope of these processes is very challenging, as the proteome of a cell represents a highly dynamic entity. Importantly, this study aimed to measure and detect all newly synthesised proteins in ferroptotic cells (the secretome) and compare them to those produced by unharmed cells, focusing specifically on the critical time frame between the onset of ferroptosis and membrane rupture, during which cells can still produce biomolecules¹⁷⁹. However, to obtain an even more transparent insight into the immunogenic potential of ferroptosis and characterise potential DAMPs, it could be valuable to further identify and quantify all proteins, as well as other components released into the surroundings following plasma membrane rupture.

4.3. Immunological responses of bystander immune cells to ferroptosis

4.3.1. Ferroptosis-provoked cytokine release by immune cells

Alongside the investigation of potential immunomodulatory factors released from ferroptotic cells, it seemed equally exigent to illuminate which effects ferroptotic cells would exercise on their extracellular milieu and bystander immune cells of the innate immune system. It was particularly intriguing to examine whether ferroptosis would result in the activation of the innate immune system and whether it triggers anti- or proinflammatory responses. In order to study the stimulant influence of ferroptosis on cells of the immune system, human (THP1) and murine macrophage cell lines (CL13, CL45, RAW264.7) were used for the experiments. Macrophages are typically derived from hematopoietic stem cells of the granulocytic-monocytic lineage in the bone marrow that first develop into monocytes before they migrate into connective tissue and ultimately evolve into macrophages²⁰¹. They reside in different tissues as wardens of the innate immune system to quickly detect and respond to exogenous and endogenous danger molecules. To this end, macrophages are equipped with TLRs and scavenger receptors that bind PAMPs and DAMPs (see 2.2.)². Macrophages are important immune cells that trigger and mediate immune responses employing different mechanisms. Besides their ability to present antigens of foreign microbes to lymphocytes via the MHC II receptors, macrophages also use cytokine secretion to alarm other players of the immune system¹⁶⁴. Cytokines regulate inflammation by promoting or antagonising inflammatory signalling cascades and pathways²⁰². They are not only produced by macrophages but also by a variety of other cell types, such as lymphocytes, fibroblasts, endothelial cells, and adipocytes²⁰². Depending on the site of impact, cytokines can operate in an autocrine, paracrine, or endocrine fashion. Albeit the small molecules frequently act on the secreting cell itself (autocrine) or in a specific location (paracrine), they are also able to signal to distant target sites in the body (endocrine)²⁰². The

broad spectrum of cytokine functions encompasses chemotaxis, intercellular communication, as well as de novo synthesis of cytokines²⁰². Therefore, macrophages are of great interest in the exploration of immune responses. Notably, although cytokines play an integral part in host defence, deregulated cytokine secretion can also result in harmful conditions in the human body^{202,203}.

To investigate the effect of ferroptotic cells on bystander immune cells, cytokine arrays were performed, similar to the experiments shown in Figure 13. In this case, however, untreated supernatants (control condition) and ferroptotic supernatants (RSL3 treatment; treatment condition) from H441 and MEFs were used respectively to study the stimulant influence of ferroptosis on human (THP1) and murine macrophage (RAW264.7) cell lines. In this experimental model, PMA was used to differentiate human monocytes (THP1 cells) in cell culture into macrophages. After exposing the macrophage cell lines to control or ferroptotic supernatants from the corresponding cells, the supernatants from the macrophages were analysed for chemokine and cytokine secretion.

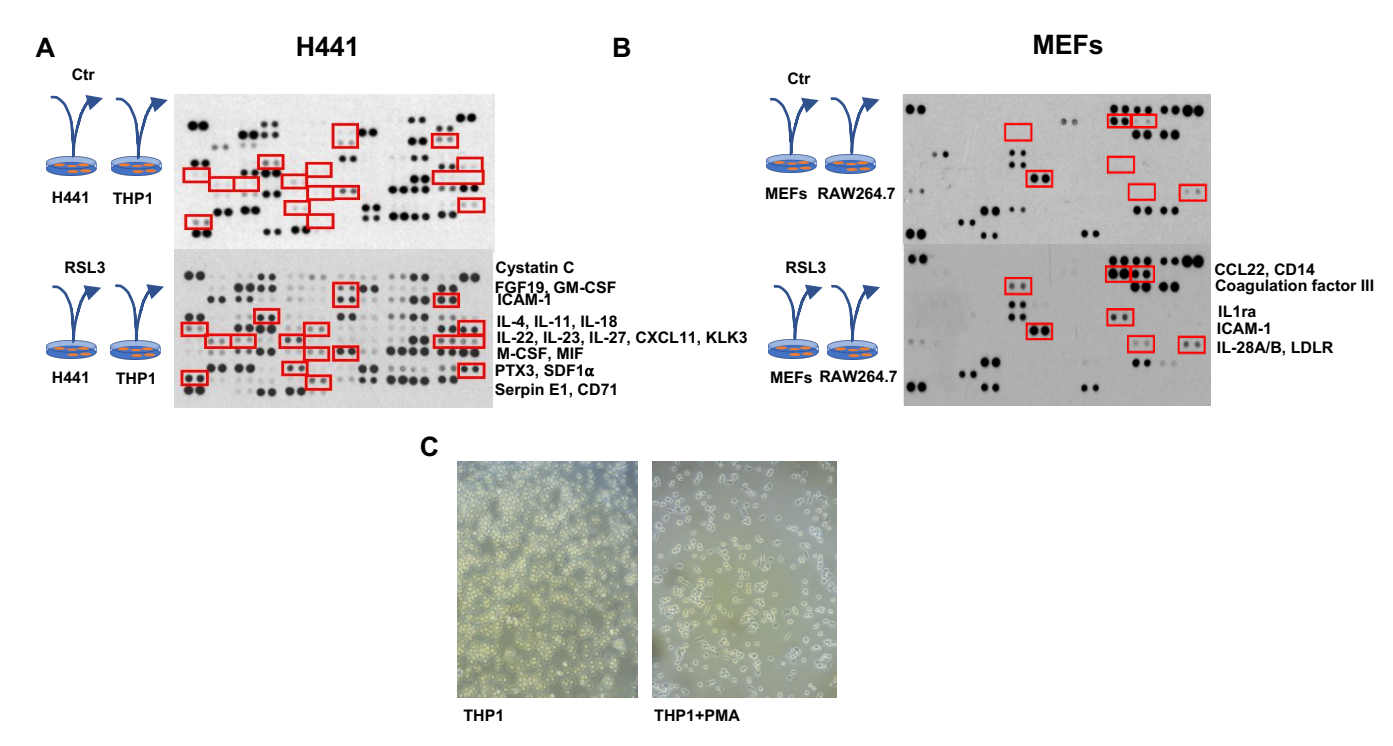


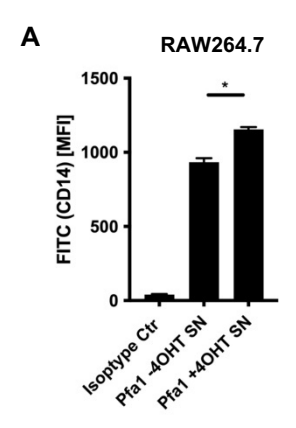
Figure 18. Experimental induction of ferroptosis in murine and human cells triggers paracrine chemo- and cytokine release from corresponding macrophages. (A) Supernatants from H441 cells treated with RSL3 [1 μ M] or untreated were used to stimulate pre-activated THP1 cells for 24 hours. Supernatants of THP1 were analysed for cytokine secretion. (B) Supernatants from MEF cells treated with RSL3 [1 μ M] or untreated were used to stimulate RAW264.7 cells for 24 hours. Supernatants of RAW264.7 cells were analysed for cytokine secretion. (C) Visualisation of human monocytes (THP1) and differentiation into macrophages through PMA treatment.

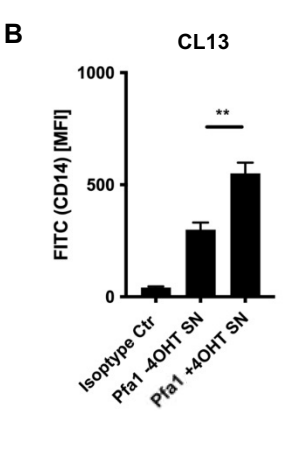
As in the cytokine arrays presented in Figure 13, distinctive chemiluminescent signals could again be detected in these cytokine arrays. IL-27, IL-18, C-X-C motif chemokine ligand 11 (CXCL-11) in the human macrophage cell line (Figure 18A), as well as CD14 and IL1ra

secreted by murine macrophages (Figure 18B) presented particularly intensified signals in the treatment condition compared to the control condition.

Together, the presented findings suggest an upregulation of cytokine secretion in both human and murine macrophage cell lines when stimulated with ferroptotic supernatants. These results further imply that macrophages increase cytokine secretion in response to immunomodulatory mediators released after ferroptotic cell death.

Of note, cytokine arrays of macrophages exposed to ferroptotic supernatants revealed increased signals for CD14. This cell surface protein was shown to be a crucial co-receptor of TLR4-mediated pathways²⁰⁴. TLR4 belongs to the superfamily of TLRs that bind PAMPs and DAMPs (see introduction 2.2.) and elicit the production of pro-inflammatory cytokines in macrophages^{2,204}. TLR4 activation can follow a CD14-dependant signalling pathway that involves the adaptor protein Toll/interleukin-1 receptor domain-containing adaptor protein inducing interferon-β (TRIF)²⁰⁵. CD14 is further linked to the essential endocytosis of the activated TLR4 receptor²⁰⁵. Interestingly, ferroptotic cell death was shown to be essential for neutrophil recruitment in an in vivo model of IRI associated with the TLR4/TRIF-mediated pathway⁴. These findings suggest that ferroptotic DAMPs may stimulate and activate the immune system. Given that the TLR4/TRIF pathway depends on the presence of CD14, it was considered a potential indicator of macrophage activation in response to ferroptosis and was used as such in this experiment. Hence, CD14 antibodies conjugated with fluorescein isothiocyanate (FITC) were used to detect CD14 expression on three untreated murine macrophage cell lines and compared to ferroptotically primed macrophages. Expression levels were measured by FACS analysis. Slightly increased levels of CD14 in the ferroptotic conditions compared to the control conditions (Figure 19) could be observed in all three different cell lines. This trend towards a higher expression of CD14 in ferroptotically primed macrophages could indicate that ferroptosis might facilitate immune responses as a sort of sensitiser.





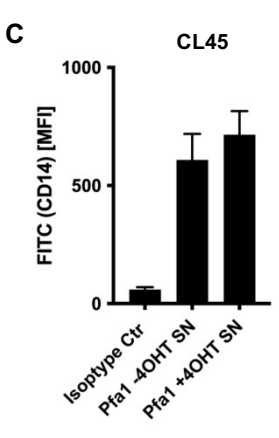


Figure 19. Macrophages exposed to ferroptotic supernatants hint at CD14 expression.

(A-C) Murine macrophage cell lines (A: RAW264.7, B: CL13, C: CL45) were exposed to untreated Pfa1 cell supernatants (Pfa1 -4OHT SN) and exposed to ferroptotic supernatants from Pfa1 cells (Pfa1 +4OHT SN) for 24 hours (24 hours after seeding). Macrophages were incubated for 60 minutes with anti-mouse antibody CD14 and analysed with flow cytometry for CD14 expression. Levels of CD14 were determined as MFI-mean fluorescence intensity by flow cytometry. Error bars show SEM. n=3.

Conclusively, the results imply that ferroptotic cell death induces the release of immunomodulatory factors that enhance cytokine/chemokine secretion and activate immune defence, particularly by influencing macrophage responses. Additionally, the presented data suggest that ferroptosis might act as a sensitising primer for the immune system. It may prepare the immune system for a more robust inflammatory response by potentially releasing immunomodulatory factors and upregulating key receptors, thereby amplifying both innate immune activation and inflammatory pathways.

4.3.2. RNA sequencing analysis of ferroptotically primed immune cells

Immunogenic signals from ferroptotic cells are hypothesised to stimulate PRRs on the plasma membrane of innate immune cells. As a consequence, it might be reasonably assumed that these cells show modulated gene expression in a diverse set of transcriptional alterations. Therefore, this study aimed to complement the previous research with investigations into the immunological implications of ferroptosis at the genetic level of immune cells. RNA sequencing provides an excellent tool to capture a snapshot of the cell's transcriptome through the quantification of gene expression in a certain condition. This high-throughput sequencing experiment delivered insight into biological activities in the cell, which is reflected in the transcription of a subset of genes into complementary RNA molecules. An RNA sequencing experimental approach was chosen in this thesis since it allows the quantification of present RNA in macrophages stimulated with ferroptotic supernatants in comparison to unstimulated macrophages. For this purpose, the three aforementioned murine macrophage cell lines were used as biological replicates (CL13, CL45, RAW264.7). Sequenced reads were mapped to their matching reference genes. Further analysis was performed using read count data (obtained from the Bioinformatics Facility, CECAD) for DESeq2-analysis.

In this study, DESeq2 was used to normalise data since commonly used normalisation methods, such as RPKM and FPKM, are not suitable for the analysis of differential gene expression. Importantly, DESeq2 uses negative binomial modelling to further account for variability in the variance between biological replicates (biological bias) in the same group. As a result, genes that are not differentially expressed will show greater similarity across the samples, while genes with high dispersion, which are presumed not to adhere to modelling assumptions, will be identified. This can then be attributed to a biological phenomenon¹⁸⁶.

Illumina high throughput RNA sequencing data analysis of the biological replicates showed that macrophages stimulated with ferroptotic supernatants (Fer.med) and naïve (Ctr.med) macrophages, respectively, cluster into two separate groups (Figure 20A). Furthermore, it revealed differentially expressed genes which hint at up- and downregulated proteins in macrophages in response to ferroptotic stimuli (Figure 20B and C). The heat map shown in Figure 20A plots the top 50 enriched genes ranked by p-value and visualises the clustering of the two conditions. However, differentially expressed genes with an adjusted p-value lower than 0.05 could not be detected.

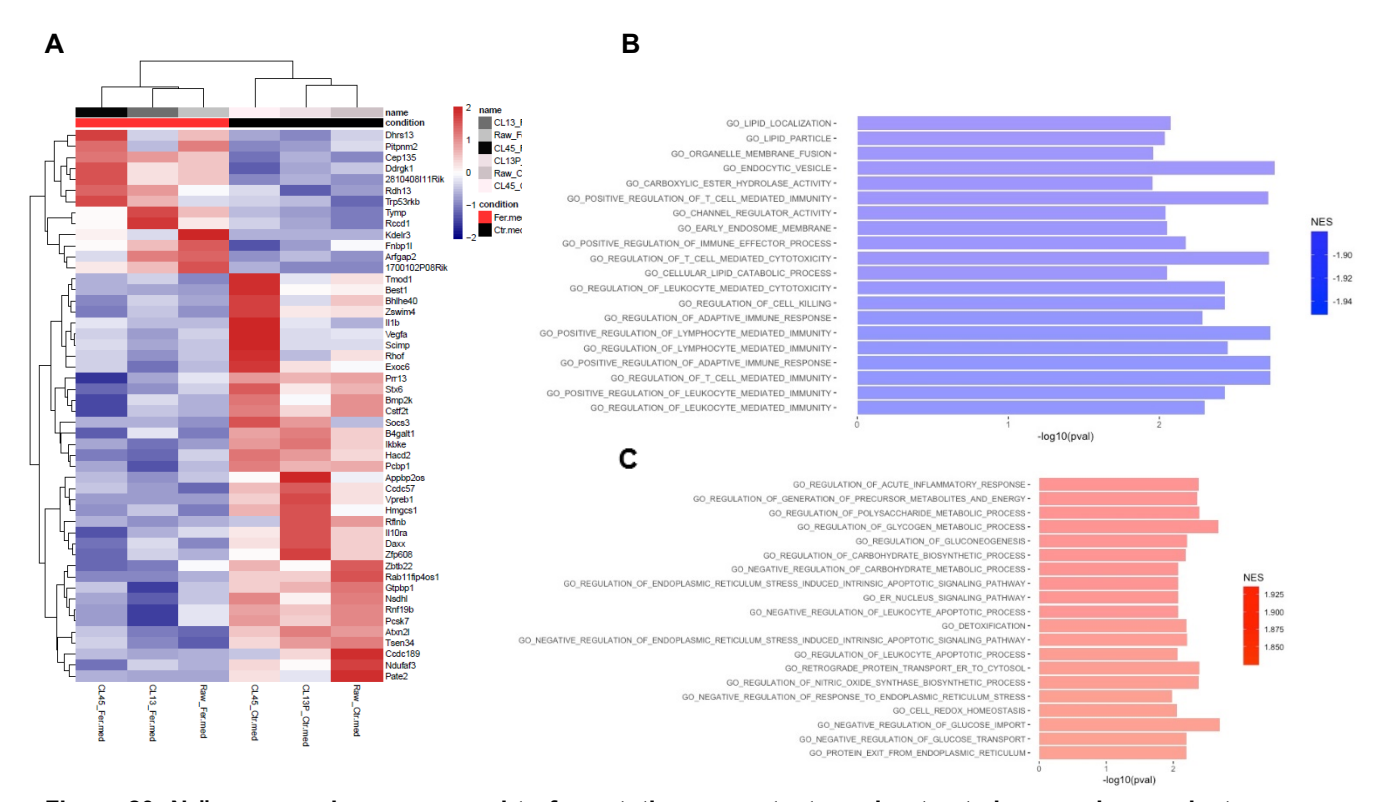


Figure 20. Naïve macrophages exposed to ferroptotic supernatants and untreated macrophages cluster into two groups. (A) Heat map of the top 50 enriched genes ranked by p-value shows clustering into two distinct groups. Genes were detected in an RNA sequencing screening analysis of unstimulated and ferroptotically stimulated macrophages. Cells were incubated in ferroptotic supernatants for 24 hours before RNA isolation. (B) Enriched gene sets in unstimulated macrophages. (C) Enriched gene sets in ferroptotically stimulated macrophages.

Strikingly, the inhibitor of nuclear factor kappa-B kinase subunit epsilon (IKBKE) gene, which encodes the inhibitor of nuclear factor kappa-B kinase epsilon (IKK ϵ), appeared to be downregulated in all three Fer.med-conditioned cell lines. Intriguingly, IKK ϵ has been described as essential for regulating inflammatory signalling pathways^{206–209}.

Collectively, these results indicate that ferroptotic supernatants can modulate macrophage gene expression, as genes are up- or downregulated in response to ferroptotic stimuli. Though differentially expressed genes with an adjusted p-value lower than 0.05 could not be detected, the presented data nonetheless hint at the immunomodulatory potential of ferroptosis.

4.4. Investigation of immunological responses to ferroptosis in vivo

Due to the physiological and intercellular dependencies of different cell types in complex tissue structures, in vitro results are not unconditionally representative of biological events and interactions in vivo. Therefore, it seemed vital to also investigate the immunomodulatory effects and consequences of ferroptosis in vivo. Recently, inflammatory implications of ferroptosis induction have been reported in several different conditional KO mouse models. In this respect, GPX4 deletion in kidneys has shown mononuclear interstitial infiltrations¹²⁶. In in vivo models of acute kidney injury (AKI) and acute renal failure, it was also implicated that Fer-1 decreased immune cell infiltrations in diseased tissues 175,176 and reduced cytokine and chemokine expression levels (CXCL-2, IL-6, p65 subunit of NF- κB^{175} , IL-33, TNF- α , monocyte chemoattractant protein 1 [MCP-1]¹⁷⁶)¹⁰⁵. These results suggest that ferroptotic DAMPs may initiate secondary immune cell activation and production of cytokines. Alternatively, the production of these alarmins may be directly blocked by Fer-1¹⁰⁵. Ferroptosis inhibition in diseased liver tissue was further shown to decrease expression levels of proinflammatory cytokines (TNF-α, IL-6, IL-1β) in a mouse model of steatohepatitis¹⁷⁸. Furthermore, a correlation between ferroptosis and neutrophil recruitment in heart tissue following ischemia/reperfusion became apparent in the work of Li and colleagues⁴. In sum, recent in vivo studies strongly implicate that ferroptosis exerts a critical role in inflammatory processes across a large spectrum of different tissues^{4,175–178}. Interestingly, pancreatic cells in a mouse model of iron overload have been shown to exhibit local oxidative damage and undergo cell death, leading to the death of mice between 7 and 14 months²¹⁰. This indicates that pancreatic cells might be a ferroptosis-prone type of tissue. Although it has further been shown that neutrophil infiltration can be observed early on during pancreatic inflammation²¹¹, it remains elusive as to whether ferroptosis is involved in the pathogenesis of pancreatic diseases or pancreatic cancer.

The mouse model presented in this thesis was designed to characterise the impact of ferroptosis induction in the pancreas through tissue-specific genetic deletion of GPX4. For this purpose, PDX1-Cre expressing mice¹⁹² were crossbred with GPX4^{FL/FL} mice¹⁹³ to induce a targeted knockout of GPX4 in the pancreas. Successful pancreas-specific deletion of GPX4 and expression of PDX1-Cre was assessed through the identification of genotypes (PDX1-Cre; GPX4^{WT/WT}, PDX1-Cre; GPX4^{WT/FL}, PDX1-Cre; GPX4^{FL/FL}; Figure 21A). The histological sections of 20-week-old mice were analysed in collaboration with the Department of Pathology at the University Clinic of Cologne to identify signs of phenotypic abnormalities, pancreatic tissue damage, and spontaneous pancreatic diseases, including pancreatitis, fibrosis, oedema or inflammatory infiltrates of immune cells. The mosaic knockout of GPX4 in mice, however,

did not seem to affect pancreatic development, according to microscopic examination. Additionally, no significant alterations in the size and appearance of the extracted organs, including pancreases and spleens, were macroscopically observed (Figure 21B). Pathological changes in structure were absent as well, and there was no sign of immune cell infiltration in the pancreas (Figure 21D).

In sum, the results presented here using a pancreas-specific GPX4 knockout model did not reveal significant pathological changes or immune cell infiltration in the pancreas, contrary to expectations. This underscores the complexity of ferroptosis in different tissues and highlights the need for further investigation into its potential role in immunity and inflammation.

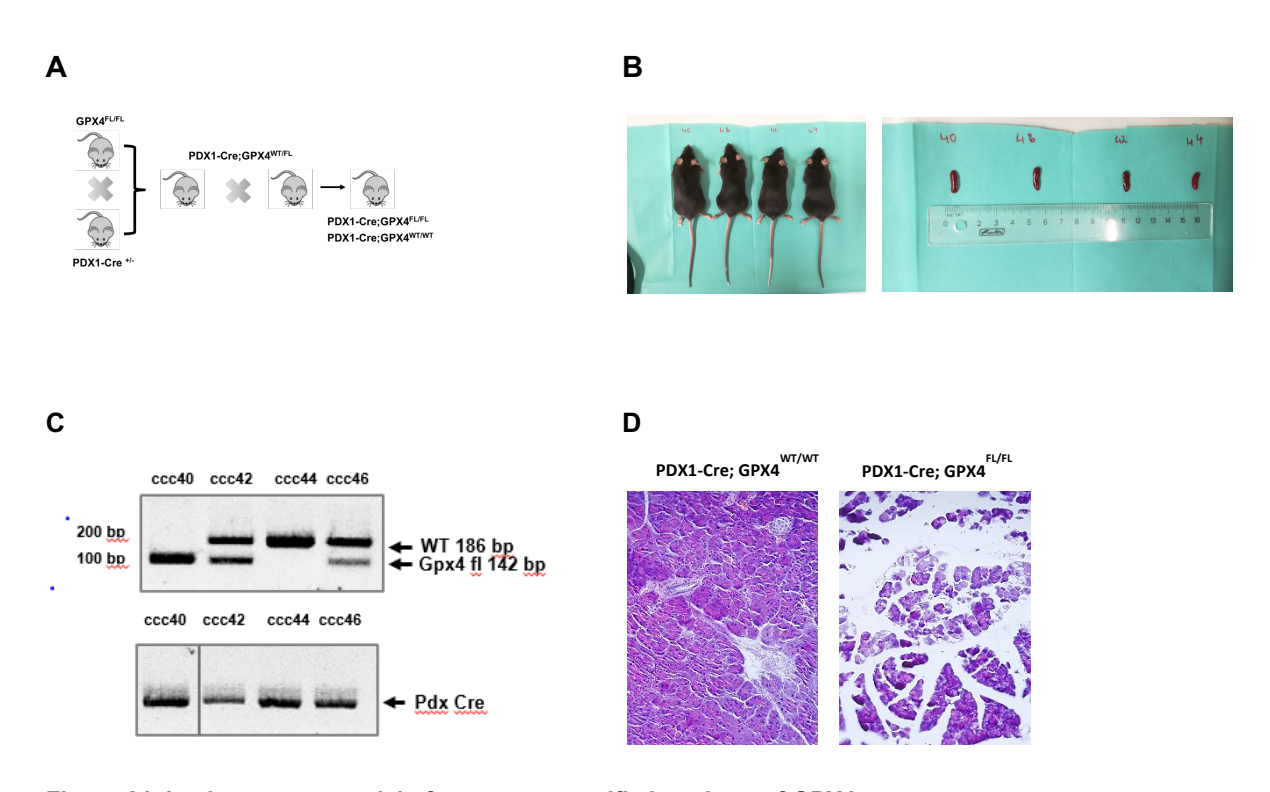


Figure 21. In vivo mouse model of pancreas-specific knockout of GPX4.

(A) Crossbreeding of GPX4^{FL/FL} mice with PDX1-Cre expressing mice was performed to generate the conditional knockout GPX4 in PDX1-Cre; GPX4^{FL/FL} mice. (B) Visualisation of mice: 40, 46, 42 and 44 with respective extracted spleen. (C) Depicted are the genotyping results of wild-type, heterozygous and homozygous GPX4 knock-out mice, as well as for PDX1-Cre expression. The GPX4 gene alleles were analysed in wild-type and mutant forms, using DNA extracted from the ears of 20-week-old mice. (D) H&E staining of pancreatic tissue from 20-week-old mice, which did not show significant pathological changes.

5. Discussion

5.1. Characterisation of a ferroptosis-induced secretome

Throughout the last decades, a large panel of different types of regulated necrosis have revolutionised the field of cell death research. As more and more distinct cell death pathways were identified, researchers have increasingly focused not only on uncovering cell death mechanisms but also on exploring immunological implications of cell death. Importantly, regulated necrosis pathways are characterised by plasma membrane rupture and cell lysis 167. Consequently, cytosolic content is exposed to the extracellular space¹⁶⁷. In this context, endogenous noninflammatory components and cell organelles of viable cells can be recognised as DAMPs when released, secreted or exposed during cell death or cell damage and acquire immunomodulatory functions^{212,213}. Alarmins on the other hand are molecules with cytokine-like properties that modulate inflammatory processes when released upon cell lysis²¹⁴. Mechanistically, DAMPs and alarmins operate as ligands that stimulate PRRexpressing immune cells resulting in the production of immune factors, such as cytokines and chemokines². To characterise the DAMP-PRR axis in ferroptosis that bridges cell death and immunity, it is essential to explore the nature of DAMPs and alarmins released upon cell death. This thesis provides an unbiased approach to identifying proteins in the secretome of Pfa1 cells that succumbed to ferroptosis. In total, 589 different protein groups were identified in the experiment, 110 of which were detected in all three of the samples. Interestingly, only 23 proteins that significantly (p < 0.05) differed between the knockout and control conditions (Table 4-1) were found. According to the data analysis, results showed a lower abundance of prostaglandin E synthase 3 (PTGES3) in the knockout condition compared to the control secretome. PTGES3 is an enzyme that converts prostaglandin endoperoxide H2 (PGH2) to prostaglandin E2 (PGE2)²¹⁵, which in turn has been reported to be released in high abundance during various forms of cell death²¹⁶. It was further shown to operate as an inhibitory DAMP by suppressing the expression of inflammatory genes²¹⁶. In the context of ferroptosis, a previous study showed upregulation of the prostaglandin-endoperoxide synthase 2 (PTGS2) gene, suggesting its importance as a tissue marker of ferroptosis 129. Thus, the results presented here show contradictory results with current findings in ferroptosis research.

Importantly, the experimental setup only allowed for the incorporation of labeled amino acids during protein biosynthesis in the cells, enabling detection through mass spectrometry. Consequently, proteins that are released passively during or after ferroptotic cell death, including potential cell organelles that function as DAMPs following plasma membrane rupture, are not represented in the results. It is conceivable that the discrepancies between the current research results and the results from this experiment could be linked to the complexity of the experimental setup. Additionally, the relatively low number of proteins detected in this

experiment could be improved by increasing the number of seeded cells. Protein translation in cells that undergo ferroptosis may also be generally attenuated or suppressed. Expanding the replicate count would further help to average out random variations in the data, reduce the level of noise and improve statistical power. Moreover, mouse immortalised fibroblasts with a 4-OHT-inducible GPX4 knockout (Pfa1 cells) were used for secretome analysis. Since each cell line displays unique characteristics, including differences in gene expression, protein production, secretion profiles, and response to stress or ferroptosis induction, the secretome can vary significantly between different cell lines. Furthermore, cell viability in Pfa1 cells decreased when DMEM high glucose medium was replaced with SILAC medium, as shown in Figure 15D. Thus, the specific cell line used in this study may have also influenced the outcome of the presented secretome analysis. Using different cell lines would be necessary to assess the effects of SILAC medium on cell viability and to further confirm the findings of the analysis.

To date, a multitude of biological molecules have been identified as DAMPs, each varying in their biological structure and quality. Not only proteins but also lipids, as well as metabolites can acquire immunomodulatory functions and operate as DAMPs²¹⁷. High mobility group protein B1 (HMGB1), histones, heat shock proteins, DNA fragments, ATP, as well as IL-1 family members are examples of common DAMPs^{213,218}. Though apoptosis was generally considered to be a non-inflammatory type of cell death, ATP, HMGB1 and histones have also been reported to be released during apoptosis^{219–221}. Elliott and colleagues have demonstrated that the release of the extracellular nucleotides ATP and UTP by apoptotic cells triggers phagocyte recruitment, thereby promoting cell clearance²²¹. However, a previous study used a mass spectrometry-based approach to show that the protein abundance released from early apoptotic cells is lower compared to necroptotic cells²²². Investigations of DAMP release associated with pathways of regulated types of necrosis have reported the release of HMGB1 in necroptosis²²³. This nuclear DAMP for example is known to bind to the receptor for advanced glycation end-products (RAGE) and is thought to foment inflammation in the context of sepsis²²⁴. When investigating a pyroptosis-induced secretome using mass spectrometry and proteomics, the release of conventional cytokines (e.g. TNF- α and IL-6) and chemokines (e.g. CXCL-10) was observed in TLR4-activated cells^{225,226}. Interestingly, it was also reported that IL-1β, IL-1α, IL-18, and HMGB1 are released by GSDMD pores or after cell lysis in response to TLR4 plus NLRP3-stimulation²²⁶.

Taken together, these results reinforce the notion that regulated necrosis has a high immunomodulatory potential. Yet, common inflammatory cytokines and chemokines that are known to be released during other types of RCD could not be detected in the results presented here. Moreover, DAMPs, such as HMGB1, could not be identified in the ferroptosis-induced secretome here, though it has been reported to be released in ferroptotic cells in an autophagy-

dependent manner²²⁷. Importantly, the lipid peroxidation by-product 4-hydroxynonenal (4-HNE), as well as ATP were equally described in a recent study to be released from ferroptotic cells²²⁸. While the exact mechanisms have yet to be determined, growing evidence suggests that ferroptosis may be inflammatory through lipid peroxidation-mediated plasma membrane rupture¹⁷⁴.

Given that the proteome of a cell is a highly dynamic entity, capturing all aspects of a secretome is highly demanding due to the complexity of this experimental setup. This study aimed to measure and detect all newly synthesised proteins of ferroptotic cells (secretome) and compare these to the proteins generated by unstimulated Pfa1 cells. However, to gain a clearer understanding of the implications of ferroptosis and its immunogenic potential, it is of great interest to further identify and quantify all proteins in the ferroptosis-induced secretome, rather than focusing solely on newly translated proteins. Furthermore, it is conceivable that DAMPs released during ferroptosis or secondary to ferroptosis are not limited to proteins but would also display lipid or metabolic biological structures. To date, it remains unclear which small metabolites are released from ferroptotic cells. To this end, a multi-omics approach, including lipidomics and metabolomics, would broaden our perspective in the investigation of ferroptotic immunogenicity. Inflammation that is thought to be triggered by inter alia DAMPs is involved in human disorders, such as sepsis and cancer²²⁹. Thus, the identification of specific DAMPs and their blockade could provide targets for potential therapeutic strategies for these pathologies. Furthermore, it would be of great interest to investigate an induced secretome from ferroptotic cancer cells to explore immunomodulatory implications on the tumour microenvironment.

5.2. Inflammatory responses in bystander immune cells

This study aimed to further investigate the immunomodulatory capacity of ferroptosis and its effect on immune cells. The conducted cytokine arrays of two macrophage cell lines showed intensified chemiluminescent signals in macrophages stimulated with ferroptotic supernatants in comparison to untreated macrophages (Figure 18). Murine macrophages appeared to display higher levels of CD14 following exposure to ferroptotic supernatants. While multiple PRRs, such as RAGE and the cytoplasmic DNA sensor cyclic guanosine monophosphate—adenosine monophosphate synthase (cGAS), have been shown to respond to ferroptotic DAMPs¹⁶², TLR4, in particular, was recently reported to play a pivotal role in the recruitment of immune cells in response to ferroptosis in an in vivo model of ischemia-reperfusion injury⁴. The research further shows that this effect could be entirely abrogated by ferroptosis inhibition⁴. Mechanistically, Li et al. demonstrated that ferroptotic cell death can trigger inflammation by the activation of a TLR4/Trif/type I IFN signalling pathway. CD14 is a cell surface molecule known to be a crucial co-receptor for TLR4²⁰⁴. It is further responsible for the essential LPS-

induced endocytosis of the activated TLR4 receptor^{205,230}. In this study, CD14 stainings of three different macrophage cell lines were performed and CD14 levels of macrophages stimulated with ferroptotic supernatants were compared to those of unstimulated macrophages (Figure 19). As a result, a tendency towards a higher expression of CD14 in response to ferroptotic supernatants could be observed. Interestingly, the activation of CD14 and TLR4 results in the activation of NF-kB²³¹. Taking into consideration that the TLR4/TRIF pathway is mediated by CD14⁴, it could be hypothesised that ferroptosis has an immunostimulatory effect on immune cells and that ferroptosis might boost stimulation by TLR4 ligands. However, according to the results from this experiment, this effect alone does not appear to be a sufficient trigger for inflammatory pathways. The presented findings hint at an immunogenic capacity of ferroptosis but underscore the importance of further research, notably on the genetic level.

RNA sequencing of three different macrophage cell lines was performed to further investigate the effect of ferroptosis on bystander immune cells and revealed that ferroptotic supernatant-exposed macrophages and unstimulated naïve macrophages clustered into two distinct groups (Figure 20A). Notably, the possibility of a death-inducing effect of the small molecule RSL3 or erastin on macrophages was circumvented in the experiments by using GPX4 knockout-inducible Pfa1 cells. Strikingly, this outcome could be observed despite the biological differences between the three different macrophage cell lines. These differentially expressed genes are indicative of potential up- and downregulations in response to the given stimulus and grant insight into genetic modifications triggered by ferroptosis. STRING analysis of the top 50 genes upregulated in ferroptosis-exposed macrophages revealed Gene Ontology (GO) terms associated with acute inflammatory responses (Figure 20B and C). Furthermore, GO analysis also indicated that ferroptosis seems to interfere with metabolic processes in the stimulated cells. Several metabolic pathways have been shown to influence sensitivity to ferroptosis²³². Further research, such as metabolic profiling, is needed to explore ferroptosis's capacity to influence bystander immune cells and to sensitise cells for additional cell death.

Interestingly, the gene encoding for IKKs was downregulated in all three ferroptotically stimulated macrophage cell lines in the RNA sequencing data (Figure 20A). IKKs has been shown to prevent TNF-induced cell death²³³. Hence, the loss of IKKs may sensitise for cell death. IKKs was also reported to inhibit T cell-mediated immune responses¹⁹⁶, suggesting its role as a negative regulator of T-cell activation. Therefore, it is plausible that T-cell-mediated immune responses could potentially be enhanced in ferroptotically primed macrophages, as IKKs was observed to be downregulated in this experiment. In this context, ferroptosis could potentially be a sensitiser for more efficient immune responses, given its downregulation in these immune cells. It could further be hypothesised to sensitise for cell death in promoting

tumour-associated macrophages (TAMs), resulting in more efficient anti-tumour immune responses (see 5.3).

However, it is important to note that no differentially expressed genes with an adjusted p-value below 0.05 were detected. Additionally, sequenced data did not reveal the upregulation of genes encoding common chemo- and cytokines. Ferroptosis alone therefore seems to be insufficient to drive macrophage inflammatory activation. The results from CD14 stainings (Figure 19) may also support the idea of a sensitising function of ferroptosis, rather than it being a direct trigger. In summary, the results presented here suggest that ferroptosis may not be sufficient to induce an immune response. However, it could play an important role as a sensitiser.

5.3. The influence of ferroptosis on cancer immunity

Recently, it was shown that the activation of innate immune cells can be initiated through the release of DAMPs from necroptotic cancer cells²³⁵. In 2000, Mills et al. provided a framework to distinguish between two macrophage phenotypes and introduced the concept of M1/M2 polarisation²³⁶. In the context of cancer biology, the M1 macrophage phenotype has been associated with tumour regression²³⁷ and inhibition of tumour growth²³⁸. Conversely, the M2 macrophage phenotype has been reported to promote tumour activity by facilitating angiogenesis²³⁹ and by suppressing anti-tumour immune responses²⁴⁰. It was demonstrated that cytokine secretion from cancer cells, drive polarisation to M2-like macrophages in the tumour microenvironment²⁴⁰. Importantly, M1/M2 macrophages can influence adaptive T helper (Th)1/Th2 lymphocyte responses, respectively²³⁶. Tumour-suppressing M1/Th1 activity is typically linked to the production of pro-inflammatory cytokines (TNF²⁴¹ and IFN-v²⁴²)¹⁰⁵. In this context, IFN-y has been reported to again stimulate M1 polarisation in a positive feedback loop²⁴². Conversely, macrophage-driven Th2 responses are associated with anti-inflammatory cytokines^{241,243}, and were shown to counteract cytokine secretion from Th1 cells^{236,244}. Therefore, cancer cells apply different mechanisms to establish a high M2 to M1 ratio in the vicinity of the tumour^{245–247}. Accordingly, the tumour microenvironment predominantly consists of M2 macrophages²⁴⁸.

Consequently, cancer research has focused on driving polarisation of TAMs towards an antitumour M1 phenotype to improve the M1/M2 ratio^{249,250}. It was demonstrated that combining gemcitabine with an agonist CD40 antibody, which promotes anti-tumour T cell responses, resulted in tumour regression in a mouse model of PDAC²⁵¹. Strikingly, this effect seemed to be linked to CD40-activated macrophages²⁵¹.

Given that immunogenic factors released during ferroptosis may either enhance M2 tumourpromoting activity or support an M1 anti-tumour immune response, it appears highly important to investigate the immunomodulatory features of ferroptosis in cancer research to find novel therapeutic strategies to combat cancer. Interestingly, induced ferroptosis in neuroblastoma caused tumour immune cell migration to the tumour¹⁵², suggesting that ferroptosis is indeed inflammatory in the context of cancer. Recent studies also suggest that increasing the susceptibility of cancer cells to ferroptosis could enhance the efficacy of combination immunotherapies²⁵². Immunotherapy-activated IFNy^{252,253}, and radiotherapy-induced ataxiatelangiectasia mutated gene (ATM) have been shown to suppress SLC7A11, leading to increased lipid peroxidation in tumour cells and ferroptosis²⁵². Immunotherapy was also shown to be associated with the differentiation in melanoma cells that sensitised tumour cells to ferroptosis²⁵⁴. Additionally, early ferroptotic cancer cells have been reported by Efimova et al. to induce anti-tumour immunity through the promotion and activation of BMDMs²⁵⁵. Therefore, not only the induction but also the sensitisation of tumour cells to ferroptosis may supply a novel tool for anti-tumour immunity and may serve the optimisation of established immunotherapies. Conversely, early ferroptotic cancer cells were shown to hinder antigenpresenting immune cells, thereby impeding an adaptive immune response²⁵⁶. Overall, the immunomodulatory impact of ferroptosis on cancer immunity seems to be strongly influenced by context and timing, and remains not fully understood.

5.4. Ferroptosis and inflammation in pathology – in vivo models

In this study, a targeted knockout of GPX4 in the pancreas of PDX-Cre transgenic mice was used to analyse the impact of organ-specific ferroptosis induction in vivo, focusing on its immunostimulatory potential (Figure 21). Surprisingly, no signs of tissue damage, inflammation, or changes in the pancreatic parenchyma were detected in the histopathological analysis (Figure 21D). At its time, it was assumed that this might be due to the implications of a mosaic knockout. It could be anticipated that this knockout might have a sensitising effect on the pancreatic tissue but was not sufficient enough to induce inflammation itself. This presumption was confirmed by a study from Dai and colleagues who reported very similar observations in WT versus KO mice using the same conditional knockout in vivo model 180. Indeed, they demonstrated that KO mice showed increased mortality and pancreatic injury in comparison to WT mice secondary to cerulean- or arginine-induced pancreatitis 180. Hence, KO mice appeared to be more susceptible to pancreatic tissue damage than WT mice. Additionally, it was demonstrated that GPX4 depletion or high-iron diets resulted in the release of oxidative DAMPs in the pancreas, namely 4-HNE and 8-hydroxy-2'-deoxyguanosine (8-OHG), which were in turn shown to activate a TMEM173/STING-dependent pathway 180. Additionally,

increased macrophage infiltration in the tumour microenvironment was observed in a model of Kras-driven PDAC¹⁸⁰. These findings support the notion that ferroptotic damage promotes pancreatic tumourigenesis.

It has been shown that Fer-1 decreases immune cell infiltrations into diseased tissues in models of acute kidney injury (AKI)^{175,176}, and reduces cytokine and chemokine secretion (CXCL-2, IL-6, p65 subunit of NF-κB¹⁷⁵, IL-33, TNF-α, MCP-1¹⁷⁶)¹⁰⁵. These findings propose that immunogenic signals released during ferroptosis may trigger secondary immune cell responses or enhance cytokine secretion. Notably, the use of other cell death inhibitors, such as zVAD-fmk and necrostatin-1 (Nec-1), did not seem to alleviate folic acid-induced AKI^{105,176}. Taken together, it is strongly suggested that ferroptosis may trigger inflammation in acute kidney injury. Furthermore, the accumulation of immune cells was shown to be hindered after Fer-1 treatment following IRI through a TLR4-mediated signalling pathway⁴, suggesting once again that ferroptotic cell death may be closely associated with inflammatory processes. Interestingly, elevated levels of proinflammatory cytokines, which were linked to neuronal degeneration, could also be detected following a conditional neuron-specific Gpx4 knockout in vivo¹⁷⁷.

Overall, ferroptotic cell death has been implicated in the pathogenesis of not only kidney injury and neurological disorders, such as intracerebral haemorrhage²⁵⁷ and neurodegeneration^{177,258}, but has also been shown to be involved in liver damage^{105,178}. Similar to the aforementioned findings, the expression of proinflammatory cytokines was observed to be reduced in a model of steatohepatitis through the application of the radical scavenger trolox¹⁷⁸. Since this metabolic liver disease is marked by the transition from steatosis to fibrosis via inflammatory processes²⁵⁹, it is reasonable to assume that ferroptosis inhibition may serve as a novel therapeutic approach for the treatment of inflammatory tissue damage and related diseases.

Collectively, it is strongly suggested that ferroptosis is closely linked to distinct inflammatory signatures, characterised by elevated levels of proinflammatory cytokines in damaged tissues 105,175–178. Recent research further implies that ferroptosis exerts a critical role in early inflammatory processes in vivo and that its prevention could dampen necroinflammatory chain reactions. Thus, ferroptosis may be present from the outset of inflammation 4,176,178,260. One might infer that ferroptosis could act as a trigger or sensitiser for subsequent inflammatory events. It has been hypothesised that other regulated necrotic cell death pathways may be initiated through recruited immune cells following immunogenic cell death, culminating in a necroinflammatory feedback loop 21,105. However, the exact molecular pathways and mechanisms driving primary and secondary necroinflammation remain to be elucidated.

6. References

- (1) Tonnus, W.; Meyer, C.; Paliege, A.; Belavgeni, A.; von Mässenhausen, A.; Bornstein, S. R.; Hugo, C.; Becker, J. U.; Linkermann, A. The Pathological Features of Regulated Necrosis. *J. Pathol.* **2019**, *247* (5), 697–707. https://doi.org/10.1002/path.5248.
- (2) Sarhan, M.; Land, W. G.; Tonnus, W.; Hugo, C. P.; Linkermann, A. Origin and Consequences of Necroinflammation. *Physiological Reviews* **2018**, 98 (2), 727–780. https://doi.org/10.1152/physrev.00041.2016.
- (3) Cao, J. Y.; Dixon, S. J. Mechanisms of Ferroptosis. *Cell. Mol. Life Sci.* **2016**, 73 (11–12), 2195–2209. https://doi.org/10.1007/s00018-016-2194-1.
- (4) Li, W.; Feng, G.; Gauthier, J. M.; Lokshina, I.; Higashikubo, R.; Evans, S.; Liu, X.; Hassan, A.; Tanaka, S.; Cicka, M.; Hsiao, H.-M.; Ruiz-Perez, D.; Bredemeyer, A.; Gross, R. W.; Mann, D. L.; Tyurina, Y. Y.; Gelman, A. E.; Kagan, V. E.; Linkermann, A.; Lavine, K. J.; Kreisel, D. Ferroptotic Cell Death and TLR4/Trif Signaling Initiate Neutrophil Recruitment after Heart Transplantation. *Journal of Clinical Investigation* 2019, 10.1172/JCI126428. https://doi.org/10.1172/JCI126428.
- (5) Gilbert, S. F. The Cell Death Pathways. *Developmental Biology. 6th edition* **2000**.
- (6) D'Arcy, M. S. Cell Death: A Review of the Major Forms of Apoptosis, Necrosis and Autophagy. *Cell Biology International* **2019**, *43* (6), 582–592. https://doi.org/10.1002/cbin.11137.
- (7) Moujalled, D.; Strasser, A.; Liddell, J. R. Molecular Mechanisms of Cell Death in Neurological Diseases. *Cell Death Differ* **2021**, *28* (7), 2029–2044. https://doi.org/10.1038/s41418-021-00814-y.
- (8) Su, Y.; Sai, Y.; Zhou, L.; Liu, Z.; Du, P.; Wu, J.; Zhang, J. Current Insights into the Regulation of Programmed Cell Death by TP53 Mutation in Cancer. *Frontiers in Oncology* **2022**, *12*.
- (9) Clarke, P. G. H.; Clarke, S. Nineteenth Century Research on Naturally Occurring Cell Death and Related Phenomena. *Anat Embryol* **1996**, *1*93 (2), 81–99. https://doi.org/10.1007/BF00214700.
- (10) Lockshin, R. A.; Williams, C. M. Programmed Cell Death—II. Endocrine Potentiation of the Breakdown of the Intersegmental Muscles of Silkmoths. *Journal of Insect Physiology* **1964**, *10* (4), 643–649. https://doi.org/10.1016/0022-1910(64)90034-4.
- (11) Saunders, J. W. Death in Embryonic Systems. *Science* **1966**, *154* (3749), 604–612. https://doi.org/10.1126/science.154.3749.604.
- (12) Tata, J. R. Requirement for RNA and Protein Synthesis for Induced Regression of the Tadpole Tail in Organ Culture. *Dev Biol* **1966**, *13* (1), 77–94. https://doi.org/10.1016/0012-1606(66)90050-9.
- (13) Lockshin, R. A. Programmed Cell Death. Activation of Lysis by a Mechanism Involving the Synthesis of Protein. *J Insect Physiol* **1969**, *15* (9), 1505–1516. https://doi.org/10.1016/0022-1910(69)90172-3.
- (14) Kerr, J. F. R.; Wyllie, A. H.; Currie, A. R. Apoptosis: A Basic Biological Phenomenon with Wide-Ranging Implications in Tissue Kinetics. *Br J Cancer* **1972**, *26* (4), 239–257.
- (15) Kerr, J. F. Shrinkage Necrosis: A Distinct Mode of Cellular Death. *J Pathol* **1971**, *105* (1), 13–20. https://doi.org/10.1002/path.1711050103.
- (16) Bursch, W.; Kleine, L.; Tenniswood, M. The Biochemistry of Cell Death by Apoptosis. *Biochem Cell Biol* **1990**, *68* (9), 1071–1074. https://doi.org/10.1139/o90-160.
- (17) Wyllie, A. H.; Kerr, J. F.; Currie, A. R. Cell Death: The Significance of Apoptosis. *Int Rev Cytol* **1980**, *68*, 251–306. https://doi.org/10.1016/s0074-7696(08)62312-8.
- (18) Savill, J.; Fadok, V. Corpse Clearance Defines the Meaning of Cell Death. *Nature* **2000**, *407* (6805), 784–788. https://doi.org/10.1038/35037722.
- (19) Kurosaka, K.; Takahashi, M.; Watanabe, N.; Kobayashi, Y. Silent Cleanup of Very Early Apoptotic Cells by Macrophages. *J Immunol* **2003**, *171* (9), 4672–4679. https://doi.org/10.4049/jimmunol.171.9.4672.
- (20) Berghe, T. V.; Linkermann, A.; Jouan-Lanhouet, S.; Walczak, H.; Vandenabeele, P. Regulated Necrosis: The Expanding Network of Non-Apoptotic Cell Death Pathways. *Nat Rev Mol Cell Biol* **2014**, *15* (2), 135–147. https://doi.org/10.1038/nrm3737.
- (21) Linkermann, A.; Stockwell, B. R.; Krautwald, S.; Anders, H.-J. Regulated Cell Death and Inflammation: An Auto-Amplification Loop Causes Organ Failure. *Nature Reviews Immunology* **2014**, *14* (11), 759–767. https://doi.org/10.1038/nri3743.
- (22) Zakeri, Z.; Lockshin, R. Cell Death: History and Future. *Advances in experimental medicine and biology* **2008**, *615*, 1–11. https://doi.org/10.1007/978-1-4020-6554-5_1.

- (23)Galluzzi, L.; Vitale, I.; Aaronson, S. A.; Abrams, J. M.; Adam, D.; Agostinis, P.; Alnemri, E. S.; Altucci, L.; Amelio, I.; Andrews, D. W.; Annicchiarico-Petruzzelli, M.; Antonov, A. V.; Arama, E.; Baehrecke, E. H.; Barlev, N. A.; Bazan, N. G.; Bernassola, F.; Bertrand, M. J. M.; Bianchi, K.; Blagosklonny, M. V.; Blomgren, K.; Borner, C.; Boya, P.; Brenner, C.; Campanella, M.; Candi, E.; Carmona-Gutierrez, D.; Cecconi, F.; Chan, F. K.-M.; Chandel, N. S.; Cheng, E. H.; Chipuk, J. E.; Cidlowski, J. A.; Ciechanover, A.; Cohen, G. M.; Conrad, M.; Cubillos-Ruiz, J. R.; Czabotar, P. E.; D'Angiolella, V.; Dawson, T. M.; Dawson, V. L.; De Laurenzi, V.; De Maria, R.; Debatin, K.-M.; DeBerardinis, R. J.; Deshmukh, M.; Di Daniele, N.; Di Virgilio, F.; Dixit, V. M.; Dixon, S. J.; Duckett, C. S.; Dynlacht, B. D.; El-Deiry, W. S.; Elrod, J. W.; Fimia, G. M.; Fulda, S.; García-Sáez, A. J.; Garg, A. D.; Garrido, C.; Gavathiotis, E.; Golstein, P.; Gottlieb, E.; Green, D. R.; Greene, L. A.; Gronemeyer, H.; Gross, A.; Hajnoczky, G.; Hardwick, J. M.; Harris, I. S.; Hengartner, M. O.; Hetz, C.; Ichijo, H.; Jäättelä, M.; Joseph, B.; Jost, P. J.; Juin, P. P.; Kaiser, W. J.; Karin, M.; Kaufmann, T.; Kepp, O.; Kimchi, A.; Kitsis, R. N.; Klionsky, D. J.; Knight, R. A.; Kumar, S.; Lee, S. W.; Lemasters, J. J.; Levine, B.; Linkermann, A.; Lipton, S. A.; Lockshin, R. A.; López-Otín, C.; Lowe, S. W.; Luedde, T.; Lugli, E.; MacFarlane, M.; Madeo, F.; Malewicz, M.; Malorni, W.; Manic, G.; Marine, J.-C.; Martin, S. J.; Martinou, J.-C.; Medema, J. P.; Mehlen, P.; Meier, P.; Melino, S.; Miao, E. A.; Molkentin, J. D.; Moll, U. M.; Muñoz-Pinedo, C.: Nagata, S.: Nuñez, G.: Oberst, A.: Oren, M.: Overholtzer, M.: Pagano, M.: Panaretakis, T.: Pasparakis, M.; Penninger, J. M.; Pereira, D. M.; Pervaiz, S.; Peter, M. E.; Piacentini, M.; Pinton, P.; Prehn, J. H. M.; Puthalakath, H.; Rabinovich, G. A.; Rehm, M.; Rizzuto, R.; Rodrigues, C. M. P.; Rubinsztein, D. C.; Rudel, T.; Ryan, K. M.; Sayan, E.; Scorrano, L.; Shao, F.; Shi, Y.; Silke, J.; Simon, H.-U.; Sistigu, A.; Stockwell, B. R.; Strasser, A.; Szabadkai, G.; Tait, S. W. G.; Tang, D.; Tavernarakis, N.; Thorburn, A.; Tsujimoto, Y.; Turk, B.; Vanden Berghe, T.; Vandenabeele, P.; Vander Heiden, M. G.; Villunger, A.; Virgin, H. W.; Vousden, K. H.; Vucic, D.; Wagner, E. F.; Walczak, H.; Wallach, D.; Wang, Y.; Wells, J. A.; Wood, W.; Yuan, J.; Zakeri, Z.; Zhivotovsky, B.; Zitvogel, L.; Melino, G.; Kroemer, G. Molecular Mechanisms of Cell Death: Recommendations of the Nomenclature Committee on Cell Death 2018. Cell Death Differ 2018, 25 (3), 486–541. https://doi.org/10.1038/s41418-017-0012-4.
- Chung, K. M.; Yu, S.-W. Interplay between Autophagy and Programmed Cell Death in Mammalian Neural Stem Cells. *BMB Rep* **2013**, *46* (8), 383–390. https://doi.org/10.5483/BMBRep.2013.46.8.164.
- (25) Clarke, P. G. Developmental Cell Death: Morphological Diversity and Multiple Mechanisms. *Anat Embryol (Berl)* **1990**, *181* (3), 195–213. https://doi.org/10.1007/BF00174615.
- (26) Elmore, S. Apoptosis: A Review of Programmed Cell Death. *Toxicol Pathol* **2007**, 35 (4), 495–516. https://doi.org/10.1080/01926230701320337.
- (27) Norbury, C. J.; Hickson, I. D. Cellular Responses to DNA Damage. *Annu Rev Pharmacol Toxicol* **2001**, *41*, 367–401. https://doi.org/10.1146/annurev.pharmtox.41.1.367.
- (28) Leist, M.; Single, B.; Castoldi, A. F.; Kühnle, S.; Nicotera, P. Intracellular Adenosine Triphosphate (ATP) Concentration: A Switch in the Decision between Apoptosis and Necrosis. *J Exp Med* **1997**, *185* (8), 1481–1486. https://doi.org/10.1084/jem.185.8.1481.
- (29) Denecker, G.; Vercammen, D.; Declercq, W.; Vandenabeele, P. Apoptotic and Necrotic Cell Death Induced by Death Domain Receptors. *Cell Mol Life Sci* **2001**, *58* (3), 356–370. https://doi.org/10.1007/PL00000863.
- (30) McIlwain, D. R.; Berger, T.; Mak, T. W. Caspase Functions in Cell Death and Disease. *Cold Spring Harb Perspect Biol* **2013**, *5* (4), a008656. https://doi.org/10.1101/cshperspect.a008656.
- (31) D'Arcy, M. S. Cell Death: A Review of the Major Forms of Apoptosis, Necrosis and Autophagy. *Cell Biology International* **2019**, *43* (6), 582–592. https://doi.org/10.1002/cbin.11137.
- (32) Zeiss, C. J. The Apoptosis-Necrosis Continuum: Insights from Genetically Altered Mice. *Vet Pathol* **2003**, *40* (5), 481–495. https://doi.org/10.1354/vp.40-5-481.
- (33) Kerr, J. F. R. Shrinkage Necrosis of Adrenal Cortical Cells. *The Journal of Pathology* **1972**, *107* (3), 217–219. https://doi.org/10.1002/path.1711070309.
- (34) Wyllie, A. H.; Kerr, J. F.; Currie, A. R. Cell Death in the Normal Neonatal Rat Adrenal Cortex. *J Pathol* **1973**, *111* (4), 255–261. https://doi.org/10.1002/path.1711110406.
- (35) Bratton, D. L.; Fadok, V. A.; Richter, D. A.; Kailey, J. M.; Guthrie, L. A.; Henson, P. M. Appearance of Phosphatidylserine on Apoptotic Cells Requires Calcium-Mediated Nonspecific Flip-Flop and Is Enhanced by Loss of the Aminophospholipid Translocase. *J Biol Chem* **1997**, 272 (42), 26159–26165. https://doi.org/10.1074/jbc.272.42.26159.
- (36) van Engeland, M.; Nieland, L. J.; Ramaekers, F. C.; Schutte, B.; Reutelingsperger, C. P. Annexin V-Affinity Assay: A Review on an Apoptosis Detection System Based on Phosphatidylserine Exposure. *Cytometry* **1998**, *31* (1), 1–9. https://doi.org/10.1002/(sici)1097-0320(19980101)31:1<1::aid-cyto1>3.0.co;2-r.

- (37) Arur, S.; Uche, U. E.; Rezaul, K.; Fong, M.; Scranton, V.; Cowan, A. E.; Mohler, W.; Han, D. K. Annexin I Is an Endogenous Ligand That Mediates Apoptotic Cell Engulfment. *Developmental Cell* **2003**, *4* (4), 587–598. https://doi.org/10.1016/S1534-5807(03)00090-X.
- (38) Igney, F. H.; Krammer, P. H. Death and Anti-Death: Tumour Resistance to Apoptosis. *Nat Rev Cancer* **2002**, *2* (4), 277–288. https://doi.org/10.1038/nrc776.
- (39) Locksley, R. M.; Killeen, N.; Lenardo, M. J. The TNF and TNF Receptor Superfamilies: Integrating Mammalian Biology. *Cell* **2001**, *104* (4), 487–501. https://doi.org/10.1016/S0092-8674(01)00237-9.
- (40) Nagata, S. Apoptosis by Death Factor. *Cell* **1997**, *88* (3), 355–365. https://doi.org/10.1016/s0092-8674(00)81874-7.
- (41) Bossen, C.; Ingold, K.; Tardivel, A.; Bodmer, J.-L.; Gaide, O.; Hertig, S.; Ambrose, C.; Tschopp, J.; Schneider, P. Interactions of Tumor Necrosis Factor (TNF) and TNF Receptor Family Members in the Mouse and Human. *J Biol Chem* 2006, 281 (20), 13964–13971. https://doi.org/10.1074/jbc.M601553200.
- (42) Walczak, H. Death Receptor–Ligand Systems in Cancer, Cell Death, and Inflammation. *Cold Spring Harb Perspect Biol* **2013**, *5* (5), a008698. https://doi.org/10.1101/cshperspect.a008698.
- (43) Krammer, P. H. CD95's Deadly Mission in the Immune System. *Nature* **2000**, *407* (6805), 789–795. https://doi.org/10.1038/35037728.
- (44) Lavrik, I. N.; Krammer, P. H. Regulation of CD95/Fas Signaling at the DISC. *Cell Death Differ* **2012**, *19* (1), 36–41. https://doi.org/10.1038/cdd.2011.155.
- (45) Kischkel, F. C.; Hellbardt, S.; Behrmann, I.; Germer, M.; Pawlita, M.; Krammer, P. H.; Peter, M. E. Cytotoxicity-Dependent APO-1 (Fas/CD95)-Associated Proteins Form a Death-Inducing Signaling Complex (DISC) with the Receptor. *EMBO J* 1995, 14 (22), 5579–5588.
- (46) Kim, J. H.; Lee, S. Y.; Oh, S. Y.; Han, S. I.; Park, H. G.; Yoo, M.-A.; Kang, H. S. Methyl Jasmonate Induces Apoptosis through Induction of Bax/Bcl-XS and Activation of Caspase-3 via ROS Production in A549 Cells. *Oncol Rep* **2004**, *12* (6), 1233–1238.
- (47) Hsu, H.; Xiong, J.; Goeddel, D. V. The TNF Receptor 1-Associated Protein TRADD Signals Cell Death and NF-Kappa B Activation. *Cell* **1995**, *81* (4), 495–504. https://doi.org/10.1016/0092-8674(95)90070-5.
- (48) Wajant, H. The Fas Signaling Pathway: More than a Paradigm. *Science* **2002**, 296 (5573), 1635–1636. https://doi.org/10.1126/science.1071553.
- (49) Samraj, A. K.; Keil, E.; Ueffing, N.; Schulze-Osthoff, K.; Schmitz, I. Loss of Caspase-9 Provides Genetic Evidence for the Type I/II Concept of CD95-Mediated Apoptosis. *J Biol Chem* **2006**, 281 (40), 29652–29659. https://doi.org/10.1074/jbc.M603487200.
- (50) Jost, P. J.; Grabow, S.; Gray, D.; McKenzie, M. D.; Nachbur, U.; Huang, D. C. S.; Bouillet, P.; Thomas, H. E.; Borner, C.; Silke, J.; Strasser, A.; Kaufmann, T. XIAP Discriminates between Type I and Type II FAS-Induced Apoptosis. *Nature* **2009**, *460* (7258), 1035–1039. https://doi.org/10.1038/nature08229.
- (51) Strasser, A.; Jost, P. J.; Nagata, S. The Many Roles of FAS Receptor Signaling in the Immune System. *Immunity* **2009**, *30* (2), 180–192. https://doi.org/10.1016/j.immuni.2009.01.001.
- (52) Krammer, P. H. CD95's Deadly Mission in the Immune System. *Nature* **2000**, *407* (6805), 789–795. https://doi.org/10.1038/35037728.
- (53) Brenner, D.; Mak, T. W. Mitochondrial Cell Death Effectors. *Curr Opin Cell Biol* **2009**, *21* (6), 871–877. https://doi.org/10.1016/j.ceb.2009.09.004.
- (54) Cory, S.; Adams, J. M. The Bcl2 Family: Regulators of the Cellular Life-or-Death Switch. *Nat Rev Cancer* **2002**, *2* (9), 647–656. https://doi.org/10.1038/nrc883.
- (55) Czabotar, P. E.; Lessene, G.; Strasser, A.; Adams, J. M. Control of Apoptosis by the BCL-2 Protein Family: Implications for Physiology and Therapy. *Nat Rev Mol Cell Biol* **2014**, *15* (1), 49–63. https://doi.org/10.1038/nrm3722.
- (56) Tait, S. W. G.; Green, D. R. Mitochondrial Regulation of Cell Death. *Cold Spring Harb Perspect Biol* **2013**, *5* (9), a008706. https://doi.org/10.1101/cshperspect.a008706.
- (57) Du, C.; Fang, M.; Li, Y.; Li, L.; Wang, X. Smac, a Mitochondrial Protein That Promotes Cytochrome c-Dependent Caspase Activation by Eliminating IAP Inhibition. *Cell* **2000**, *102* (1), 33–42. https://doi.org/10.1016/s0092-8674(00)00008-8.
- (58) Cai, J.; Yang, J.; Jones, D. P. Mitochondrial Control of Apoptosis: The Role of Cytochrome c. *Biochim Biophys Acta* **1998**, *1366* (1–2), 139–149. https://doi.org/10.1016/s0005-2728(98)00109-1.
- (59) Garrido, C.; Galluzzi, L.; Brunet, M.; Puig, P. E.; Didelot, C.; Kroemer, G. Mechanisms of Cytochrome c Release from Mitochondria. *Cell Death Differ* **2006**, *13* (9), 1423–1433. https://doi.org/10.1038/sj.cdd.4401950.

- (60) van Loo, G.; Saelens, X.; van Gurp, M.; MacFarlane, M.; Martin, S. J.; Vandenabeele, P. The Role of Mitochondrial Factors in Apoptosis: A Russian Roulette with More than One Bullet. *Cell Death Differ* **2002**, *9* (10), 1031–1042. https://doi.org/10.1038/sj.cdd.4401088.
- (61) Saelens, X.; Festjens, N.; Vande Walle, L.; van Gurp, M.; van Loo, G.; Vandenabeele, P. Toxic Proteins Released from Mitochondria in Cell Death. *Oncogene* **2004**, *23* (16), 2861–2874. https://doi.org/10.1038/sj.onc.1207523.
- (62) van Loo, G.; van Gurp, M.; Depuydt, B.; Srinivasula, S. M.; Rodriguez, I.; Alnemri, E. S.; Gevaert, K.; Vandekerckhove, J.; Declercq, W.; Vandenabeele, P. The Serine Protease Omi/HtrA2 Is Released from Mitochondria during Apoptosis. Omi Interacts with Caspase-Inhibitor XIAP and Induces Enhanced Caspase Activity. Cell Death Differ 2002, 9 (1), 20–26. https://doi.org/10.1038/sj.cdd.4400970.
- (63) Chinnaiyan, A. M. The Apoptosome: Heart and Soul of the Cell Death Machine. *Neoplasia* **1999**, *1* (1), 5–15.
- (64) Acehan, D.; Jiang, X.; Morgan, D. G.; Heuser, J. E.; Wang, X.; Akey, C. W. Three-Dimensional Structure of the Apoptosome: Implications for Assembly, Procaspase-9 Binding, and Activation. *Molecular Cell* **2002**, *9* (2), 423–432. https://doi.org/10.1016/S1097-2765(02)00442-2.
- (65) Cain, K.; Bratton, S. B.; Cohen, G. M. The Apaf-1 Apoptosome: A Large Caspase-Activating Complex. *Biochimie* **2002**, *84* (2–3), 203–214. https://doi.org/10.1016/s0300-9084(02)01376-7.
- (66) Sakahira, H.; Enari, M.; Nagata, S. Cleavage of CAD Inhibitor in CAD Activation and DNA Degradation during Apoptosis. *Nature* **1998**, *391* (6662), 96–99. https://doi.org/10.1038/34214.
- (67) Fadok, V. A.; Cathelineau, A. de; Daleke, D. L.; Henson, P. M.; Bratton, D. L. Loss of Phospholipid Asymmetry and Surface Exposure of Phosphatidylserine Is Required for Phagocytosis of Apoptotic Cells by Macrophages and Fibroblasts *. *Journal of Biological Chemistry* 2001, 276 (2), 1071–1077. https://doi.org/10.1074/jbc.M003649200.
- (68) Klionsky, D. J. Autophagy Revisited: A Conversation with Christian de Duve. *Autophagy* **2008**, *4* (6), 740–743. https://doi.org/10.4161/auto.6398.
- (69) Bialik, S.; Dasari, S. K.; Kimchi, A. Autophagy-Dependent Cell Death Where, How and Why a Cell Eats Itself to Death. *Journal of Cell Science* **2018**, *131* (18), jcs215152. https://doi.org/10.1242/jcs.215152.
- (70) Mizushima, N.; Levine, B.; Cuervo, A. M.; Klionsky, D. J. Autophagy Fights Disease through Cellular Self-Digestion. *Nature* **2008**, *451* (7182), 1069–1075. https://doi.org/10.1038/nature06639.
- (71) Kroemer, G.; Mariño, G.; Levine, B. Autophagy and the Integrated Stress Response. *Mol Cell* **2010**, *40* (2), 280–293. https://doi.org/10.1016/j.molcel.2010.09.023.
- (72) Murrow, L.; Debnath, J. Autophagy as a Stress-Response and Quality-Control Mechanism: Implications for Cell Injury and Human Disease. *Annu Rev Pathol* **2013**, *8*, 105–137. https://doi.org/10.1146/annurev-pathol-020712-163918.
- (73) Cuervo, A. M. Autophagy: Many Paths to the Same End. *Mol Cell Biochem* **2004**, *263* (1–2), 55–72.
- (74) Liu, J.; Kuang, F.; Kroemer, G.; Klionsky, D. J.; Kang, R.; Tang, D. Autophagy-Dependent Ferroptosis: Machinery and Regulation. *Cell Chem Biol* **2020**, 27 (4), 420–435. https://doi.org/10.1016/j.chembiol.2020.02.005.
- (75) Ohashi, Y. Class III Phosphatidylinositol 3-Kinase Complex I Subunit NRBF2/Atg38 from Cell and Structural Biology to Health and Disease. *Autophagy* **2021**, *17* (12), 3897–3907. https://doi.org/10.1080/15548627.2021.1872240.
- (76) Ndoye, A.; Weeraratna, A. T. Autophagy- An Emerging Target for Melanoma Therapy. *F1000Res* **2016**, *5*, F1000 Faculty Rev-1888. https://doi.org/10.12688/f1000research.8347.1.
- (77) Xie, Y.; Kang, R.; Sun, X.; Zhong, M.; Huang, J.; Klionsky, D. J.; Tang, D. Posttranslational Modification of Autophagy-Related Proteins in Macroautophagy. *Autophagy* **2014**, *11* (1), 28–45. https://doi.org/10.4161/15548627.2014.984267.
- (78) Li, W.; Li, J.; Bao, J. Microautophagy: Lesser-Known Self-Eating. *Cell Mol Life Sci* **2012**, *69* (7), 1125–1136. https://doi.org/10.1007/s00018-011-0865-5.
- (79) Dice, J. F. Chaperone-Mediated Autophagy. *Autophagy* **2007**, *3* (4), 295–299. https://doi.org/10.4161/auto.4144.
- (80) Zhou, B.; Liu, J.; Kang, R.; Klionsky, D. J.; Kroemer, G.; Tang, D. Ferroptosis Is a Type of Autophagy-Dependent Cell Death. Semin Cancer Biol 2020, 66, 89–100. https://doi.org/10.1016/j.semcancer.2019.03.002.
- (81) Mancias, J. D.; Wang, X.; Gygi, S. P.; Harper, J. W.; Kimmelman, A. C. Quantitative Proteomics Identifies NCOA4 as the Cargo Receptor Mediating Ferritinophagy. *Nature* **2014**, *509* (7498), 105–109. https://doi.org/10.1038/nature13148.

- (82) Galluzzi, L.; Bravo-San Pedro, J. M.; Kepp, O.; Kroemer, G. Regulated Cell Death and Adaptive Stress Responses. *Cell Mol Life Sci* **2016**, 73 (11–12), 2405–2410. https://doi.org/10.1007/s00018-016-2209-y.
- (83) Kroemer, G.; Galluzzi, L.; Vandenabeele, P.; Abrams, J.; Alnemri, E.; Baehrecke, E.; Blagosklonny, M.; El-Deiry, W.; Golstein, P.; Green, D.; Hengartner, M.; Knight, R.; Kumar, S.; Lipton, S.; Malorni, W.; Nuñez, G.; Peter, M.; Tschopp, J.; Yuan, J.; Piacentini, M.; Zhivotovsky, B.; Melino, G. Classification of Cell Death. Cell Death Differ 2009, 16 (1), 3–11. https://doi.org/10.1038/cdd.2008.150.
- (84) Nirmala, J. G.; Lopus, M. Cell Death Mechanisms in Eukaryotes. *Cell Biol Toxicol* **2020**, 36 (2), 145–164. https://doi.org/10.1007/s10565-019-09496-2.
- (85) Trump, B. F.; Berezesky, I. K.; Chang, S. H.; Phelps, P. C. The Pathways of Cell Death: Oncosis, Apoptosis, and Necrosis. *Toxicol Pathol* **1997**, *25* (1), 82–88. https://doi.org/10.1177/019262339702500116.
- (86) Dhuriya, Y. K.; Sharma, D. Necroptosis: A Regulated Inflammatory Mode of Cell Death. *Journal of Neuroinflammation* **2018**, *15* (1), 199. https://doi.org/10.1186/s12974-018-1235-0.
- (87) Dai, W.; Cheng, J.; Leng, X.; Hu, X.; Ao, Y. The Potential Role of Necroptosis in Clinical Diseases (Review). *Int J Mol Med* **2021**, *47* (5), 89. https://doi.org/10.3892/ijmm.2021.4922.
- (88) Tewari, M.; Beidler, D. R.; Dixit, V. M. CrmA-Inhibitable Cleavage of the 70-KDa Protein Component of the U1 Small Nuclear Ribonucleoprotein during Fas- and Tumor Necrosis Factor-Induced Apoptosis (*). *Journal of Biological Chemistry* **1995**, *270* (32), 18738–18741. https://doi.org/10.1074/jbc.270.32.18738.
- (89) Meng, Y.; Sandow, J. J.; Czabotar, P. E.; Murphy, J. M. The Regulation of Necroptosis by Post-Translational Modifications. *Cell Death Differ* 2021, 28 (3), 861–883. https://doi.org/10.1038/s41418-020-00722-7.
- (90) Samson, A. L.; Zhang, Y.; Geoghegan, N. D.; Gavin, X. J.; Davies, K. A.; Mlodzianoski, M. J.; Whitehead, L. W.; Frank, D.; Garnish, S. E.; Fitzgibbon, C.; Hempel, A.; Young, S. N.; Jacobsen, A. V.; Cawthorne, W.; Petrie, E. J.; Faux, M. C.; Shield-Artin, K.; Lalaoui, N.; Hildebrand, J. M.; Silke, J.; Rogers, K. L.; Lessene, G.; Hawkins, E. D.; Murphy, J. M. MLKL Trafficking and Accumulation at the Plasma Membrane Control the Kinetics and Threshold for Necroptosis. *Nat Commun* 2020, 11 (1), 3151. https://doi.org/10.1038/s41467-020-16887-1.
- (91) Wang, H.; Sun, L.; Su, L.; Rizo, J.; Liu, L.; Wang, L.-F.; Wang, F.-S.; Wang, X. Mixed Lineage Kinase Domain-like Protein MLKL Causes Necrotic Membrane Disruption upon Phosphorylation by RIP3. *Mol Cell* **2014**, *54* (1), 133–146. https://doi.org/10.1016/j.molcel.2014.03.003.
- (92) Chen, X.; Dai, Y.; Wan, X.; Hu, X.; Zhao, W.; Ban, X.; Wan, H.; Huang, K.; Zhang, Q.; Xiong, K. ZBP1-Mediated Necroptosis: Mechanisms and Therapeutic Implications. *Molecules* **2022**, *28* (1), 52. https://doi.org/10.3390/molecules28010052.
- (93) Kuriakose, T.; Man, S. M.; Malireddi, R. K. S.; Karki, R.; Kesavardhana, S.; Place, D. E.; Neale, G.; Vogel, P.; Kanneganti, T.-D. ZBP1/DAI Is an Innate Sensor of Influenza Virus Triggering the NLRP3 Inflammasome and Programmed Cell Death Pathways. *Sci Immunol* **2016**, *1* (2), aag2045. https://doi.org/10.1126/sciimmunol.aag2045.
- (94) Szczesny, B.; Marcatti, M.; Ahmad, A.; Montalbano, M.; Brunyánszki, A.; Bibli, S.-I.; Papapetropoulos, A.; Szabo, C. Mitochondrial DNA Damage and Subsequent Activation of Z-DNA Binding Protein 1 Links Oxidative Stress to Inflammation in Epithelial Cells. *Sci Rep* **2018**, 8 (1), 914. https://doi.org/10.1038/s41598-018-19216-1.
- (95) Rao, Z.; Zhu, Y.; Yang, P.; Chen, Z.; Xia, Y.; Qiao, C.; Liu, W.; Deng, H.; Li, J.; Ning, P.; Wang, Z. Pyroptosis in Inflammatory Diseases and Cancer. *Theranostics* **2022**, *12* (9), 4310–4329. https://doi.org/10.7150/thno.71086.
- (96) D'Souza, C. A.; Heitman, J. Dismantling the Cryptococcus Coat. *Trends Microbiol* **2001**, *9* (3), 112–113. https://doi.org/10.1016/s0966-842x(00)01945-4.
- (97) Yu, P.; Zhang, X.; Liu, N.; Tang, L.; Peng, C.; Chen, X. Pyroptosis: Mechanisms and Diseases. *Sig Transduct Target Ther* **2021**, *6* (1), 1–21. https://doi.org/10.1038/s41392-021-00507-5.
- (98) Strowig, T.; Henao-Mejia, J.; Elinav, E.; Flavell, R. Inflammasomes in Health and Disease. *Nature* **2012**, *481* (7381), 278–286. https://doi.org/10.1038/nature10759.
- (99) Rathinam, V. A. K.; Fitzgerald, K. A. Inflammasome Complexes: Emerging Mechanisms and Effector Functions. *Cell* **2016**, *165* (4), 792–800. https://doi.org/10.1016/j.cell.2016.03.046.
- (100) Broz, P.; Dixit, V. M. Inflammasomes: Mechanism of Assembly, Regulation and Signalling. *Nat Rev Immunol* **2016**, *16* (7), 407–420. https://doi.org/10.1038/nri.2016.58.
- (101) Sborgi, L.; Rühl, S.; Mulvihill, E.; Pipercevic, J.; Heilig, R.; Stahlberg, H.; Farady, C. J.; Müller, D. J.; Broz, P.; Hiller, S. GSDMD Membrane Pore Formation Constitutes the Mechanism of

- Pyroptotic Cell Death. *EMBO J* **2016**, 35 (16), 1766–1778. https://doi.org/10.15252/embj.201694696.
- (102) Fink, S. L.; Cookson, B. T. Caspase-1-Dependent Pore Formation during Pyroptosis Leads to Osmotic Lysis of Infected Host Macrophages. *Cellular Microbiology* **2006**, *8* (11), 1812–1825. https://doi.org/10.1111/j.1462-5822.2006.00751.x.
- (103) Shi, J.; Zhao, Y.; Wang, Y.; Gao, W.; Ding, J.; Li, P.; Hu, L.; Shao, F. Inflammatory Caspases Are Innate Immune Receptors for Intracellular LPS. *Nature* **2014**, *514* (7521), 187–192. https://doi.org/10.1038/nature13683.
- (104) Dixon, S. J.; Lemberg, K. M.; Lamprecht, M. R.; Skouta, R.; Zaitsev, E. M.; Gleason, C. E.; Patel, D. N.; Bauer, A. J.; Cantley, A. M.; Yang, W. S.; Morrison, B.; Stockwell, B. R. Ferroptosis: An Iron-Dependent Form of Nonapoptotic Cell Death. *Cell* **2012**, *149* (5), 1060–1072. https://doi.org/10.1016/j.cell.2012.03.042.
- (105) Bebber, C. M.; Müller, F.; Prieto Clemente, L.; Weber, J.; von Karstedt, S. Ferroptosis in Cancer Cell Biology. *Cancers (Basel)* **2020**, *12* (1), E164. https://doi.org/10.3390/cancers12010164.
- (106) Xie, Y.; Hou, W.; Song, X.; Yu, Y.; Huang, J.; Sun, X.; Kang, R.; Tang, D. Ferroptosis: Process and Function. *Cell Death Differ* **2016**, *23* (3), 369–379. https://doi.org/10.1038/cdd.2015.158.
- (107) Dixon, S. J.; Stockwell, B. R. The Hallmarks of Ferroptosis. *Annual Review of Cancer Biology* **2019**, 3 (1), 35–54. https://doi.org/10.1146/annurev-cancerbio-030518-055844.
- (108) Betteridge, D. J. What Is Oxidative Stress? *Metabolism* **2000**, *49* (2, Supplement 1), 3–8. https://doi.org/10.1016/S0026-0495(00)80077-3.
- (109) Ayala, A.; Muñoz, M. F.; Argüelles, S. Lipid Peroxidation: Production, Metabolism, and Signaling Mechanisms of Malondialdehyde and 4-Hydroxy-2-Nonenal. *Oxid Med Cell Longev* **2014**, *2014*, 360438. https://doi.org/10.1155/2014/360438.
- (110) Gao, M.; Monian, P.; Quadri, N.; Ramasamy, R.; Jiang, X. Glutaminolysis and Transferrin Regulate Ferroptosis. *Mol Cell* **2015**, *59* (2), 298–308. https://doi.org/10.1016/j.molcel.2015.06.011.
- (111) Hao, S.; Liang, B.; Huang, Q.; Dong, S.; Wu, Z.; He, W.; Shi, M. Metabolic Networks in Ferroptosis. Oncol Lett 2018, 15 (4), 5405–5411. https://doi.org/10.3892/ol.2018.8066.
- (112) Kakhlon, O.; Cabantchik, Z. I. The Labile Iron Pool: Characterization, Measurement, and Participation in Cellular Processes(1). *Free Radic Biol Med* **2002**, 33 (8), 1037–1046. https://doi.org/10.1016/s0891-5849(02)01006-7.
- (113) Cheng, Z.; Li, Y. What Is Responsible for the Initiating Chemistry of Iron-Mediated Lipid Peroxidation: An Update. *Chem Rev* **2007**, *107* (3), 748–766. https://doi.org/10.1021/cr040077w.
- (114) Sullivan, L. B.; Chandel, N. S. Mitochondrial Reactive Oxygen Species and Cancer. *Cancer Metab* **2014**, *2*, 17. https://doi.org/10.1186/2049-3002-2-17.
- (115) Papa, S.; Martino, P. L.; Capitanio, G.; Gaballo, A.; De Rasmo, D.; Signorile, A.; Petruzzella, V. The Oxidative Phosphorylation System in Mammalian Mitochondria. *Adv Exp Med Biol* **2012**, 942, 3–37. https://doi.org/10.1007/978-94-007-2869-1_1.
- (116) Martínez-Reyes, I.; Chandel, N. S. Mitochondrial TCA Cycle Metabolites Control Physiology and Disease. *Nat Commun* **2020**, *11* (1), 102. https://doi.org/10.1038/s41467-019-13668-3.
- (117) Tang, Y.; Zhou, J.; Hooi, S. C.; Jiang, Y.-M.; Lu, G.-D. Fatty Acid Activation in Carcinogenesis and Cancer Development: Essential Roles of Long-Chain Acyl-CoA Synthetases. *Oncol Lett* **2018**, *16* (2), 1390–1396. https://doi.org/10.3892/ol.2018.8843.
- (118) Doll, S.; Proneth, B.; Tyurina, Y. Y.; Panzilius, E.; Kobayashi, S.; Ingold, I.; Irmler, M.; Beckers, J.; Aichler, M.; Walch, A.; Prokisch, H.; Trümbach, D.; Mao, G.; Qu, F.; Bayir, H.; Füllekrug, J.; Scheel, C. H.; Wurst, W.; Schick, J. A.; Kagan, V. E.; Angeli, J. P. F.; Conrad, M. ACSL4 Dictates Ferroptosis Sensitivity by Shaping Cellular Lipid Composition. *Nat Chem Biol* **2017**, *13* (1), 91–98. https://doi.org/10.1038/nchembio.2239.
- (119) Gaschler, M. M.; Stockwell, B. R. Lipid Peroxidation in Cell Death. *Biochem Biophys Res Commun* **2017**, *482* (3), 419–425. https://doi.org/10.1016/j.bbrc.2016.10.086.
- (120) Dixon, S. J.; Winter, G. E.; Musavi, L. S.; Lee, E. D.; Snijder, B.; Rebsamen, M.; Superti-Furga, G.; Stockwell, B. R. Human Haploid Cell Genetics Reveals Roles for Lipid Metabolism Genes in Nonapoptotic Cell Death. ACS Chem Biol 2015, 10 (7), 1604–1609. https://doi.org/10.1021/acschembio.5b00245.
- (121) Yang, W. S.; Kim, K. J.; Gaschler, M. M.; Patel, M.; Shchepinov, M. S.; Stockwell, B. R. Peroxidation of Polyunsaturated Fatty Acids by Lipoxygenases Drives Ferroptosis. *Proc Natl Acad Sci U S A* **2016**, *113* (34), E4966-4975. https://doi.org/10.1073/pnas.1603244113.
- (122) Lei, P.; Bai, T.; Sun, Y. Mechanisms of Ferroptosis and Relations With Regulated Cell Death: A Review. *Frontiers in Physiology* **2019**, *10*. https://doi.org/10.3389/fphys.2019.00139.

- (123) Feng, H.; Stockwell, B. R. Unsolved Mysteries: How Does Lipid Peroxidation Cause Ferroptosis? *PLOS Biology* **2018**, *16* (5), e2006203. https://doi.org/10.1371/journal.pbio.2006203.
- (124) Agmon, E.; Solon, J.; Bassereau, P.; Stockwell, B. R. Modeling the Effects of Lipid Peroxidation during Ferroptosis on Membrane Properties. *Sci Rep* **2018**, *8* (1), 5155. https://doi.org/10.1038/s41598-018-23408-0.
- (125) Kagan, V. E.; Mao, G.; Qu, F.; Angeli, J. P. F.; Doll, S.; Croix, C. S.; Dar, H. H.; Liu, B.; Tyurin, V. A.; Ritov, V. B.; Kapralov, A. A.; Amoscato, A. A.; Jiang, J.; Anthonymuthu, T.; Mohammadyani, D.; Yang, Q.; Proneth, B.; Klein-Seetharaman, J.; Watkins, S.; Bahar, I.; Greenberger, J.; Mallampalli, R. K.; Stockwell, B. R.; Tyurina, Y. Y.; Conrad, M.; Bayır, H. Oxidized Arachidonic and Adrenic PEs Navigate Cells to Ferroptosis. *Nat Chem Biol* 2017, 13 (1), 81–90. https://doi.org/10.1038/nchembio.2238.
- (126) Friedmann Angeli, J. P.; Schneider, M.; Proneth, B.; Tyurina, Y. Y.; Tyurin, V. A.; Hammond, V. J.; Herbach, N.; Aichler, M.; Walch, A.; Eggenhofer, E.; Basavarajappa, D.; Rådmark, O.; Kobayashi, S.; Seibt, T.; Beck, H.; Neff, F.; Esposito, I.; Wanke, R.; Förster, H.; Yefremova, O.; Heinrichmeyer, M.; Bornkamm, G. W.; Geissler, E. K.; Thomas, S. B.; Stockwell, B. R.; O'Donnell, V. B.; Kagan, V. E.; Schick, J. A.; Conrad, M. Inactivation of the Ferroptosis Regulator Gpx4 Triggers Acute Renal Failure in Mice. *Nat. Cell Biol.* **2014**, *16* (12), 1180–1191. https://doi.org/10.1038/ncb3064.
- (127) Seiler, A.; Schneider, M.; Förster, H.; Roth, S.; Wirth, E. K.; Culmsee, C.; Plesnila, N.; Kremmer, E.; Rådmark, O.; Wurst, W.; Bornkamm, G. W.; Schweizer, U.; Conrad, M. Glutathione Peroxidase 4 Senses and Translates Oxidative Stress into 12/15-Lipoxygenase Dependent-and AIF-Mediated Cell Death. *Cell Metab.* **2008**, *8* (3), 237–248. https://doi.org/10.1016/j.cmet.2008.07.005.
- (128) Pallast, S.; Arai, K.; Wang, X.; Lo, E. H.; van Leyen, K. 12/15-Lipoxygenase Targets Neuronal Mitochondria under Oxidative Stress. *J Neurochem* **2009**, *111* (3), 882–889. https://doi.org/10.1111/j.1471-4159.2009.06379.x.
- (129) Yang, W. S.; SriRamaratnam, R.; Welsch, M. E.; Shimada, K.; Skouta, R.; Viswanathan, V. S.; Cheah, J. H.; Clemons, P. A.; Shamji, A. F.; Clish, C. B.; Brown, L. M.; Girotti, A. W.; Cornish, V. W.; Schreiber, S. L.; Stockwell, B. R. Regulation of Ferroptotic Cancer Cell Death by GPX4. Cell 2014, 156 (0), 317–331. https://doi.org/10.1016/j.cell.2013.12.010.
- (130) Meister, A. Selective Modification of Glutathione Metabolism. *Science* **1983**, 220 (4596), 472–477. https://doi.org/10.1126/science.6836290.
- (131) Serru, V.; Baudin, B.; Ziegler, F.; David, J. P.; Cals, M. J.; Vaubourdolle, M.; Mario, N. Quantification of Reduced and Oxidized Glutathione in Whole Blood Samples by Capillary Electrophoresis. *Clin Chem* **2001**, *47* (7), 1321–1324.
- (132) Habib, E.; Linher-Melville, K.; Lin, H.-X.; Singh, G. Expression of XCT and Activity of System Xc– Are Regulated by NRF2 in Human Breast Cancer Cells in Response to Oxidative Stress. *Redox Biology* **2015**, *5*, 33–42. https://doi.org/10.1016/j.redox.2015.03.003.
- (133) Yu, X.; Long, Y. C. Crosstalk between Cystine and Glutathione Is Critical for the Regulation of Amino Acid Signaling Pathways and Ferroptosis. *Sci Rep* **2016**, *6* (1), 30033. https://doi.org/10.1038/srep30033.
- (134) Mcbean, G. J. The Transsulfuration Pathway: A Source of Cysteine for Glutathione in Astrocytes. *Amino Acids* **2011**, *42* (1).
- (135) Lu, S. C. GLUTATHIONE SYNTHESIS. *Biochim Biophys Acta* **2013**, *1830* (5), 3143–3153. https://doi.org/10.1016/j.bbagen.2012.09.008.
- (136) Proneth, B.; Conrad, M. Ferroptosis and Necroinflammation, a yet Poorly Explored Link. *Cell Death Differ* **2019**, *26* (1), 14–24. https://doi.org/10.1038/s41418-018-0173-9.
- (137) Dixon, S. J.; Patel, D. N.; Welsch, M.; Skouta, R.; Lee, E. D.; Hayano, M.; Thomas, A. G.; Gleason, C. E.; Tatonetti, N. P.; Slusher, B. S.; Stockwell, B. R. Pharmacological Inhibition of Cystine–Glutamate Exchange Induces Endoplasmic Reticulum Stress and Ferroptosis. *eLife* **2014**, *3*, e02523. https://doi.org/10.7554/eLife.02523.
- (138) Gao, M.; Yi, J.; Zhu, J.; Minikes, A. M.; Monian, P.; Thompson, C. B.; Jiang, X. Role of Mitochondria in Ferroptosis. *Molecular Cell* **2019**, 73 (2), 354-363.e3. https://doi.org/10.1016/j.molcel.2018.10.042.
- (139) Stockwell, B. R. Ferroptosis Turns 10: Emerging Mechanisms, Physiological Functions, and Therapeutic Applications. *Cell* **2022**, *185* (14), 2401–2421. https://doi.org/10.1016/j.cell.2022.06.003.
- (140) Doll, S.; Freitas, F. P.; Shah, R.; Aldrovandi, M.; da Silva, M. C.; Ingold, I.; Goya Grocin, A.; Xavier da Silva, T. N.; Panzilius, E.; Scheel, C. H.; Mourão, A.; Buday, K.; Sato, M.; Wanninger, J.; Vignane, T.; Mohana, V.; Rehberg, M.; Flatley, A.; Schepers, A.; Kurz, A.; White, D.; Sauer,

- M.; Sattler, M.; Tate, E. W.; Schmitz, W.; Schulze, A.; O'Donnell, V.; Proneth, B.; Popowicz, G. M.; Pratt, D. A.; Angeli, J. P. F.; Conrad, M. FSP1 Is a Glutathione-Independent Ferroptosis Suppressor. *Nature* **2019**, *575* (7784), 693–698. https://doi.org/10.1038/s41586-019-1707-0.
- (141) Bersuker, K.; Hendricks, J. M.; Li, Z.; Magtanong, L.; Ford, B.; Tang, P. H.; Roberts, M. A.; Tong, B.; Maimone, T. J.; Zoncu, R.; Bassik, M. C.; Nomura, D. K.; Dixon, S. J.; Olzmann, J. A. The CoQ Oxidoreductase FSP1 Acts Parallel to GPX4 to Inhibit Ferroptosis. *Nature* **2019**, *575* (7784), 688–692. https://doi.org/10.1038/s41586-019-1705-2.
- (142) Mao, C.; Liu, X.; Zhang, Y.; Lei, G.; Yan, Y.; Lee, H.; Koppula, P.; Wu, S.; Zhuang, L.; Fang, B.; Poyurovsky, M. V.; Olszewski, K.; Gan, B. DHODH-Mediated Ferroptosis Defence Is a Targetable Vulnerability in Cancer. *Nature* 2021, 593 (7860), 586–590. https://doi.org/10.1038/s41586-021-03539-7.
- (143) Kraft, V. A. N.; Bezjian, C. T.; Pfeiffer, S.; Ringelstetter, L.; Müller, C.; Zandkarimi, F.; Merl-Pham, J.; Bao, X.; Anastasov, N.; Kössl, J.; Brandner, S.; Daniels, J. D.; Schmitt-Kopplin, P.; Hauck, S. M.; Stockwell, B. R.; Hadian, K.; Schick, J. A. GTP Cyclohydrolase 1/Tetrahydrobiopterin Counteract Ferroptosis through Lipid Remodeling. *ACS Cent Sci* **2020**, *6* (1), 41–53. https://doi.org/10.1021/acscentsci.9b01063.
- (144) Dixon, S. J.; Stockwell, B. R. The Role of Iron and Reactive Oxygen Species in Cell Death. *Nat Chem Biol* **2014**, *10* (1), 9–17. https://doi.org/10.1038/nchembio.1416.
- (145) Conrad, M.; Friedmann Angeli, J. P. Glutathione Peroxidase 4 (Gpx4) and Ferroptosis: What's so Special about It? *Mol Cell Oncol* **2015**, 2 (3), e995047. https://doi.org/10.4161/23723556.2014.995047.
- (146) Aquilano, K.; Baldelli, S.; Ciriolo, M. R. Glutathione: New Roles in Redox Signaling for an Old Antioxidant. *Frontiers in Pharmacology* **2014**, *5*.
- (147) Yang, W. S.; Stockwell, B. R. Synthetic Lethal Screening Identifies Compounds Activating Iron-Dependent, Nonapoptotic Cell Death in Oncogenic-RAS-Harboring Cancer Cells. *Chem Biol* **2008**, *15* (3), 234–245. https://doi.org/10.1016/j.chembiol.2008.02.010.
- (148) Abdalkader, M.; Lampinen, R.; Kanninen, K. M.; Malm, T. M.; Liddell, J. R. Targeting Nrf2 to Suppress Ferroptosis and Mitochondrial Dysfunction in Neurodegeneration. *Frontiers in Neuroscience* **2018**, *12*.
- (149) Petsouki, E.; Cabrera, S. N. S.; Heiss, E. H. AMPK and NRF2: Interactive Players in the Same Team for Cellular Homeostasis? *Free Radical Biology and Medicine* **2022**, *190*, 75–93. https://doi.org/10.1016/j.freeradbiomed.2022.07.014.
- (150) Ishii, T.; Itoh, K.; Takahashi, S.; Sato, H.; Yanagawa, T.; Katoh, Y.; Bannai, S.; Yamamoto, M. Transcription Factor Nrf2 Coordinately Regulates a Group of Oxidative Stress-Inducible Genes in Macrophages. *J Biol Chem* **2000**, 275 (21), 16023–16029. https://doi.org/10.1074/jbc.275.21.16023.
- (151) Sun, X.; Ou, Z.; Chen, R.; Niu, X.; Chen, D.; Kang, R.; Tang, D. Activation of the P62-Keap1-NRF2 Pathway Protects against Ferroptosis in Hepatocellular Carcinoma Cells. *Hepatology* **2016**, 63 (1), 173–184. https://doi.org/10.1002/hep.28251.
- (152) Hassannia, B.; Wiernicki, B.; Ingold, I.; Qu, F.; Van Herck, S.; Tyurina, Y. Y.; Bayır, H.; Abhari, B. A.; Angeli, J. P. F.; Choi, S. M.; Meul, E.; Heyninck, K.; Declerck, K.; Chirumamilla, C. S.; Lahtela-Kakkonen, M.; Van Camp, G.; Krysko, D. V.; Ekert, P. G.; Fulda, S.; De Geest, B. G.; Conrad, M.; Kagan, V. E.; Vanden Berghe, W.; Vandenabeele, P.; Vanden Berghe, T. Nano-Targeted Induction of Dual Ferroptotic Mechanisms Eradicates High-Risk Neuroblastoma. *J Clin Invest* 2018, 128 (8), 3341–3355. https://doi.org/10.1172/JCl99032.
- (153) Sun, X.; Ou, Z.; Xie, M.; Kang, R.; Fan, Y.; Niu, X.; Wang, H.; Cao, L.; Tang, D. HSPB1 as a Novel Regulator of Ferroptotic Cancer Cell Death. *Oncogene* **2015**, *34* (45), 5617–5625. https://doi.org/10.1038/onc.2015.32.
- (154) Gao, M.; Monian, P.; Pan, Q.; Zhang, W.; Xiang, J.; Jiang, X. Ferroptosis Is an Autophagic Cell Death Process. *Cell Res* **2016**, *26* (9), 1021–1032. https://doi.org/10.1038/cr.2016.95.
- (155) Hou, W.; Xie, Y.; Song, X.; Sun, X.; Lotze, M. T.; Zeh, H. J.; Kang, R.; Tang, D. Autophagy Promotes Ferroptosis by Degradation of Ferritin. *Autophagy* **2016**, *12* (8), 1425–1428. https://doi.org/10.1080/15548627.2016.1187366.
- (156) Yapici, F. I.; Bebber, C. M.; Karstedt, S. von. A Guide to Ferroptosis in Cancer. *Molecular Oncology* **2024**, *18* (6), 1378. https://doi.org/10.1002/1878-0261.13649.
- (157) Zilka, O.; Shah, R.; Li, B.; Friedmann Angeli, J. P.; Griesser, M.; Conrad, M.; Pratt, D. A. On the Mechanism of Cytoprotection by Ferrostatin-1 and Liproxstatin-1 and the Role of Lipid Peroxidation in Ferroptotic Cell Death. ACS Cent Sci 2017, 3 (3), 232–243. https://doi.org/10.1021/acscentsci.7b00028.
- (158) Demaurex, N.; Petheö, G. L. Electron and Proton Transport by NADPH Oxidases. *Philos Trans R Soc Lond B Biol Sci* **2005**, 360 (1464), 2315–2325. https://doi.org/10.1098/rstb.2005.1769.

- (159) Konijn, A. M.; Glickstein, H.; Vaisman, B.; Meyron-Holtz, E. G.; Slotki, I. N.; Cabantchik, Z. I. The Cellular Labile Iron Pool and Intracellular Ferritin in K562 Cells. *Blood* **1999**, *94* (6), 2128–2134. https://doi.org/10.1182/blood.V94.6.2128.
- (160) LaVaute, T.; Smith, S.; Cooperman, S.; Iwai, K.; Land, W.; Meyron-Holtz, E.; Drake, S. K.; Miller, G.; Abu-Asab, M.; Tsokos, M.; Switzer, R.; Grinberg, A.; Love, P.; Tresser, N.; Rouault, T. A. Targeted Deletion of the Gene Encoding Iron Regulatory Protein-2 Causes Misregulation of Iron Metabolism and Neurodegenerative Disease in Mice. *Nat Genet* 2001, 27 (2), 209–214. https://doi.org/10.1038/84859.
- (161) Sun, Y.; Berleth, N.; Wu, W.; Schlütermann, D.; Deitersen, J.; Stuhldreier, F.; Berning, L.; Friedrich, A.; Akgün, S.; Mendiburo, M. J.; Wesselborg, S.; Conrad, M.; Berndt, C.; Stork, B. Fin56-Induced Ferroptosis Is Supported by Autophagy-Mediated GPX4 Degradation and Functions Synergistically with MTOR Inhibition to Kill Bladder Cancer Cells. *Cell Death Dis* **2021**, *12* (11), 1–14. https://doi.org/10.1038/s41419-021-04306-2.
- (162) Chen, X.; Kang, R.; Kroemer, G.; Tang, D. Ferroptosis in Infection, Inflammation, and Immunity. *Journal of Experimental Medicine* **2021**, *218* (6), e20210518. https://doi.org/10.1084/jem.20210518.
- (163) Pedrera, L.; Espiritu, R. A.; Ros, U.; Weber, J.; Schmitt, A.; Stroh, J.; Hailfinger, S.; von Karstedt, S.; García-Sáez, A. J. Ferroptotic Pores Induce Ca2+ Fluxes and ESCRT-III Activation to Modulate Cell Death Kinetics. *Cell Death Differ* **2021**, *28* (5), 1644–1657. https://doi.org/10.1038/s41418-020-00691-x.
- (164) Charles A Janeway, J.; Travers, P.; Walport, M.; Shlomchik, M. J. Principles of Innate and Adaptive Immunity. In *Immunobiology: The Immune System in Health and Disease. 5th edition*; Garland Science, 2001.
- (165) Sun, L.; Wang, X.; Saredy, J.; Yuan, Z.; Yang, X.; Wang, H. Innate-Adaptive Immunity Interplay and Redox Regulation in Immune Response. *Redox Biol* **2020**, *37*, 101759. https://doi.org/10.1016/j.redox.2020.101759.
- (166) Marshall, J. S.; Warrington, R.; Watson, W.; Kim, H. L. An Introduction to Immunology and Immunopathology. *Allergy Asthma Clin Immunol* 2018, 14 (Suppl 2), 49. https://doi.org/10.1186/s13223-018-0278-1.
- (167) Galluzzi, L.; Bravo-San Pedro, J. M.; Vitale, I.; Aaronson, S. A.; Abrams, J. M.; Adam, D.; Alnemri, E. S.; Altucci, L.; Andrews, D.; Annicchiarico-Petruzzelli, M.; Baehrecke, E. H.; Bazan, N. G.; Bertrand, M. J.; Bianchi, K.; Blagosklonny, M. V.; Blomgren, K.; Borner, C.; Bredesen, D. E.; Brenner, C.; Campanella, M.; Candi, E.; Cecconi, F.; Chan, F. K.; Chandel, N. S.; Cheng, E. H.; Chipuk, J. E.; Cidlowski, J. A.; Ciechanover, A.; Dawson, T. M.; Dawson, V. L.; De Laurenzi, V.; De Maria, R.; Debatin, K.-M.; Di Daniele, N.; Dixit, V. M.; Dynlacht, B. D.; El-Deiry, W. S.; Fimia, G. M.; Flavell, R. A.; Fulda, S.; Garrido, C.; Gougeon, M.-L.; Green, D. R.; Gronemeyer, H.; Hajnoczky, G.; Hardwick, J. M.; Hengartner, M. O.; Ichijo, H.; Joseph, B.; Jost, P. J.; Kaufmann, T.; Kepp, O.; Klionsky, D. J.; Knight, R. A.; Kumar, S.; Lemasters, J. J.; Levine, B.; Linkermann, A.; Lipton, S. A.; Lockshin, R. A.; López-Otín, C.; Lugli, E.; Madeo, F.; Malorni, W.; Marine, J.-C.; Martin, S. J.; Martinou, J.-C.; Medema, J. P.; Meier, P.; Melino, S.; Mizushima, N.; Moll, U.; Muñoz-Pinedo, C.; Nuñez, G.; Oberst, A.; Panaretakis, T.; Penninger, J. M.; Peter, M. E.; Piacentini, M.; Pinton, P.; Prehn, J. H.; Puthalakath, H.; Rabinovich, G. A.; Ravichandran, K. S.; Rizzuto, R.; Rodrigues, C. M.; Rubinsztein, D. C.; Rudel, T.; Shi, Y.; Simon, H.-U.; Stockwell, B. R.; Szabadkai, G.; Tait, S. W.; Tang, H. L.; Tavernarakis, N.; Tsujimoto, Y.; Vanden Berghe, T.; Vandenabeele, P.; Villunger, A.; Wagner, E. F.; Walczak, H.; White, E.; Wood, W. G.; Yuan, J.; Zakeri, Z.; Zhivotovsky, B.; Melino, G.; Kroemer, G. Essential versus Accessory Aspects of Cell Death: Recommendations of the NCCD 2015. Cell Death Differ. 2015, 22 (1), 58-73. https://doi.org/10.1038/cdd.2014.137.
- (168) Green, D. R.; Ferguson, T.; Zitvogel, L.; Kroemer, G. Immunogenic and Tolerogenic Cell Death. *Nat Rev Immunol* **2009**, *9* (5), 353–363. https://doi.org/10.1038/nri2545.
- (169) Yang, D.; Han, Z.; Oppenheim, J. J. ALARMINS AND IMMUNITY. *Immunol Rev* **2017**, *280* (1), 41–56. https://doi.org/10.1111/imr.12577.
- (170) Tang, D.; Kang, R.; Coyne, C. B.; Zeh, H. J.; Lotze, M. T. PAMPs and DAMPs: Signal 0s That Spur Autophagy and Immunity. *Immunological Reviews* **2012**, 249 (1), 158–175. https://doi.org/10.1111/j.1600-065X.2012.01146.x.
- (171) Zindel, J.; Kubes, P. DAMPs, PAMPs, and LAMPs in Immunity and Sterile Inflammation. *Annual Review of Pathology: Mechanisms of Disease* **2020**, *15* (1), 493–518. https://doi.org/10.1146/annurev-pathmechdis-012419-032847.
- (172) Sarhan, M.; von Mässenhausen, A.; Hugo, C.; Oberbauer, R.; Linkermann, A. Immunological Consequences of Kidney Cell Death. *Cell Death Dis* **2018**, 9 (2), 114. https://doi.org/10.1038/s41419-017-0057-9.

- (173) Ros, U.; Peña-Blanco, A.; Hänggi, K.; Kunzendorf, U.; Krautwald, S.; Wong, W. W.-L.; García-Sáez, A. J. Necroptosis Execution Is Mediated by Plasma Membrane Nanopores Independent of Calcium. *Cell Rep* **2017**, *19* (1), 175–187. https://doi.org/10.1016/j.celrep.2017.03.024.
- (174) Tonnus, W.; Linkermann, A. "Death Is My Heir"—Ferroptosis Connects Cancer Pharmacogenomics and Ischemia-Reperfusion Injury. *Cell Chemical Biology* **2016**, 23 (2), 202–203. https://doi.org/10.1016/j.chembiol.2016.02.005.
- (175) Linkermann, A.; Skouta, R.; Himmerkus, N.; Mulay, S. R.; Dewitz, C.; Zen, F. D.; Prokai, A.; Zuchtriegel, G.; Krombach, F.; Welz, P.-S.; Weinlich, R.; Berghe, T. V.; Vandenabeele, P.; Pasparakis, M.; Bleich, M.; Weinberg, J. M.; Reichel, C. A.; Bräsen, J. H.; Kunzendorf, U.; Anders, H.-J.; Stockwell, B. R.; Green, D. R.; Krautwald, S. Synchronized Renal Tubular Cell Death Involves Ferroptosis. PNAS 2014, 111 (47), 16836–16841. https://doi.org/10.1073/pnas.1415518111.
- (176) Martin-Sanchez, D.; Ruiz-Andres, O.; Poveda, J.; Carrasco, S.; Cannata-Ortiz, P.; Sanchez-Niño, M. D.; Ruiz Ortega, M.; Egido, J.; Linkermann, A.; Ortiz, A.; Sanz, A. B. Ferroptosis, but Not Necroptosis, Is Important in Nephrotoxic Folic Acid–Induced AKI. *J Am Soc Nephrol* **2017**, 28 (1), 218–229. https://doi.org/10.1681/ASN.2015121376.
- (177) Hambright, W. S.; Fonseca, R. S.; Chen, L.; Na, R.; Ran, Q. Ablation of Ferroptosis Regulator Glutathione Peroxidase 4 in Forebrain Neurons Promotes Cognitive Impairment and Neurodegeneration. *Redox Biol* 2017, 12, 8–17. https://doi.org/10.1016/j.redox.2017.01.021.
- (178) Tsurusaki, S.; Tsuchiya, Y.; Koumura, T.; Nakasone, M.; Sakamoto, T.; Matsuoka, M.; Imai, H.; Kok, C. Y.-Y.; Okochi, H.; Nakano, H.; Miyajima, A.; Tanaka, M. Hepatic Ferroptosis Plays an Important Role as the Trigger for Initiating Inflammation in Nonalcoholic Steatohepatitis. *Cell Death Dis* **2019**, *10* (6), 1–14. https://doi.org/10.1038/s41419-019-1678-y.
- (179) Espiritu, R. A.; Pedrera, L.; Ros, U. Chapter Seven Tuning the Way to Die: Implications of Membrane Perturbations in Necroptosis. In *Advances in Biomembranes and Lipid Self-Assembly*; Iglič, A., Rappolt, M., García-Sáez, A. J., Eds.; Advances in Biomembranes and Lipid Self-Assembly; Academic Press, 2019; Vol. 29, pp 201–247. https://doi.org/10.1016/bs.abl.2019.01.006.
- (180) Dai, E.; Han, L.; Liu, J.; Xie, Y.; Zeh, H. J.; Kang, R.; Bai, L.; Tang, D. Ferroptotic Damage Promotes Pancreatic Tumorigenesis through a TMEM173/STING-Dependent DNA Sensor Pathway. *Nat Commun* **2020**, *11*, 6339. https://doi.org/10.1038/s41467-020-20154-8.
- (181) De Nardo, D.; Kalvakolanu, D. V.; Latz, E. Immortalization of Murine Bone Marrow-Derived Macrophages. In *Macrophages: Methods and Protocols*; Rousselet, G., Ed.; Springer: New York, NY, 2018; pp 35–49. https://doi.org/10.1007/978-1-4939-7837-3_4.
- (182) Brower, M.; Carney, D. N.; Oie, H. K.; Gazdar, A. F.; Minna, J. D. Growth of Cell Lines and Clinical Specimens of Human Non-Small Cell Lung Cancer in a Serum-Free Defined Medium. *Cancer Res* **1986**, *46* (2), 798–806.
- (183) Bozkurt, A. S. Publication Status of Mouse Embryonic Fibroblast Cells in Scientific Journals. *European Journal of Therapeutics* **2021**, 27 (2), 135–141. https://doi.org/10.5152/eurjther.2021.20111.
- (184) Raschke, W. C.; Baird, S.; Ralph, P.; Nakoinz, I. Functional Macrophage Cell Lines Transformed by Abelson Leukemia Virus. *Cell* **1978**, *15* (1), 261–267. https://doi.org/10.1016/0092-8674(78)90101-0.
- (185) Tsuchiya, S.; Yamabe, M.; Yamaguchi, Y.; Kobayashi, Y.; Konno, T.; Tada, K. Establishment and Characterization of a Human Acute Monocytic Leukemia Cell Line (THP-1). *Int J Cancer* **1980**, 26 (2), 171–176. https://doi.org/10.1002/ijc.2910260208.
- (186) Rapaport, F.; Khanin, R.; Liang, Y.; Pirun, M.; Krek, A.; Zumbo, P.; Mason, C. E.; Socci, N. D.; Betel, D. Comprehensive Evaluation of Differential Gene Expression Analysis Methods for RNA-Seq Data. *Genome Biol* **2013**, *14* (9), R95. https://doi.org/10.1186/gb-2013-14-9-r95.
- (187) Lowry, O. H.; Rosebrough, N. J.; Farr, A. L.; Randall, R. J. Protein Measurement with the Folin Phenol Reagent. *J Biol Chem* **1951**, *193* (1), 265–275.
- (188) Eichelbaum, K.; Krijgsveld, J. Combining Pulsed SILAC Labeling and Click-Chemistry for Quantitative Secretome Analysis. In *Exocytosis and Endocytosis*; Ivanov, A. I., Ed.; Springer New York: New York, NY, 2014; Vol. 1174, pp 101–114. https://doi.org/10.1007/978-1-4939-0944-5_7.
- (189) Tyanova, S.; Temu, T.; Sinitcyn, P.; Carlson, A.; Hein, M. Y.; Geiger, T.; Mann, M.; Cox, J. The Perseus Computational Platform for Comprehensive Analysis of (Prote)Omics Data. *Nat Methods* **2016**, *13* (9), 731–740. https://doi.org/10.1038/nmeth.3901.
- (190) Nolte, H.; MacVicar, T. D.; Tellkamp, F.; Krüger, M. Instant Clue: A Software Suite for Interactive Data Visualization and Analysis. *Sci Rep* **2018**, *8* (1), 12648. https://doi.org/10.1038/s41598-018-31154-6.

- (191) Starr, T.; Bauler, T. J.; Malik-Kale, P.; Steele-Mortimer, O. The Phorbol 12-Myristate-13-Acetate Differentiation Protocol Is Critical to the Interaction of THP-1 Macrophages with Salmonella Typhimurium. *PLoS One* **2018**, *13* (3), e0193601. https://doi.org/10.1371/journal.pone.0193601.
- (192) von Karstedt, S.; Conti, A.; Nobis, M.; Montinaro, A.; Hartwig, T.; Lemke, J.; Legler, K.; Annewanter, F.; Campbell, A. D.; Taraborrelli, L.; Grosse-Wilde, A.; Coy, J. F.; El-Bahrawy, M. A.; Bergmann, F.; Koschny, R.; Werner, J.; Ganten, T. M.; Schweiger, T.; Hoetzenecker, K.; Kenessey, I.; Hegedüs, B.; Bergmann, M.; Hauser, C.; Egberts, J.-H.; Becker, T.; Röcken, C.; Kalthoff, H.; Trauzold, A.; Anderson, K. I.; Sansom, O. J.; Walczak, H. Cancer Cell-Autonomous TRAIL-R Signaling Promotes KRAS-Driven Cancer Progression, Invasion, and Metastasis. *Cancer Cell* **2015**, *27* (4), 561–573. https://doi.org/10.1016/j.ccell.2015.02.014.
- (193) Yoo, S.-E.; Chen, L.; Na, R.; Liu, Y.; Rios, C.; Van Remmen, H.; Richardson, A.; Ran, Q. Gpx4 Ablation in Adult Mice Results in a Lethal Phenotype Accompanied by Neuronal Loss in Brain. *Free Radic Biol Med* **2012**, *52* (9), 1820–1827. https://doi.org/10.1016/j.freeradbiomed.2012.02.043.
- (194) Aebersold, R.; Goodlett, D. R. Mass Spectrometry in Proteomics. *Chem Rev* **2001**, *101* (2), 269–295. https://doi.org/10.1021/cr990076h.
- (195) Chen, X.; Wei, S.; Ji, Y.; Guo, X.; Yang, F. Quantitative Proteomics Using SILAC: Principles, Applications, and Developments. *Proteomics* **2015**, *15* (18), 3175–3192. https://doi.org/10.1002/pmic.201500108.
- (196) Ong, S.-E.; Mann, M. Mass Spectrometry–Based Proteomics Turns Quantitative. *Nat Chem Biol* **2005**, *1* (5), 252–262. https://doi.org/10.1038/nchembio736.
- (197) Wang, K.; Zhang, Z.; Wang, M.; Cao, X.; Qi, J.; Wang, D.; Gong, A.; Zhu, H. Role of GRP78 Inhibiting Artesunate-Induced Ferroptosis in KRAS Mutant Pancreatic Cancer Cells. *Drug Des Devel Ther* **2019**, *13*, 2135–2144. https://doi.org/10.2147/DDDT.S199459.
- (198) Zhu, S.; Zhang, Q.; Sun, X.; Zeh, H. J.; Lotze, M. T.; Kang, R.; Tang, D. HSPA5 Regulates Ferroptotic Cell Death in Cancer Cells. *Cancer Res* 2017, 77 (8), 2064–2077. https://doi.org/10.1158/0008-5472.CAN-16-1979.
- (199) Mázló, A.; Tang, Y.; Jenei, V.; Brauman, J.; Yousef, H.; Bácsi, A.; Koncz, G. Resolution Potential of Necrotic Cell Death Pathways. *International Journal of Molecular Sciences* **2023**, *24* (1), 16. https://doi.org/10.3390/ijms24010016.
- (200) Corrigall, V. M.; Bodman-Smith, M. D.; Brunst, M.; Cornell, H.; Panayi, G. S. Inhibition of Antigen-Presenting Cell Function and Stimulation of Human Peripheral Blood Mononuclear Cells to Express an Antiinflammatory Cytokine Profile by the Stress Protein BiP: Relevance to the Treatment of Inflammatory Arthritis. *Arthritis Rheum* **2004**, *50* (4), 1164–1171. https://doi.org/10.1002/art.20134.
- (201) Sieweke, M. H.; Allen, J. E. Beyond Stem Cells: Self-Renewal of Differentiated Macrophages. *Science* **2013**, 342 (6161), 1242974. https://doi.org/10.1126/science.1242974.
- (202) Arango Duque, G.; Descoteaux, A. Macrophage Cytokines: Involvement in Immunity and Infectious Diseases. *Front Immunol* **2014**, *5*. https://doi.org/10.3389/fimmu.2014.00491.
- (203) Cavaillon, J. M. Cytokines and Macrophages. *Biomedicine & Pharmacotherapy* **1994**, *48* (10), 445–453. https://doi.org/10.1016/0753-3322(94)90005-1.
- (204) He, Z.; Riva, M.; Björk, P.; Swärd, K.; Mörgelin, M.; Leanderson, T.; Ivars, F. CD14 Is a Co-Receptor for TLR4 in the S100A9-Induced Pro-Inflammatory Response in Monocytes. *PLoS One* **2016**, *11* (5), e0156377. https://doi.org/10.1371/journal.pone.0156377.
- (205) Ciesielska, A.; Matyjek, M.; Kwiatkowska, K. TLR4 and CD14 Trafficking and Its Influence on LPS-Induced pro-Inflammatory Signaling. *Cell Mol Life Sci* **2021**, 78 (4), 1233–1261. https://doi.org/10.1007/s00018-020-03656-y.
- (206) Fitzgerald, K. A.; McWhirter, S. M.; Faia, K. L.; Rowe, D. C.; Latz, E.; Golenbock, D. T.; Coyle, A. J.; Liao, S.-M.; Maniatis, T. IKKepsilon and TBK1 Are Essential Components of the IRF3 Signaling Pathway. *Nat. Immunol.* **2003**, *4* (5), 491–496. https://doi.org/10.1038/ni921.
- (207) Sharma, S.; tenOever, B. R.; Grandvaux, N.; Zhou, G.-P.; Lin, R.; Hiscott, J. Triggering the Interferon Antiviral Response through an IKK-Related Pathway. *Science* **2003**, *300* (5622), 1148–1151. https://doi.org/10.1126/science.1081315.
- (208) Tenoever, B. R.; Ng, S.-L.; Chua, M. A.; McWhirter, S. M.; García-Sastre, A.; Maniatis, T. Multiple Functions of the IKK-Related Kinase IKKepsilon in Interferon-Mediated Antiviral Immunity. Science 2007, 315 (5816), 1274–1278. https://doi.org/10.1126/science.1136567.
- (209) Wang, Y.; Lu, X.; Zhu, L.; Shen, Y.; Chengedza, S.; Feng, H.; Wang, L.; Jung, J. U.; Gutkind, J. S.; Feng, P. IKK Epsilon Kinase Is Crucial for Viral G Protein-Coupled Receptor Tumorigenesis. Proc Natl Acad Sci U S A 2013, 110 (27), 11139–11144. https://doi.org/10.1073/pnas.1219829110.

- (210) Altamura, S.; Kessler, R.; Gröne, H.-J.; Gretz, N.; Hentze, M. W.; Galy, B.; Muckenthaler, M. U. Resistance of Ferroportin to Hepcidin Binding Causes Exocrine Pancreatic Failure and Fatal Iron Overload. *Cell Metabolism* **2014**, *20* (2), 359–367. https://doi.org/10.1016/j.cmet.2014.07.007.
- (211) Yang, Z.; Meng, X.; Xu, P. Central Role of Neutrophil in the Pathogenesis of Severe Acute Pancreatitis. *J Cell Mol Med* **2015**, *19* (11), 2513–2520. https://doi.org/10.1111/jcmm.12639.
- (212) Rock, K. L.; Kono, H. The Inflammatory Response to Cell Death. *Annu Rev Pathol* **2008**, 3, 99–126. https://doi.org/10.1146/annurev.pathmechdis.3.121806.151456.
- (213) Kaczmarek, A.; Vandenabeele, P.; Krysko, D. V. Necroptosis: The Release of Damage-Associated Molecular Patterns and Its Physiological Relevance. *Immunity* **2013**, *38* (2), 209–223. https://doi.org/10.1016/j.immuni.2013.02.003.
- (214) Oppenheim, J. J.; Yang, D. Alarmins: Chemotactic Activators of Immune Responses. *Curr Opin Immunol* **2005**, *17* (4), 359–365. https://doi.org/10.1016/j.coi.2005.06.002.
- (215) Nakatani, Y.; Kudo, I. [Prostaglandin E2 synthases]. *Nihon Yakurigaku Zasshi* **2002**, *120* (6), 373–378. https://doi.org/10.1254/fpj.120.373.
- (216) Hangai, S.; Ao, T.; Kimura, Y.; Matsuki, K.; Kawamura, T.; Negishi, H.; Nishio, J.; Kodama, T.; Taniguchi, T.; Yanai, H. PGE2 Induced in and Released by Dying Cells Functions as an Inhibitory DAMP. *Proc Natl Acad Sci U S A* **2016**, *113* (14), 3844–3849. https://doi.org/10.1073/pnas.1602023113.
- (217) Patel, S. Danger-Associated Molecular Patterns (DAMPs): The Derivatives and Triggers of Inflammation. *Curr Allergy Asthma Rep* **2018**, *18* (11), 63. https://doi.org/10.1007/s11882-018-0817-3.
- (218) Vénéreau, E.; Ceriotti, C.; Bianchi, M. E. DAMPs from Cell Death to New Life. *Front Immunol* **2015**, *6*, 422. https://doi.org/10.3389/fimmu.2015.00422.
- (219) Radic, M.; Marion, T.; Monestier, M. Nucleosomes Are Exposed at the Cell Surface in Apoptosis. *J Immunol* **2004**, *172* (11), 6692–6700. https://doi.org/10.4049/jimmunol.172.11.6692.
- (220) Jiang, W.; Bell, C. W.; Pisetsky, D. S. The Relationship between Apoptosis and High-Mobility Group Protein 1 Release from Murine Macrophages Stimulated with Lipopolysaccharide or Polyinosinic-Polycytidylic Acid. *J Immunol* **2007**, *178* (10), 6495–6503. https://doi.org/10.4049/jimmunol.178.10.6495.
- (221) Elliott, M. R.; Chekeni, F. B.; Trampont, P. C.; Lazarowski, E. R.; Kadl, A.; Walk, S. F.; Park, D.; Woodson, R. I.; Ostankovich, M.; Sharma, P.; Lysiak, J. J.; Harden, T. K.; Leitinger, N.; Ravichandran, K. S. Nucleotides Released by Apoptotic Cells Act as a Find-Me Signal to Promote Phagocytic Clearance. *Nature* **2009**, *461* (7261), 282–286. https://doi.org/10.1038/nature08296.
- (222) Tanzer, M. C.; Frauenstein, A.; Stafford, C. A.; Phulphagar, K.; Mann, M.; Meissner, F. Quantitative and Dynamic Catalogs of Proteins Released during Apoptotic and Necroptotic Cell Death. *Cell Rep* **2020**, *30* (4), 1260-1270.e5. https://doi.org/10.1016/j.celrep.2019.12.079.
- (223) Murai, S.; Yamaguchi, Y.; Shirasaki, Y.; Yamagishi, M.; Shindo, R.; Hildebrand, J. M.; Miura, R.; Nakabayashi, O.; Totsuka, M.; Tomida, T.; Adachi-Akahane, S.; Uemura, S.; Silke, J.; Yagita, H.; Miura, M.; Nakano, H. A FRET Biosensor for Necroptosis Uncovers Two Different Modes of the Release of DAMPs. *Nat Commun* 2018, 9 (1), 4457. https://doi.org/10.1038/s41467-018-06985-6.
- (224) Fiuza, C.; Bustin, M.; Talwar, S.; Tropea, M.; Gerstenberger, E.; Shelhamer, J. H.; Suffredini, A. F. Inflammation-Promoting Activity of HMGB1 on Human Microvascular Endothelial Cells. *Blood* **2003**, *101* (7), 2652–2660. https://doi.org/10.1182/blood-2002-05-1300.
- (225) Meissner, F.; Scheltema, R. A.; Mollenkopf, H.-J.; Mann, M. Direct Proteomic Quantification of the Secretome of Activated Immune Cells. *Science* 2013, 340 (6131), 475–478. https://doi.org/10.1126/science.1232578.
- (226) Phulphagar, K.; Kühn, L. I.; Ebner, S.; Frauenstein, A.; Swietlik, J. J.; Rieckmann, J.; Meissner, F. Proteomics Reveals Distinct Mechanisms Regulating the Release of Cytokines and Alarmins during Pyroptosis. *Cell Rep* 2021, 34 (10), 108826. https://doi.org/10.1016/j.celrep.2021.108826.
- (227) Wen, Q.; Liu, J.; Kang, R.; Zhou, B.; Tang, D. The Release and Activity of HMGB1 in Ferroptosis. *Biochem Biophys Res Commun* **2019**, *510* (2), 278–283. https://doi.org/10.1016/j.bbrc.2019.01.090.
- (228) Zhang, X.; Ma, Y.; Lv, G.; Wang, H. Ferroptosis as a Therapeutic Target for Inflammation-Related Intestinal Diseases. *Front Pharmacol* **2023**, *14*, 1095366. https://doi.org/10.3389/fphar.2023.1095366.

- (229) Murao, A.; Aziz, M.; Wang, H.; Brenner, M.; Wang, P. Release Mechanisms of Major DAMPs. *Apoptosis* **2021**, *26* (3), 152–162. https://doi.org/10.1007/s10495-021-01663-3.
- (230) Zanoni, I.; Ostuni, R.; Marek, L. R.; Barresi, S.; Barbalat, R.; Barton, G. M.; Granucci, F.; Kagan, J. C. CD14 Controls the LPS-Induced Endocytosis of Toll-like Receptor 4. *Cell* **2011**, 147 (4), 868–880. https://doi.org/10.1016/j.cell.2011.09.051.
- (231) Jiang, Q.; Akashi, S.; Miyake, K.; Petty, H. R. Cutting Edge: Lipopolysaccharide Induces Physical Proximity Between CD14 and Toll-Like Receptor 4 (TLR4) Prior to Nuclear Translocation of NF-KB1. *The Journal of Immunology* **2000**, *165* (7), 3541–3544. https://doi.org/10.4049/jimmunol.165.7.3541.
- (232) Stockwell, B. R.; Friedmann Angeli, J. P.; Bayir, H.; Bush, A. I.; Conrad, M.; Dixon, S. J.; Fulda, S.; Gascón, S.; Hatzios, S. K.; Kagan, V. E.; Noel, K.; Jiang, X.; Linkermann, A.; Murphy, M. E.; Overholtzer, M.; Oyagi, A.; Pagnussat, G. C.; Park, J.; Ran, Q.; Rosenfeld, C. S.; Salnikow, K.; Tang, D.; Torti, F. M.; Torti, S. V.; Toyokuni, S.; Woerpel, K. A.; Zhang, D. D. Ferroptosis: A Regulated Cell Death Nexus Linking Metabolism, Redox Biology, and Disease. *Cell* 2017, 171 (2), 273–285. https://doi.org/10.1016/j.cell.2017.09.021.
- (233) Lafont, E.; Draber, P.; Rieser, E.; Reichert, M.; Kupka, S.; de Miguel, D.; Draberova, H.; von Mässenhausen, A.; Bhamra, A.; Henderson, S.; Wojdyla, K.; Chalk, A.; Surinova, S.; Linkermann, A.; Walczak, H. TBK1 and IKKε Prevent TNF-Induced Cell Death by RIPK1 Phosphorylation. *Nat. Cell Biol.* **2018**, *20* (12), 1389–1399. https://doi.org/10.1038/s41556-018-0229-6.
- (234) Zhang, J.; Feng, H.; Zhao, J.; Feldman, E. R.; Chen, S.-Y.; Yuan, W.; Huang, C.; Akbari, O.; Tibbetts, S. A.; Feng, P. IκB Kinase ε Is an NFATc1 Kinase That Inhibits T Cell Immune Response. *Cell Rep* **2016**, *16* (2), 405–418. https://doi.org/10.1016/j.celrep.2016.05.083.
- (235) Aaes, T. L.; Kaczmarek, A.; Delvaeye, T.; De Craene, B.; De Koker, S.; Heyndrickx, L.; Delrue, I.; Taminau, J.; Wiernicki, B.; De Groote, P.; Garg, A. D.; Leybaert, L.; Grooten, J.; Bertrand, M. J. M.; Agostinis, P.; Berx, G.; Declercq, W.; Vandenabeele, P.; Krysko, D. V. Vaccination with Necroptotic Cancer Cells Induces Efficient Anti-Tumor Immunity. *Cell Reports* **2016**, *15* (2), 274–287. https://doi.org/10.1016/j.celrep.2016.03.037.
- (236) Mills, C. D.; Kincaid, K.; Alt, J. M.; Heilman, M. J.; Hill, A. M. M-1/M-2 Macrophages and the Th1/Th2 Paradigm. *The Journal of Immunology* 2000, 164 (12), 6166–6173. https://doi.org/10.4049/jimmunol.164.12.6166.
- (237) Watkins, S. K.; Egilmez, N. K.; Suttles, J.; Stout, R. D. IL-12 Rapidly Alters the Functional Profile of Tumor-Associated and Tumor-Infiltrating Macrophages In Vitro and In Vivo. *The Journal of Immunology* **2007**, *178* (3), 1357–1362. https://doi.org/10.4049/jimmunol.178.3.1357.
- (238) Mills, C. D.; Shearer, J.; Evans, R.; Caldwell, M. D. Macrophage Arginine Metabolism and the Inhibition or Stimulation of Cancer. *The Journal of Immunology* **1992**, *149* (8), 2709–2714.
- (239) Nucera, S.; Biziato, D.; Palma, M. D. The Interplay between Macrophages and Angiogenesis in Development, Tissue Injury and Regeneration. *Int. J. Dev. Biol.* **2011**, *55* (4–5), 495–503. https://doi.org/10.1387/ijdb.103227sn.
- (240) Hartwig, T.; Montinaro, A.; Karstedt, S. von; Sevko, A.; Surinova, S.; Chakravarthy, A.; Taraborrelli, L.; Draber, P.; Lafont, E.; Vargas, F. A.; El-Bahrawy, M. A.; Quezada, S. A.; Walczak, H. The TRAIL-Induced Cancer Secretome Promotes a Tumor-Supportive Immune Microenvironment via CCR2. *Molecular Cell* **2017**, *65* (4), 730-742.e5. https://doi.org/10.1016/j.molcel.2017.01.021.
- (241) Martinez, F. O.; Gordon, S.; Locati, M.; Mantovani, A. Transcriptional Profiling of the Human Monocyte-to-Macrophage Differentiation and Polarization: New Molecules and Patterns of Gene Expression. *The Journal of Immunology* 2006, 177 (10), 7303–7311. https://doi.org/10.4049/jimmunol.177.10.7303.
- (242) Ley, K. M1 Means Kill; M2 Means Heal. *The Journal of Immunology* **2017**, *199* (7), 2191–2193. https://doi.org/10.4049/jimmunol.1701135.
- (243) Goerdt, S.; Politz, O.; Schledzewski, K.; Birk, R.; Gratchev, A.; Guillot, P.; Hakiy, N.; Klemke, C.-D.; Dippel, E.; Kodelja, V.; Orfanos, C. E. Alternative versus Classical Activation of Macrophages. *PAT* **1999**, *67* (5–6), 222–226. https://doi.org/10.1159/000028096.
- (244) Fiorentino, D. F.; Bond, M. W.; Mosmann, T. R. Two Types of Mouse T Helper Cell. IV. Th2 Clones Secrete a Factor That Inhibits Cytokine Production by Th1 Clones. *J. Exp. Med.* **1989**, 170 (6), 2081–2095. https://doi.org/10.1084/jem.170.6.2081.
- (245) Biswas, S. K.; Mantovani, A. Macrophage Plasticity and Interaction with Lymphocyte Subsets: Cancer as a Paradigm. *Nat Immunol* **2010**, *11* (10), 889–896. https://doi.org/10.1038/ni.1937.
- (246) Solinas, G.; Schiarea, S.; Liguori, M.; Fabbri, M.; Pesce, S.; Zammataro, L.; Pasqualini, F.; Nebuloni, M.; Chiabrando, C.; Mantovani, A.; Allavena, P. Tumor-Conditioned Macrophages

- Secrete Migration-Stimulating Factor: A New Marker for M2-Polarization, Influencing Tumor Cell Motility. *The Journal of Immunology* **2010**, *185* (1), 642–652. https://doi.org/10.4049/jimmunol.1000413.
- (247) Mantovani, A.; Allavena, P.; Sica, A.; Balkwill, F. Cancer-Related Inflammation. *Nature* **2008**, *454* (7203), 436–444. https://doi.org/10.1038/nature07205.
- (248) Sica, A.; Schioppa, T.; Mantovani, A.; Allavena, P. Tumour-Associated Macrophages Are a Distinct M2 Polarised Population Promoting Tumour Progression: Potential Targets of Anti-Cancer Therapy. *European Journal of Cancer* **2006**, *42* (6), 717–727. https://doi.org/10.1016/j.ejca.2006.01.003.
- (249) Mantovani, A.; Allavena, P. The Interaction of Anticancer Therapies with Tumor-Associated Macrophages. *Journal of Experimental Medicine* **2015**, *212* (4), 435–445. https://doi.org/10.1084/jem.20150295.
- (250) Ries, C. H.; Cannarile, M. A.; Hoves, S.; Benz, J.; Wartha, K.; Runza, V.; Rey-Giraud, F.; Pradel, L. P.; Feuerhake, F.; Klaman, I.; Jones, T.; Jucknischke, U.; Scheiblich, S.; Kaluza, K.; Gorr, I. H.; Walz, A.; Abiraj, K.; Cassier, P. A.; Sica, A.; Gomez-Roca, C.; de Visser, K. E.; Italiano, A.; Le Tourneau, C.; Delord, J.-P.; Levitsky, H.; Blay, J.-Y.; Rüttinger, D. Targeting Tumor-Associated Macrophages with Anti-CSF-1R Antibody Reveals a Strategy for Cancer Therapy. *Cancer Cell* **2014**, *25* (6), 846–859. https://doi.org/10.1016/j.ccr.2014.05.016.
- (251) Beatty, G. L.; Chiorean, E. G.; Fishman, M. P.; Saboury, B.; Teitelbaum, U. R.; Sun, W.; Huhn, R. D.; Song, W.; Li, D.; Sharp, L. L.; Torigian, D. A.; O'Dwyer, P. J.; Vonderheide, R. H. CD40 Agonists Alter Tumor Stroma and Show Efficacy Against Pancreatic Carcinoma in Mice and Humans. *Science* **2011**, *331* (6024), 1612–1616. https://doi.org/10.1126/science.1198443.
- (252) Lang, X.; Green, M. D.; Wang, W.; Yu, J.; Choi, J. E.; Jiang, L.; Liao, P.; Zhou, J.; Zhang, Q.; Dow, A.; Saripalli, A. L.; Kryczek, I.; Wei, S.; Szeliga, W.; Vatan, L.; Stone, E. M.; Georgiou, G.; Cieslik, M.; Wahl, D. R.; Morgan, M. A.; Chinnaiyan, A. M.; Lawrence, T. S.; Zou, W. Radiotherapy and Immunotherapy Promote Tumoral Lipid Oxidation and Ferroptosis via Synergistic Repression of SLC7A11. Cancer Discov 2019, CD-19-0338. https://doi.org/10.1158/2159-8290.CD-19-0338.
- (253) Wang, W.; Green, M.; Choi, J. E.; Gijón, M.; Kennedy, P. D.; Johnson, J. K.; Liao, P.; Lang, X.; Kryczek, I.; Sell, A.; Xia, H.; Zhou, J.; Li, G.; Li, J.; Li, W.; Wei, S.; Vatan, L.; Zhang, H.; Szeliga, W.; Gu, W.; Liu, R.; Lawrence, T. S.; Lamb, C.; Tanno, Y.; Cieslik, M.; Stone, E.; Georgiou, G.; Chan, T. A.; Chinnaiyan, A.; Zou, W. CD8+ T Cells Regulate Tumour Ferroptosis during Cancer Immunotherapy. *Nature* 2019, 569 (7755), 270–274. https://doi.org/10.1038/s41586-019-1170-y.
- (254) Tsoi, J.; Robert, L.; Paraiso, K.; Galvan, C.; Sheu, K. M.; Lay, J.; Wong, D. J. L.; Atefi, M.; Shirazi, R.; Wang, X.; Braas, D.; Grasso, C. S.; Palaskas, N.; Ribas, A.; Graeber, T. G. Multi-Stage Differentiation Defines Melanoma Subtypes with Differential Vulnerability to Drug-Induced Iron-Dependent Oxidative Stress. *Cancer Cell* **2018**, *33* (5), 890-904.e5. https://doi.org/10.1016/j.ccell.2018.03.017.
- (255) Efimova, I.; Catanzaro, E.; Van der Meeren, L.; Turubanova, V. D.; Hammad, H.; Mishchenko, T. A.; Vedunova, M. V.; Fimognari, C.; Bachert, C.; Coppieters, F.; Lefever, S.; Skirtach, A. G.; Krysko, O.; Krysko, D. V. Vaccination with Early Ferroptotic Cancer Cells Induces Efficient Antitumor Immunity. *J Immunother Cancer* 2020, 8 (2), e001369. https://doi.org/10.1136/jitc-2020-001369.
- (256) Wiernicki, B.; Maschalidi, S.; Pinney, J.; Adjemian, S.; Vanden Berghe, T.; Ravichandran, K. S.; Vandenabeele, P. Cancer Cells Dying from Ferroptosis Impede Dendritic Cell-Mediated Anti-Tumor Immunity. *Nat Commun* **2022**, *13* (1), 3676. https://doi.org/10.1038/s41467-022-31218-2.
- (257) Li, Q.; Han, X.; Lan, X.; Gao, Y.; Wan, J.; Durham, F.; Cheng, T.; Yang, J.; Wang, Z.; Jiang, C.; Ying, M.; Koehler, R. C.; Stockwell, B. R.; Wang, J. Inhibition of Neuronal Ferroptosis Protects Hemorrhagic Brain. *JCI Insight* **2017**, *2* (7), e90777. https://doi.org/10.1172/jci.insight.90777.
- (258) Chen, L.; Hambright, W. S.; Na, R.; Ran, Q. Ablation of the Ferroptosis Inhibitor Glutathione Peroxidase 4 in Neurons Results in Rapid Motor Neuron Degeneration and Paralysis. *J Biol Chem* **2015**, 290 (47), 28097–28106. https://doi.org/10.1074/jbc.M115.680090.
- (259) Yatsuji, S.; Hashimoto, E.; Tobari, M.; Taniai, M.; Tokushige, K.; Shiratori, K. Clinical Features and Outcomes of Cirrhosis Due to Non-Alcoholic Steatohepatitis Compared with Cirrhosis Caused by Chronic Hepatitis C. *Journal of Gastroenterology and Hepatology* **2009**, *24* (2), 248–254. https://doi.org/10.1111/j.1440-1746.2008.05640.x.
- (260) Friedmann Angeli, J. P.; Krysko, D. V.; Conrad, M. Ferroptosis at the Crossroads of Cancer-Acquired Drug Resistance and Immune Evasion. *Nat Rev Cancer* **2019**, *19* (7), 405–414. https://doi.org/10.1038/s41568-019-0149-1.

7. Appendix

7.1. List of Figures

- Figure 1. Major forms of cell death
- Figure 2. The extrinsic and intrinsic pathway of ferroptosis
- Figure 3. Pathways of necroptosis
- Figure 4. GSDMD-mediated pyroptosis
- Figure 5. Schematic view of the ferroptosis pathway
- Figure 6. Endogenous positive and negative regulators of ferroptosis
- Figure 7. Exogenous ferroptosis inhibitors and inducers
- Figure 8. Innate and adaptive immunity
- Figure 9. Necroinflammation
- Figure 10. Ferroptosis is induced in murine Pfa1 cells through genetic knockout of GPX4
- Figure 11. H441 and MEF cells display loss of cell viability upon GPX4 inhibition with RSL3
- Figure 12. H441 and MEF cells exhibit increased levels of lipid ROS upon induction of ferroptosis which can be reverted by co-treatment with Fer-1
- Figure 13. Cytokine array analysis of supernatants from ferroptotic H441 and MEF cells display augmented cytokine contents
- Figure 14. SILAC model
- Figure 15. AHA does not display toxicity on Pfa1 cells or interference with 4-OHT and Fer-1
- Figure 16. Mass spectrometry-based proteomics workflow for secretome analysis
- Figure 17. Quantitative secretome analysis
- Figure 18. Experimental induction of ferroptosis in murine and human cells triggers paracrine chemo-cytokine release from corresponding macrophages
- Figure 19. Macrophages exposed to ferroptotic supernatant hint at CD14 expression
- Figure 20. Naïve macrophages exposed to ferroptotic supernatants and untreated macrophages cluster into two groups
- Figure 21. In vivo mouse model of pancreas-specific knockout of GPX4

7.2. List of Tables

- Table 3-1 Primary antibodies used in this study
- Table 3-2 Secondary antibodies used in this study
- Table 3-3 Buffers used in this study
- Table 3-4 Cell culture materials
- Table 3-5 Cell lines used in this study
- Table 3-6 Consumable materials and chemicals
- Table 3-7 Enzymes and enzyme buffers used in this study
- Table 3-8 Kits used in this study
- Table 3-9 Equipment used in this study
- Table 3-10 Primers used in this study
- Table 3-11 Components used for PCR
- Table 3-12 PCR program for amplification of DNA fragments
- Table 3-13 Electrophoresis gel composition
- Table 3-14 H&E staining protocol
- Table 4-1 Proteins detected with t-test significance

8. Publications

- Bebber, C. M.; Müller, F.; Prieto Clemente, L.; Weber, J.; von Karstedt, S. Ferroptosis in Cancer Cell Biology. *Cancers* (Basel) 2020, 12 (1), E164. https://doi.org/10.3390/cancers12010164
- Pedrera, L.; Espiritu, R. A.; Ros, U.; Weber, J.; Schmitt, A.; Stroh, J.; Hailfinger, S.; von Karstedt, S.; García-Sáez, A. J. Ferroptotic Pores Induce Ca2+ Fluxes and ESCRT-III Activation to Modulate Cell Death Kinetics. *Cell Death Differ* 2021, 28 (5), 1644– 1657. https://doi.org/10.1038/s41418-020-00691-x.
- Yapici FI, Seidel E, Dahlhaus A, Weber J, Schmidt C, Chaves Filho AB, Yang M, Nenchova M, Güngör E, Kotouza I, Beck J, Stroh J, Abdallah AT, Lackmann JW, Bebber CM, Androulidaki A, Kreuzalar P, Schulze A, Frezza C & von Karstedt S. An Atlas of Ferroptosis-induced Secretomes (submitted)